

**SPARSE FORMULATION OF LYAPUNOV DIRECT METHOD APPLIED TO
TRANSIENT STABILITY OF LARGE-SCALE POWER SYSTEMS**

By

MONEER M. ABU-ELNAGA

A Thesis

Submitted to the School of Graduate Studies
in Partial Fulfilment of the Requirement
for the Degree,
Doctor of Philosophy

McMaster University

September 1987

TO MY MOTHER AND MY WIFE

SPARSE FORMULATION OF LYAPUNOV DIRECT METHOD
FOR TRANSIENT STABILITY

DOCTOR OF PHILOSOPHY (1987)

McMASTER UNIVERSITY

(Electrical Engineering)

Hamilton, Ontario

TITLE : Sparse Formulation of Lyapunov Direct Method Applied
to Transient Power System Stability."

AUTHOR : Moneer M. Abu-Elnaga

B.Sc. (Elect. Eng., Ain Shams University, Egypt)
M.Sc. (Elect. Eng., Ain Shams University, Egypt)
Student Member, Institute of Electrical and Electronics
Engineers (USA)

SUPERVISOR : Mohamed A. El-Kady

Associate Professor of Electrical and Computer
Engineering
Development Manager, Ontario Hydro, Canada
B.Sc. and M.Sc. (Elect. Eng., Cairo University, Egypt)
Ph.D. (McMaster University, Canada)
Senior Member, Institute of Electrical and Electronics
Engineers (USA)
P. Eng. (Province of Ontario, Canada)

COSUPERVISOR : Raymond D. Findlay

Professor of Electrical and Computer Engineering
B.Sc. and M.Sc. (Elect. Eng., Toronto Univ. , Canada)
Ph.D. (Elect. Eng., Toronto University, Canada)
Senior Member, Institute of Electrical and Electronics
Engineers (USA)
P. Eng. (Province of Ontario, Canada)

NUMBER OF PAGES : xvii, 178

ABSTRACT

The Transient Energy Function (TEF) method represents a powerful technique to analyze the transient stability of large-scale power systems. Currently, in the applications of the TEF method, the power network is reduced by eliminating all buses and retaining only the internal nodes of the generators. This Reduced Network Formulation (RNF) yields dense (non-sparse) matrices in the computations and consumes significant computational time. This represents a serious drawback of the RNF, especially in applications to large power networks. Also, all system loads are modeled as constant impedance loads in order to use conventional techniques to reduce the network to the internal nodes of the generators. Many loads in practical power systems can be represented as constant power loads. Such loads are conventionally approximated as constant impedance type based on the pre-fault conditions. Consequently, accurate results may not be obtained. Moreover, the TEF is not applicable to very large-scale power systems due to the computer storage-related problems (e.g. file paging) and excessive computational time.

A novel formulation of the TEF method, retaining the original structure of the system network, is presented and the associated computerized algorithm is described. All the above mentioned problems are solved using the proposed Sparse Formulation (SF).

The sparse formulation avoids network reduction completely. All matrices used in the calculation of both the Stable Equilibrium Point (SEP) and the Unstable Equilibrium Point (UEP), for which the computational times are dominant in the calculation process of the energy margin (the stability index), are very sparse. This leads to a significant saving in computational time, i.e. the sparse formulation is more efficient as compared with the RNF approach.

The sparse formulation is applied to different (realistic) utility systems of up to 300 generators and 1724 buses. The results prove the superiority of the sparse formulation in contrast with other current methods.

In addition, either constant impedance or constant power load models, or any combination thereof, can be handled explicitly. Considering these actual load models, the stability indices (the critical clearing time and the transient stability limit) can be calculated more accurately.

The proposed technique can handle very large scale power systems which are beyond the scope of RNF approach. Consequently, it enables an improved design methodology of transmission networks by including provision for modeling the network in more detail. Using the sparse formulation, it is possible to perform a transient stability analysis on a microcomputer. This will render cost-effective the use of such analysis throughout the world. Also, a very powerful and robust numerical technique to deal with ill-conditioned power systems is

described. Therefore, practical (stressed) power systems can be handled, i.e. the sparse formulation is more reliable than other techniques such as RNF.

ACKNOWLEDGEMENTS

I wish to express my sincere gratitude to Dr. M.A. El-Kady for expert technical guidance and supervision throughout the course of this work. I gratefully express my appreciation to Dr. R.D. Findlay, my co-supervisor for his kind supervision and continuing encouragement. I also thank Dr. R.T.H. Alden and Dr. V.F. Carvalho, members of my supervisory committee, for their useful suggestions and continuing interest.

I would also like to express my appreciation to the Power System Operations Division of Ontario Hydro for providing the data without which this work would not have been completed.

Special thanks are due to my dear wife Seham for her patience, understanding and encouragement.

It is my pleasure to acknowledge useful discussion with my sister Samia and my friends M.S. El-Hennaway and M.S. El-Sobky.

TABLE OF CONTENTS

	PAGE
ABSTRACT	iii
ACKNOWLEDGEMENTS	vi
LIST OF FIGURES	xii
LIST OF TABLES	xvi
CHAPTER 1 INTRODUCTION	1
1.1 Statement of the Problem	1
1.2 Methods for Transient Stability Assessment	4
1.2.1 Time Domain Simulation Method	4
1.2.2 Lyapunov Direct Method	5
1.2.2.1 The Transient Stability Margin Concept	6
1.3 The New Proposed Method	7
1.3.1 Assumptions	8
1.4 Scope of the Thesis	8
CHAPTER 2 GENERAL REVIEW AND BACKGROUND	11
2.1 Introduction	11
2.2 Lyapunov Direct Method and Asymptotic Stability	13
2.3 Mathematical Models for Multimachine Power Systems	13
2.3.1 State Space Model in a Synchronously Rotating Reference (SRR)	16
2.3.1.1 State Space Model with Post-Fault SEP Transferred to Origin	18

2.3.2	State Space Model in Center Of Angle (COA) Reference Frame	19
2.4	Direct Methods for One-Machine and Two-Machine Systems	21
2.4.1	Equal Area Criterion (EAC) Method	21
2.4.2	Phase Plane Method	21
2.5	Direct Methods for Multimachine Systems	22
2.5.1	Zobov Method	23
2.5.2	Luré Type Lyapunov Functions	23
2.5.2.1	Moore and Anderson Theorem (Generalized Popov Criterion)	24
2.5.3	The Energy Type Lyapunov Functions	25
2.5.3.1	Determination of the Stability Region	27
2.5.3.2	Conservativeness and Difficulties of the TEF Application	28
2.5.3.3	The Transient Stability Margin Concept	31
2.5.4	The Structure Preserving Model	33
2.5.5	Vector Lyapunov Approach	34
2.6	Conclusion	35
CHAPTER 3	SPARSE TEF FORMULATION	37
3.1	Introduction	37
3.2	System Equations	38
3.3	Transient Energy Margin	42
3.3.1	Practical Considerations	43
3.4	Algorithm	45
3.5	Conclusion	48

CHAPTER 4	APPLICATIONS TO LARGE SCALE POWER SYSTEMS (CONSTANT IMPEDANCE LOADS)	49
4.1	Introduction	49
4.2	Application to a 50-Generator, 145-Bus System	50
4.2.1	System Description	50
4.2.2	TEF Results	53
4.2.3	Stability Indices	60
4.3	Application to a 100-Generator, 1095-Bus System	62
4.3.1	System Description	62
4.3.2	TEF Results and Stability Indices	62
4.4	Application to a 156-Generator, 1184-Bus System	66
4.4.1	System Description	66
4.4.2	TEF Results and Stability Indices	66
4.5	Application to a 300-Generator, 1825-Bus System	72
4.5.1	System Description	72
4.5.2	TEF Results and Stability Indices	72
4.6	Application on a TI Microcomputer	80
4.7	Conclusion.	80
CHAPTER 5	A ROBUST TECHNIQUE FOR LARGE SCALE ILL-CONDITIONED POWER SYSTEMS	82
5.1	Introduction	82
5.2	Physical Aspects	83
5.3	Techniques Used in the RNF for Ill-Conditioned Systems	84
5.3.1	The Davidon Fletcher Powel Method	85
5.3.2	The Corrected Gauss Newton Method	85

5.4	The Proposed Technique	85
5.4.1	The Least Squares Method	88
5.4.2	Fibonacci Search	90
5.4.3	Algorithm	91
5.5	Application to a 108-Generator, 252-Bus Ill-Conditioned System	92
5.5.1	System Description	92
5.5.2	TEF Results	94
5.5.3	The Effect of the Mode of Instability on the Speed of Calculation	97
5.6	Conclusion	103
CHAPTER 6	SPARSE TEF METHOD INCLUDING LOAD MODELS	104
6.1	Introduction	104
6.2	Applications to a 11-Generator, 55-Bus System	105
6.2.1	The Effect of Load Modeling on the Critical Clearing Time	105
6.2.2	The Effect of Load Modeling on the Energy Margin	117
6.2.2.1	The Effect of Load Modeling on the Clearing and UEP Points	121
6.2.2.2	The Effect of Load Modeling on the Clearing Speed	128
6.3	Applications to a 50-generator, 145-Bus System	128
6.3.1	The Effect of Load Modeling on the Stability Limit	130
6.4	Conclusion	141

CHAPTER 7	CONCLUSION	145
7.1	Research Contribution	146
7.2	Recommendations for Further Research	148
APPENDIX A	STABILITY DEFINITIONS AND LYAPUNOV STABILITY THEORY	150
APPENDIX B	DERIVATION OF SYSTEM EQUATIONS	153
APPENDIX C	DERIVATION OF JACOBIAN ELEMENTS	158
APPENDIX D	A MULTI-STAGE ALGORITHM (STAFP-1)	164
REFERENCES		171

LIST OF FIGURES

FIGURE		PAGE
3.1	A tableau form of equation (3.11).	41
4.1	The sparsity pattern of the Jacobian matrix for the 50-generator system (matrix of order 390).	52
4.2	The effect of the number of divisions in the energy margin calculation on the energy margin of the 50-generator system, clearing time = 0.108 s.	57
4.3	The effect of the number of steps in the clearing angles and speeds calculation on the energy margin - clearing time characteristic of the 50-generator system. Station B gross output = 1380 MW and loads = constant impedance.	61
4.4	The effect of the number of steps in the clearing angles and speeds calculation on the energy margin - station B output characteristic of the 50-generator system. $T_{cl} = 0.108$ s and loads = constant impedance.	63
4.5	The sparsity pattern of the Jacobian matrix for the 100-generator system (matrix of order 2386).	65
4.6	The energy margin of the 100-generator system versus the clearing time for constant impedance loads and station B gross output = 1350 MW (critical $T_{cl} = 0.1105$ s).	68
4.7	The energy margin of the 100-generator system versus station B interface flow for constant impedance loads and clearing time = 0.068 s (stability limit = 1485.7 MW).	69
4.8	The energy margin of the 156-generator system versus the clearing time for constant impedance loads and station B gross output = 3500 MW (critical $T_{cl} = 0.09665$ s).	73
4.9	The energy margin of the 156-generator system versus station B interface flow for constant impedance loads and clearing time = 0.108 s (stability limit = 3375.7 MW).	74

4.10	The sparsity pattern of the Jacobian matrix for the 300-generator system (matrix of order 4026).	76
4.11	The energy margin of the 300-generator system versus the clearing time for constant impedance loads and station B gross output = 3500 MW (critical Tc1 = 0.1146 s).	78
4.12	The energy margin of the 300-generator system versus station B interface flow for constant impedance loads and clearing time = 0.108 s (stability limit = 3557.2 MW).	79
6.1	The rotor angles of the advanced machines in time domain for 100 % constant impedance load models of the 11-generator system.	106
6.2	The energy margin of the 11-generator system versus the clearing time for 100 % constant impedance loads (critical Tc1 = 0.0956 s).	108
6.3	The rotor angles of the advanced machines in time domain for 50 % constant impedance + 50 % constant power load models for the 11-generator system.	109
6.4	The energy margin of the 11-generator system versus the clearing time for 50 % constant impedance + 50 % constant power loads (critical Tc1 = 0.1347 s).	110
6.5	The rotor angles of the advanced machines in time domain for 100 % constant power load models for the 11-generator system.	111
6.6	The energy margin of the 11-generator system versus the clearing time for 100 % constant power loads (critical Tc1 = 0.1833 s).	112
6.7	The critical clearing times of the 11-generator system for different load models using the sparse formulation and the time domain approach.	113
6.8	The percentage error in the critical clearing time calculation of the 11-generator system for different load models.	114
6.9	The energy at the UEP of the 11-generator system versus the clearing time for different load models (different % of constant impedance loads).	115
6.10	The energy at clearing of the 11-generator system versus the clearing time for different load models (different % of constant impedance loads).	116

6.11	The EAC criterion for 1 machine-infinite bus system.	118
6.12	The energy margin of the 11-generator system versus the clearing time for different load models (different % of constant impedance loads).	119
6.13	The normalized energy margin of the 11-generator system versus the clearing time for different load models (different % of constant impedance loads).	120
6.14	The energy at clearing the energy at the UEP and the energy margin of the 11-generator system for different load models, clearing time = 0.068 s.	122
6.15	The normalized energy margin of the 11-generator system for different load models, clearing time = 0.068 s.	123
6.16	The magnetic and dissipated energy and the positional energy of the 11-generator system for different load models, clearing time = 0.068 s.	125
6.17	The UEP of the advanced machines and the reference machine of the 11-generator system for different load models, clearing time = 0.068 s.	126
6.18	The clearing angles of the advanced machines and the reference machine of the 11-generator system for different load models, clearing time = 0.068 s.	127
6.19	The clearing speeds of the advanced machines and the reference machine of the 11-generator system for different load models, clearing time = 0.068 s.	129
6.20	The rotor angles of the advanced machines in time domain for 100 % constant impedance load models for the 50-generator system.	131
6.21	The energy margin of the 50-generator system versus station B interface flow for 100 % constant impedance loads (stability limit = 1426.5 MW).	132
6.22	The rotor angles of the advanced machines in time domain for 50 % constant impedance + 50% constant power load models for the 50-generator system.	133
6.23	The energy margin of the 50-generator system versus station B interface flow for 50 % constant impedance + 50% constant power loads (stability limit = 1462.5 MW).	134

6.24	The rotor angles of the advanced machines in time domain for 100 % constant power load models for the 50-generator system.	135
6.25	The energy margin of the 50-generator system versus station B interface flow for 100 % constant power loads (stability limit = 150.2.0 MW).	136
6.26	The stability limit of the 50-generator system for different load models using the sparse formulation and the time domain.	138
6.27	The percentage error in stability limit calculation of the 50-generator system for different load models.	139
6.28	The energy margin of the 50-generator system versus station B interface flow for different load models (different % of constant impedance loads).	140
6.29	The normalized energy margin of the 50-generator system versus station B interface flow for different load models (different % of constant impedance loads).	142
B.1	Generator classical model.	154
D.1	The first screen of STEFP-1.	165
D.2	The screen of stage 1 of STEFP-1.	166
D.3	The screen of stage 2 of STEFP-1.	168
D.4	The screen of stage 4 of STEFP-1.	169
D.5	The screen of stage 5 of STEFP-1.	170

LIST OF TABLES

TABLE		PAGE
4.1	The main data of the 50-generator system.	51
4.2	The clearing angles and speeds in the COA frame of reference for the 50-generator system, clearing time = 0.108 second.	54
4.3	The SEP and UEP for the 50-generator system.	55
4.4	The final results of the 50-generator system.	56
4.5	Voltage magnitudes at some buses and the corresponding angles in degrees for the 50-generator system.	58
4.6	The CPU times (seconds) taken by the sparse formulation and the corresponding times taken by the reduced network formulation for the 50-generator system.	59
4.7	The main data of the 100-generator system.	64
4.8	The CPU times (seconds) taken by the sparse formulation and the corresponding times taken by the reduced network formulation for the 100-generator system.	67
4.9	The main data of the 156-generator system.	70
4.10	The CPU times (seconds) taken by the sparse formulation and the corresponding times taken by the reduced network formulation for the 156-generator system.	71
4.11	The main data of the 300-generator system.	75
4.12	The CPU times (seconds) taken by the sparse formulation for the 300-generator system.	77
5.1	The main data of the 108-generator ill-conditioned system.	93
5.2	The clearing angles and speeds in COA frame of reference for the 108-generator ill-conditioned system, clearing time = 0.04 second.	95

5.3	The SEP and UEP for the 108-generator ill-conditioned system.	96
5.4	The final results of the 108-generator ill-conditioned system.	98
5.5	The CPU times (seconds) taken by the sparse formulation and the corresponding times taken by the RNF for the 108-generator ill-conditioned system.	99
5.6	The total mismatch, the method used in each iteration and total CPU time for different values of ITERLIM and NILL to calculate the UEP for the 108-generator ill-conditioned system.	100
5.7	The three modes of instability used to calculate the UEP for the 108-generator ill-conditioned system.	102
5.8	The total mismatch, the method used in each iteration and CPU time consumed in the UEP calculation for different modes of instability for the 108-generator ill-conditioned system.	103
6.1	The stability limits (MW) of different load models using time domain and sparse TEF methods for the 50-generator system.	137
6.2	The effect of load modeling on the status of the 50-generator system, $T_{cl} = 0.068$ s, station B gross output =1460 MW.	143

CHAPTER 1

INTRODUCTION

1.1 Statement of the Problem

Successful operation of a power system depends largely on the engineer's ability to provide reliable and uninterrupted service to the loads. This means that both voltage and frequency, at all loads, must be held within acceptable tolerances so that the consumer's equipment will operate satisfactorily. In order to achieve that two requirements are necessary; firstly, the system generators should run synchronously. (in step) and with adequate capacity to meet the load demand. Secondly, the integrity of the power network should be maintained to ensure continuity of service. Power systems occasionally suffer perturbations. These perturbations may be small originating from random changes in loads or they may be severe arising out of a fault on the network, a sudden application of a major load, or loss of a line or a generating unit. These perturbations may cause the power system to go from one equilibrium state (operating condition) to another. Continued successful operation of the system depends upon a stable transition to the new operating condition. The study of the behavior of the system in the transition period is described as power system stability analysis.

The transient following the system perturbation is oscillatory in nature. If the system is stable, these oscillations will be damped toward either: (a) the original operating condition if there is no net

change in power, or (b) a new operating condition if there is an unbalance between the supply and demand due to this perturbation. In either case all interconnected synchronous machines should maintain in synchronism if the system is to remain stable. The power system stability definitions [1], often used in the literature, are as follows:

Steady state stability refers to the stability of a power system subject to small and gradual changes in loads: the system remains stable with conventional excitation and governor controls.

Dynamic stability refers to the stability of a power system subject to a relatively small and "sudden" disturbance: the system can be described by linear differential equations. Typical examples are the low-frequency oscillations of interconnected large power systems and the torsional oscillations of a steam-electric power plant.

Transient Stability refers to the stability of a power system subject to a sudden and severe disturbance. For this definition to apply the system must be described by differential equations which may be nonlinear. Typical examples resulting in transient stability analysis include a fault on the network, sudden application of a major load, or loss of a line or a generating unit. This type of stability is analyzed throughout this thesis.

Transient stability can be explained physically as follows [2]. Assume that the system is in steady state, i.e. the power supplied by the generators exactly matches the power absorbed by the loads plus the

electric power loss in the transmission system. Suppose that a large perturbation in the system occurs, e.g. a fault on a transmission line. This disturbance upsets the energy balance existing prior to the disturbance and results in an excess or deficit of the mechanical power supplied over the electrical power produced by each generator in the system. Consequently, the generator rotors accelerate or decelerate respectively. The rotor angles either increase or decrease with respect to the synchronously rotating reference frame. When the fault is removed, possibly by isolating the faulted line so that an energy balance is again possible, the excess or deficit kinetic energy acquired by the system until the instant of fault clearance must be redistributed. If the system can absorb this energy after the fault is cleared, it is considered to be transiently stable; if the system cannot absorb all of this energy, then instability results. Synchronism must be maintained to ensure continuous operation of a power system. Hence transient stability analysis is an important consideration in all stages of power system design and operation.

The critical clearing time of circuit breakers, which isolate the faulty portion from the rest of the system, is important for the system planner in order to coordinate the relay setting for a given fault. Also, for the system operator, it is necessary to define appropriate security indices [3] (the transient stability margin described in section 1.2.2.1) to ensure a stable operating condition.

This chapter describes generally the different methods to tackle the problem of transient stability analysis, as well as the advantages

and the disadvantages of each. The physical aspects of the proposed method are also described. The scope of the thesis is summarized at the end of the chapter.

1.2 Methods for Transient Stability Assessment

1.2.1 Time Domain Simulation Method

The conventional method to solve the transient stability problem is by time domain simulation of rotor angles of the synchronous generators of the system (the swing curves). This method requires solving a set of differential equations which represent the system dynamics using step-by-step numerical integration techniques. The main advantage of this method is that it can simulate large systems with complex generator, exciter, and governor models. In addition, the load can be represented in a practical manner. However, solving the differential equations requires considerable computational effort especially when the system is large as in the case of North American networks. Moreover, the step-by-step method yields only a result to indicate whether or not stability is maintained. It does not indicate the quality of the system stability (or instability).

To calculate the critical clearing time using this method, the simulation is performed for a certain clearing time. If the system is stable, the clearing time is increased and the simulation is repeated once again. The process is repeated until the swing curves reveal instability. This is a tedious, trial-and-error process, besides being

expensive in terms of computer time. The continued growth of interconnections as well as their increased use for bulk power transfer has increased the necessary system representation size to the point where the number of possible studies is quite limited in many applications.

1.2.2 Lyapunov Direct Method

The equal area criterion [4] and phase plane methods [5,6,7] represent direct methods to solve the transient stability problem in the sense that they do not need to solve the system differential equations in the time domain. Unfortunately, such applications are limited to dual-machine systems.

In the past few decades power system researchers have been investigating a direct method to solve the transient stability problem for multimachine power systems. This method is based on the second method (also called the direct method) of the Lyapunov stability theory [8,9]. The statement of the second method of the Lyapunov stability theory and the definitions of stability and asymptotic stability [10] are given in appendix A. In this method, the transient energy of the post-fault system is used as a Lyapunov function. In agreement with most literature on the subject, we describe it as the Transient Energy Function (TEF) method. The main advantage of this method over the time simulation is that it does not need to solve the system differential equations in the time domain. Other important advantages are described in the following section.

1.2.2.1 The Transient Stability Margin Concept

The transient stability (or instability) of the system can be predicted [11] by comparing the value of the system energy function at the instant of fault clearing (the kinetic energy described in section 1.3.2) with the critical energy associated with the initial disturbed system trajectory and the post-fault system configuration. The difference between these two energies is what is called the Energy Margin (EM) which represents a quantitative measure of system stability. The energy margin can also be translated into additional disturbances that the system can withstand.

The energy margin can be normalized by relating it to the transient kinetic energy at the end of the disturbance. The Normalized Energy Margin (NEM) can then be used as an indicator of the robustness of the system, i.e. as an index for security assessment. It can also be used to rank different contingencies according to their severity.

The TEF method, though it represents a powerful technique to analyze the transient stability of large-scale power systems, faces some serious problems. The power network has to be reduced by eliminating all buses and retaining only the internal nodes of the generators. Consequently, the RNF yields dense (non-sparse) matrices in the computations and consumes significant computational time. This represents a serious drawback of the RNF, especially in applications to large power networks. Also, all system loads are modeled as constant impedance loads in order to be able to reduce the network to the internal nodes of the generators. Other types of loads (e.g.

constant power loads), which represent a majority in all practical power systems, must be approximated as constant impedance type loads based on the pre-fault conditions. Consequently, accurate results may not be obtained. Moreover, the TEF is not applicable to very large-scale power systems (e.g. 300-generator system) due to the computer storage-related problems (e.g. file paging). All these problems are solved using the proposed Sparse Formulation (SF).

1.3 The New Proposed Method

The sparse formulation proposed in this thesis uses the principle of the transient energy function but it keeps the original structure of the system network, i.e. it avoids network reduction completely. All matrices used in the calculation of both the Stable Equilibrium Point (SEP) and the Unstable Equilibrium Point (UEP), for which the computational times are dominant in the calculation process of the energy margin (the stability index), are very sparse. This leads to a significant saving in computational time.

In addition, either constant impedance or constant power load models (or any combination thereof) can be handled explicitly. Considering these actual load models, the stability indices (the critical clearing time and the transient stability limit) can be calculated accurately. Moreover, the voltage collapse can also be monitored if the system is working near the stability limit.

The proposed technique can handle very large scale power systems which are beyond the scope of the RNF approach, so a better design of

transmission networks can be obtained by modeling the network in more detail. Using the sparse formulation, it is possible to perform a transient stability analysis on a microcomputer. This will render cost-effective the use of such analysis throughout the world. Also, a robust numerical technique to deal with ill-conditioned power systems is described so that practical (stressed) power systems can be handled efficiently. The sparse formulation is claimed to be more efficient, more accurate and, in some cases, more reliable as compared to the RNF technique when applied to large scale systems.

1.3.1 Assumptions

The following assumptions are considered for convenient analysis of the problem:

- (1) The classical model of the synchronous generator is used: constant emf behind the direct axis transient reactance.
- (2) The mechanical input powers of synchronous generators are constant.
- (3) Damping is neglected.

1.4 Scope of the Thesis

The scope of the thesis can be summarized as follows:

Chapter 1, this chapter, is an introduction to the transient stability problem. It has described generally the different methods to tackle the problem, together with the advantages and the disadvantages of each. The physical aspects and the contributions of the proposed method have been emphasized.

Chapter 2 provides a comprehensive survey of direct methods for solving the transient stability problem. It describes the important aspects of different techniques since the introduction of the methods in power system transient stability analysis by Magnusson [12] in 1947.

Chapter 3 presents the sparse formulation of the system equations and the energy margin. It also describes a computerized algorithm to apply the sparse formulation technique for transient stability assessment.

Applications to several practical systems of up to 300 generators and 1724 buses using constant impedance load models are described in Chapter 4. A detailed comparison with RNF results are given showing the superiority of the sparse formulation technique with regard to both the computational time and storage. An application of the SF on a micro-computer is also given.

Chapter 5 describes a robust algorithm which applies the sparse formulation technique to ill-conditioned (stressed) systems. It also provides a general description of the ill-conditioning problem in transient stability analysis. A complete comparison with the RNF method is also presented.

Chapter 6 shows applications to several systems using different load models. The effect of load modeling on the critical clearing time and the transient stability limit is emphasized. The validity of the SF for different load model applications is proved by comparing its results with those obtained using time domain simulation.

Chapter 7 contains conclusions and recommendations for further research.

CHAPTER 2
GENERAL REVIEW AND BACKGROUND

2.1 Introduction

Stability was first recognized as a problem in the 1920's [13]. It was noted that the stability phenomenon was related to the establishment of a grid of hydraulic stations remote from the metropolitan areas they served. The methods of analysis used in early studies were dictated by the state of the art of the computation. Therefore, the models and methods of analysis had to be simple. In addition, graphical techniques such as the equal area criterion and circle diagrams were developed. Such techniques were adequate for analysing very simple systems which could be treated as two-machine systems. The ac network analyser developed in the 1930's permitted analysis of multimachine power systems. The network analyser was well suited for the solution of the network algebraic equations but not the machine differential equations. Therefore, simple machine models had to be used and the resulting swing equations were solved by hand calculations. In the early 1950's, electronic analog computers were used for analysis of special problems where the dynamics of synchronous machines, excitation systems and speed governors had to be modeled in more detail. The digital computers developed later in the 1950's allowed the analysis of the overall behaviour of multimachine power systems using simple models. The first digital computer program for power system stability was developed in

1956 [14]. Since then, digital computers have been enhanced very rapidly and complicated programs capable of handling large systems and very detailed models have been developed. Developments in control system theory and numerical techniques have had significant influence on the methods currently used for the stability analysis of power systems [15].

As power systems have grown rapidly and become more complex, the time domain simulation method (using the swing curves of different generators, as described in Chapter 1) has become more complex to apply, especially for security assessment and on-line stability calculation. In the last two decades power system researchers have been investigating a direct method to assess transient stability without having to solve the system equations in the time domain. A technique which achieves this purpose is based on the second method of Lyapunov's stability theory (see Appendix A).

The scope of this chapter can be summarized as follows:

- (i) Description of the Lyapunov criterion.
- (ii) Mathematical models of multimachine power systems.
- (iii) Direct methods for a single machine or two-machine systems.
- (iv) A review of the direct methods of multimachine power systems.

Detailed descriptions are given for the methods and techniques which are relevant to the work of this thesis. For more details, a monograph by Pai [2] or surveys by Willems [16], Ribben-Pavella [17,19] and Fouad [18] are recommended.

2.2 Lyapunov Direct Method and Asymptotic Stability

The principle of Lyapunov's criterion as applied to conventional transient stability analysis consists of constructing a suitable Lyapunov function $V(\underline{x})$, where \underline{x} is a vector of system state variables, and determining a stability domain surrounding the post-fault Stable Equilibrium Point (SEP) of the system. In other words, Lyapunov's criterion consists of two main steps. The first step is to define, in state space, a region of asymptotic stability of the post-fault SEP inside which $V(\underline{x}) > 0$ (except at $\underline{x} = 0$) and $\dot{V}(\underline{x}) < 0$. If V_{\min} is the lowest value of $V(\underline{x})$ on the surface $\dot{V}(\underline{x}) = 0$ (the boundary of the region), then that region is determined by $V(\underline{x}) < V_{\min}$. The second step is to determine the point of intersection of the system trajectory with the boundary of this region. Then by integration of system equations up to this point, the Critical Clearing Time (CCT) can be obtained. It should be noted that different Lyapunov functions yield different values of V_{\min} , and power system researchers have tried their best to construct Lyapunov functions that give less conservative results.

2.3 Mathematical Models for Multimachine Power Systems

The modeling process has been dealt with extensively [20,21]. Models of (almost) any desired degree of precision can be specified for the generator and its controls [19]. In transient stability study, it is difficult to use detailed models which provide ultimate accuracy. Therefore, it is traditional for this type of studies to make simplifying assumptions. The usual assumptions associated with setting

up the mathematical model are as follows [2]:

1. The network is assumed to be in the sinusoidal steady state, i.e. the time constants of the transmission network are negligible compared to the electro-mechanical frequency of oscillation.

2. A synchronous machine is represented by a constant voltage behind its direct axis transient reactance; i.e. the flux linkages are assumed to be constant during the transient period. Hence, flux decay and voltage regulation are not taken into consideration.

3. Damping, if not neglected, is proportional to slip speed.

4. The generator mechanical input power is constant and equal to the pre-fault value. In some applications to single machine or two-machine systems, governor action may be considered.

5. Loads are represented as constant impedances based on the pre-fault voltage conditions obtained from the load flow. So the network can be represented by the reduced bus admittance matrix (\bar{Y}_R); that is by eliminating all the network external nodes (physical buses) and retaining only the internal nodes of the generators.

Although the previous assumptions are good approximations and satisfactory for most applications, it is sometimes desirable to use more exact mathematical models. Now, consider a power system consisting of N_g synchronous machines (or groups of machines). The dynamic equation (the swing equation) which describes the motion of the g^{th} generator is given by:

$$M_g \frac{d^2 \delta_g(t)}{dt^2} + D_g \frac{d\delta_g(t)}{dt} + P_{eg}(t) - P_{mg} = 0 \quad (2.1)$$

where:

δ_g is the rotor angle of generator g in a synchronous frame of reference in radians,

M_g is the inertia constant of generator g in $(\text{second})^2/\text{radian}$,

D_g is the damping constant of generator g in $\text{second}/\text{radian}$,

P_{eg} is the electrical output power of generator g in per unit, and

P_{mg} is the mechanical input power of generator g in per unit.

The electrical output power of generator g can be expressed by the following equation:

$$P_{eg} = E_g^2 G_{gg} + \sum_{\substack{j=1 \\ j \neq g}}^{N_g} [E_g E_j B_{gj} \sin(\delta_g - \delta_j) + E_g E_j G_{gj} \cos(\delta_g - \delta_j)] \quad (2.2)$$

where:

E_g is the magnitude of generator g internal voltage (emf) behind the direct-axis transient reactance in per unit,

G_{gg} is the driving point conductance of \bar{Y}_R in per unit,

G_{gj} is the transfer conductance of \bar{Y}_R in per unit, and

B_{gj} is the transfer susceptance of \bar{Y}_R in per unit.

It should be noted that the matrix \bar{Y}_R changes with network topology during a fault and after clearing the fault (which may differ from the pre-fault conditions). Equation (2.1) can be rewritten as follows:

$$M_g \frac{d^2 \delta_g(t)}{dt^2} + D_g \frac{d \delta_g(t)}{dt} + P_{eg}^*(t) - P_g = 0 \quad (2.3)$$

where:

$$P_{eg}^* = \sum_{\substack{j=1 \\ j \neq g}}^{N_g} [E_g E_j B_{gj} \sin(\delta_g - \delta_j) + E_g E_j G_{gj} \cos(\delta_g - \delta_j)] \quad (2.4)$$

$$\text{and } P_g = P_{mg} - E_g^2 G_{gg} \quad (2.5)$$

To cast equation (2.3) in an appropriate state space form, we have to specify the state variables first. There are several types of state space models proposed in the literature expressing different aspects. These aspects are discussed in the following subsections.

2.3.1 State Space Model in a Synchronously Rotating Reference (SRR)

Frame

In power system problems, a reference angle is always required. One choice is to take the angle of one of the machines as a reference angle (generally the machine having the largest inertia) and measure the angle of each of the other machines with respect to this machine. Let us define the state variables as:

$$\underline{x}^1 = [\omega_1, \omega_2, \dots, \omega_{N_g} \mid \delta_1, \delta_2, \dots, \delta_{N_g}]^T \quad (2.6)$$

Then, equation (2.3) is equivalent to the following $2N_g$ equations:

$$\dot{\omega}_g = -\frac{D_g}{M_g} \omega_g + P_g - P_{eg}^* \quad g=1,2,\dots,N_g \quad (2.7)$$

$$\dot{\delta}_g = \omega_g$$

where ω_g is the rotor speed deviation of generator g in radian/sec.

This model has $2 N_g$ state variables. It was used in earlier works by Willems [22] and Pai [23], but Sastry and Murthy [24] and Ribben-Pavella [17] have pointed out that the Lyapunov functions used in [22,23] are valid only if the partial stability concept [25] is invoked, and not valid in the state space defined by \underline{x}^1 if stability is considered in the sense of Lyapunov. P_{ei}^* 's of equation (2.7) are functions of the angular differences only and not the absolute rotor angles, i.e. we must take the angular differences of all machines with respect to a reference machine. Hence, the proper state variables are (assuming that the N_g^{th} machine is the reference machine):

$$\underline{x}^2 = [\omega_1, \omega_2, \dots, \omega_{N_g} \mid \delta_1 - \delta_{N_g}, \delta_2 - \delta_{N_g}, \dots, \delta_{N_g-1} - \delta_{N_g}]^T \quad (2.8)$$

and the corresponding state space model is described by [17]:

$$\dot{\omega}_g = -\frac{D_g}{M_g} \omega_g + P_g - P_{eg}^* \quad g=1,2,\dots,N_g$$

$$\dot{\delta}_g - \dot{\delta}_{N_g} = \omega_g - \omega_{N_g} \quad g=1,2,\dots,N_g-1 \quad (2.9)$$

Moreover, if the case of uniform damping or zero damping is considered, the state variables will be the differences in angles and the differences in speeds as well, i.e. the order of the state space model is $2N_g - 2$. This has been discussed in detail in [26]. The state variables are:

$$\tilde{x}^3 = [\omega_1 - \omega_{N_g}, \omega_2 - \omega_{N_g}, \dots, \omega_{N_g-1} - \omega_{N_g} \mid \delta_1 - \delta_{N_g}, \delta_2 - \delta_{N_g}, \dots, \delta_{N_g-1} - \delta_{N_g}]^T \quad (2.10)$$

and the state space model in this case takes the form:

$$\dot{\omega}_g - \dot{\omega}_{N_g} = -\eta (\omega_g - \omega_{N_g}) + \frac{P_g - P_{eg}^*}{M_g} - \frac{P_{N_g} - P_{eN_g}^*}{M_{N_g}} \quad g=1, 2, \dots, N_g-1 \quad (2.11)$$

$$\dot{\delta}_g - \dot{\delta}_{N_g} = \omega_g - \omega_{N_g} \quad g=1, 2, \dots, N_g-1$$

where $\eta = \frac{D_i}{M_i}$ for all i in the uniform damping case and $\eta = 0$ in the case of zero damping. The derivation of the correct order of the state space model has also been done via:

- (i) controllability and observability notion [24], and
- (ii) minimal realization theory [27]

2.3.1.1 State Space Model with Post-Fault SEP Transferred to Origin

This form is necessary if we wish to construct Lyapunov functions in a systematic manner by one of the following methods:

- (i) First integral method [28].
- (ii) Quadratic forms (Krasovskii's method) [29].
- (iii) Variable gradient method [30].
- (iv) Zopov's method [31].
- (v) Absolute stability (Popov's method) [32].

In this case the state variables are:

$$\underline{x} = [\omega_1, \omega_2, \dots, \omega_{N_g} \mid \delta_1 - \delta_1^g, \delta_2 - \delta_2^g, \dots, \delta_{N_g} - \delta_{N_g}^g]^T \quad (2.12)$$

where δ_g^g represents the post-fault SEP of generator g . Then the state space model of equation (2.9) can be reduced to the following canonical form:

$$\begin{aligned} \dot{\underline{x}} &= A \underline{x} - B f(\underline{\sigma}) \\ \underline{\sigma} &= C \underline{x} \end{aligned} \quad (2.13)$$

where A , B and C are matrices whose elements depend on the inertia and damping constants of system generators and the network topology.

2.3.2 State Space Model in Center Of Angle (COA) Reference Frame

Another possibility to define a reference angle is what is called the Center Of Angle (COA) reference frame. This is a center of angle proportional to the inertia-weighted angle of each generator, a concept analogous to the center of mass in mechanical systems. COA was proposed

by Tavora and Smith [33], Stanton [34] and Fouad and Lugtu [35]. The COA denoted by δ_0 is defined as:

$$\delta_0 = \frac{1}{M_0} \sum_{g=1}^{N_g} M_g \delta_g \quad (2.14)$$

where

$$M_0 = \sum_{g=1}^{N_g} M_g \quad (2.15)$$

Hence, the new rotor angle and speed of generator g are

$$\theta_i = \delta_i - \delta_0 \quad (2.16)$$

and

$$\dot{\omega}_i = \dot{\theta}_i = \omega_i - \omega_0 \quad (2.17)$$

respectively, where $\omega_0 = \dot{\delta}_0$. Accordingly, the state space model in the case of uniform or zero damping takes the following form:

$$M_g \dot{\omega}_g = -D_g \omega_g + P_g - P_{eg}^* - \frac{M_g}{M_0} P_{COA} \quad g=1,2,\dots,N_g \quad (2.18)$$

$$\dot{\theta}_g = \omega_g$$

where

$$P_{COA} = \sum_{g=1}^{N_g} (P_g - P_{eg}^*) \quad (2.19)$$

while the model in the nonuniform damping case is slightly more

complicated [36]. This model, given by equation (2.18), is suitable for the energy function approach.

2.4 Direct Methods for One-Machine and Two-Machine Systems.

The transient stability problem of power systems having one or two machines has been investigated and studied using classical direct methods well before the Lyapunov direct method was applied. These classical methods are the Equal Area Criterion (EAC) and the phase plane method. In applying these methods, the assumptions mentioned in section 2.3 are considered with the exception that damping is neglected for EAC applications.

2.4.1 Equal Area Criterion (EAC) Method

The EAC method is considered as a special case of Lyapunov direct method since Lyapunov's function is a generalization of the energy function. This method was proposed by Skilling and Yamakawa [37] and, since then, many applications on EAC have been done. For a detailed study of the EAC, reference [4] is recommended. The EAC can be applied to a two-machine system by converting this system to a single machine-infinite bus system. A significant amount of research work has been done using the EAC method some of which exist in references [38-43].

2.4.2 Phase Plane Method

This method has been used extensively in the past in the theory of automatic control to analyze the second order nonlinear systems. It

has been introduced to power system applications by Dharma Rao [44] who could extend the application of this technique to multimachine power systems [45]. Kashkari [46] used the phase plane approach to show that the transient stability limit can be improved using feedback signals based on the rates of change of voltage, current, power or rotor angle. Gless [47] (one of the early papers on the application of the Lyapunov direct method to transient power system analysis) presented a valuable comparison between the direct method of Lyapunov, the phase plane technique and the EAC, with all three approaches giving identical results for the equivalent 1-machine system.

2.5 Direct Methods for Multimachine Systems.

Lyapunov's direct method was first proposed as a solution to the power system stability problem by Gless [47] and El-Abiad and Nagappan [48] who gave an algorithmic procedure for computer implementation to obtain the transient stability region and to calculate the CCT. Since then, there has been a significant growth in research work on this area. The main objective has been to improve the quality of Lyapunov functions in order to include a larger region of asymptotic stability (region of attraction) or more complex systems. A historical summary of various methods of constructing Lyapunov functions is contained in a paper by Gurel and Lapidus [49]. In the following subsections, previous research work is classified according to either the type of Lyapunov function or the type of load model.

2.5.1 Zubov Method

The main advantage of this method is that it enables us to generate a Lyapunov function together with the corresponding region of attraction or an approximation to it. Unfortunately, the inherent drawback of this method associated with solving linear partial differential equations precludes its application to large-scale systems. A description of the construction procedure of the Lyapunov function exists in a paper by Margolis and Vogt [50]. The authors showed that if the solution of linear partial differential equations of the system is obtained in a closed form, the exact stability region can be obtained. Yu and Vongasuriya [51] constructed a Lyapunov function in a series form and consequently an approximate region of attraction was obtained.

2.5.2 Luré Type Lyapunov Functions

In 1944, Luré and Postnikov [52] constructed a Lyapunov function for systems with the nonlinearity existing in the first and third quadrant. This function consists of a sum of a quadratic form in the state variables and an integral of the nonlinearity terms. Luré derived a set of nonlinear equations called Luré's resolving equations. He proved that the existence of a solution of these equations is a sufficient condition of global asymptotic stability of the nonlinear system. Kalman [53] and Yakubovitch [54] established the connection between Popov's stability criterion [32] and Luré functions by providing that satisfaction of the former is a necessary and sufficient condition for the existence of the latter. Later, Moore and Anderson [55]

succeeded in extending Popov's criterion to systems with multiple nonlinearities and, based on their theorem, a significant amount of work has been done. The mathematical model given by equation (2.13) is of Luré type and it has been used in this case.

$$\dot{\tilde{x}} = A \tilde{x} - B f(\sigma) \quad (2.13)$$

$$\sigma = C \tilde{x}$$

2.5.2.1 Moore and Anderson Theorem (Generalized Popov Criterion)

If, with s and I representing the complex frequency and the unity matrix, there exist real matrices N and Q such that

$$Z(s) = (N + Qs) C (sI - A)^{-1} B \quad (2.20)$$

is positive real, then the system (2.13) is asymptotically stable in the large providing $(N + Qs)$ does not cause pole-zero cancellation. Then the related Luré type Lyapunov function has the following form:

$$V(\tilde{x}) = \tilde{x}^T P \tilde{x} + \int_{\tilde{x}}^{\sigma} f^T(\sigma) Q d\sigma \quad (2.21)$$

and P is a positive definite matrix satisfying the following set of equations:

$$\begin{aligned}
 A^T P + P A &= -L L^T \\
 P B &= C^T N + A^T C^T Q - L W \\
 W^T W &= Q C B + B^T C^T Q
 \end{aligned}
 \tag{2.22}$$

where L and W are auxiliary matrices.

The Moore and Anderson theorem has been applied for the first time to a multimachine case by Willems [56] and by Willems and Willems [57]. They derived two functions corresponding to uniform and non-uniform damping cases, but the state space models used in this work have been corrected after a discussion with Sastry and Murthy [58,59]. The Popov' criterion has been exploited further and different forms of Lyapunov function were obtained by Pai and Murthy [27], Mansour [60] and Willems [25]. Kakimoto et al. [61,62] and Kakimoto and Hayashi [63] extended the work of Moore and Anderson to handle systems with machine models of third order. Their function has an additional term to represent the effect of field flux decay and, therefore, their method allows counting for automatic voltage regulators if the time constants lie within a limited range of values. Their work is considered as a valuable contribution to the transient stability analysis.

2.5.3 The Energy Type Lyapunov Functions

Magnusson [12] and later Aylett [6] developed the original energy based methods to determine the stability of power systems and proposed

the use of the transient energy function, obtained as a sum of first integrals of the rotor accelerating power equations, for the analysis of transient stability. Later on, DiCaprio and Saccomano [64] and Ribbens-Pavella [65] derived an energy function depending on the system model given by equations (2.10) and (2.11). This energy function has the following form (neglecting the transfer conductances):

$$\begin{aligned}
 V(\underline{\theta}, \underline{\omega}) = & \sum_{i=1}^{N_g-1} \sum_{j=i+1}^{N_g} [0.5 M_i M_j (\omega_i - \omega_j)^2 \\
 & - (P_i M_j - P_j M_i) (\theta_{ij} - \theta_{ij}^s) \\
 & - M_o E_i E_j B_{ij} (\cos \theta_{ij} - \cos \theta_{ij}^s)] \quad (2.23)
 \end{aligned}$$

where $\theta_{ij} = \theta_i - \theta_j$, M_o is the total inertia (the summation of all generator inertias) and the superscript s denotes the value of θ_{ij} at the SEP. The authors showed that V is a Lyapunov function satisfying $V > 0$ and $\dot{V} = 0$, i.e. the post-fault SEP is Lyapunov stable. The authors also showed that including a uniform damping makes the system asymptotically stable but does not enlarge the domain of stability. Athay et al. [66,67] used the state space model in the COA reference frame described by equations (2.18) and (2.19) to formulate the energy function. This function, which is known as Transient Energy Function (TEF), has the advantage that its various terms can be given physical meaning analogous to the single machine case. Neglecting damping, the system model of equation (2.18) can be rewritten as:

$$M_g \dot{\omega}_g = P_g - P_{eg}^* - \frac{M_g}{M_0} P_{COA} \quad g=1,2,\dots,N_g \quad (2.24)$$

$$\dot{\theta}_g = \omega_g$$

Then the TEF (described by Athay [66]) can be expressed as:

$$V(\theta, \omega) = 0.5 \sum_{i=1}^{N_g} M_i \omega_i^2 - \sum_{i=1}^{N_g} P_i (\theta_i - \theta_i^E)$$

$$- \sum_{i=1}^{N_g-1} \sum_{j=i+1}^{N_g} [E_i E_j B_{ij} (\cos(\theta_{ij}) - \cos(\theta_{ij}^E))]$$

$$- \int_{\theta_i^E + \theta_j^E}^{\theta_i + \theta_j} E_i E_j G_{ij} \cos(\theta_{ij}) d(\theta_i + \theta_j) \quad (2.25)$$

The first term represents the kinetic energy while the second, third and fourth terms represent the potential energy (positional, magnetic and dissipated energies respectively). All these system energies are relative to COA.

2.5.3.1 Determination of the Stability Region

Each of the system models described in section 2.3 can be written in the following general form:

$$\dot{\underline{x}} = \underline{f}(\underline{x}) \quad (2.26)$$

The equilibrium solutions are obtained by setting $\dot{\underline{x}} = \underline{0}$, i.e. by solving:

$$\underline{f}(\underline{x}) = \underline{0} \quad (2.27)$$

One solution of this set of equations (in the post-fault condition) is the SEP while all other solutions (saddle points) are Unstable Equilibrium Points (UEP's) surrounding the SEP. Since the speed is zero at the UEP's, and so the kinetic energy, the surface formed (in angle space) by these UEP's is called the Potential Energy Boundary Surface (PEBS) [67]. The system at different UEP's has different values of energies. The stability region is determined by that UEP which gives the minimum value. The TEF evaluated at that UEP is called the critical energy (V_{cr}). The CCT can then be calculated by integrating the faulted system equations until $V(\underline{x}) = V_{cr}$.

2.5.3.2 Conservativeness and Difficulties of the TEF Application

Lyapunov direct methods have generally led to conservative stability prediction for practical multimachine power systems. This characteristic can be attributed mainly to two factors:

- (a) The first factor is the conservative nature of Lyapunov theory itself; which gives only sufficient conditions for stability.
- (b) The second factor relates to the difficulties associated with the stability region calculation. The determination of the UEP corresponding

to V_{cr} represents the most difficult step to calculate the stability region. The number of possible UEP's is $2^{N_g-1} - 1$ which means that a considerable amount of calculations could be performed before the UEP with minimum energy can be obtained. Moreover, the practical experience has proved that using the concept of minimum energy UEP to calculate V_{cr} for a large system may lead to very conservative results if the fault configurations (e.g. the fault location) are not taken into account.

Much research work have been done to obviate these difficulties. To reduce the amount of calculation required to calculate the UEP's, Prabhakara and El-Abiad [68] suggested that the accurate determination of these UEP's is not necessary. The process of using the analogy of the one machine-infinite bus system gives an acceptable stability boundary. Gupta and El-Abiad [69] provided a systematic method of eliminating the UEP's which are of no interest in the search for the stability region which leads to the exact determination of the UEP closest to the post-fault SEP in the sense of energy. Pai and Narayana [70] and Ribbens-Pavella [71] showed that the UEP's of interest lie in the proximity of certain points (called the corner points) on the boundary of a polytope. These corner points which are easily identifiable can be used as approximations of the exact UEP's for different modes of instability (a mode of instability defines the advanced machines which tend to be separate from the system), e.g. the corner point associated with the mode in which the i^{th} machine being advanced is:

$(\delta_1^s, \delta_2^s, \dots, \pi - 2\delta_1^s, \dots, \delta_{N_g}^s)$ where $(\delta_1^s, \delta_2^s, \dots, \delta_{N_g}^s)$ is the post-fault SEP. Ribbens-Pavella [72] showed that the change in the energy function

in the neighborhood of an UEP is very small and, hence, she suggested that V_{cr} can be determined quickly by calculating N_g approximate UEP's only (instead of the $2N_g - 1$ possible UEP's). However, all power systems used in the previous works ([68-72]) were small systems of no more than 10 machines and no applications were done to large-scale power systems.

Another problem appeared when applying the energy function given by equation (2.25) in COA (described by Athay [66]), namely the evaluation of the integral term which depends on the unknown system trajectory between the post-fault SEP and the UEP. Therefore, it is not possible to judge analytically the sign definiteness of V or \dot{V} . Athay [66,67] used an approximation of linear trajectory between the SEP and UEP. He removed a major part of the conservativeness of the direct methods by incorporating the fault location in determining the exact mode of instability. He chose the UEP nearest to the point at which the critical unstable trajectory crosses the boundary of the PEBS. That is by integrating the faulted trajectory and at the same time monitoring the mismatch function $F(\theta)$ as an Euclidean norm of the power mismatches $f_i(\theta)$ for the post-fault system. When $F(\theta)$ reaches a maximum, the corresponding angles θ are very close to the intersection point of the fault-on trajectory with the PEBS. The UEP so chosen is then fault dependent and is referred to as the controlling UEP. The TEF with the linear approximation mentioned above takes the following closed form:

$$\begin{aligned}
 V(\theta, \omega) &= 0.5 \sum_{i=1}^{N_g} M_i \omega_i^2 - \sum_{i=1}^{N_g} P_i (\theta_i - \theta_i^s) \\
 &- \sum_{i=1}^{N_g-1} \sum_{j=i+1}^{N_g} [E_i E_j B_{ij} (\cos(\theta_{ij}) - \cos(\theta_{ij}^s)) \\
 &- \frac{\theta_i^u + \theta_j^u - \theta_i^s - \theta_j^s}{\theta_i^u - \theta_j^u - \theta_i^s + \theta_j^s} E_i E_j G_{ij} (\sin(\theta_{ij}^u) - \sin(\theta_{ij}^s))]
 \end{aligned}
 \tag{2.28}$$

where the superscript u denotes the values at the UEP. The TEF with these features has been used successfully in assessing the stability of practical, large-scale power systems.

2.5.3.3 The Transient Stability Margin Concept

The Energy Margin (EM) is the difference between system critical energy V_{cr} and the system energy at the instant of fault clearing V_{cl} : The energy margin represents a quantitative measure of system stability and can also be translated into additional disturbances that the system can withstand. Fouad and Stanton [73] added a correction term to V_{cr} to overcome the inconsistency that V_{cl} is calculated referring to the pre-fault SEP while V_{cr} is calculated referring to the post-fault SEP. Fouad and Stanton [73] and Fouad and Vittal [75] also introduced the concept of kinetic energy correction that not all the transient kinetic energy contributes to system instability. Only that part of the transient kinetic energy which contributes to system separation should be considered in calculating V_{cl} . Therefore, they classified the system generators into two groups; the first group is the critical generators

tending to separate from the system and the second group is the rest of the generators. Analogous to the two-machine system, the KE corresponding to the critical generators (advanced machines) separating from the rest is given by:

$$KE = 0.5 M_{eq} \omega_{eq}^2 \quad (2.29)$$

$$\text{where } M_{eq} = \frac{M_{adv} \cdot M_{rest}}{M_{adv} + M_{rest}}, \quad \omega_{eq} = \omega_{adv} - \omega_{rest}$$

$$M_{adv} = \sum_i M_i, \quad i \in C \text{ which contains all advanced machines,}$$

$$M_{rest} = \sum_i M_i, \quad i \in C' \text{ which contains the remaining machines,}$$

$$\omega_{adv} = \frac{1}{M_{adv}} \sum_i M_i \omega_i, \quad i \in C$$

$$\text{and } \omega_{rest} = \frac{1}{M_{rest}} \sum_i M_i \omega_i, \quad i \in C'$$

Fouad et al. [74] used the TEF technique for contingency analysis. They presented a scheme that can be used in system planning: as a screening tool to identify the critical cases for detailed study, and in system operation, as a means of performing dynamic security assessment. Fouad et al. [76] generalized the concept of the mode of instability: it is not always the case that all advanced machines associated with a certain mode are initially seen to be unstable. Some machines, although are

advanced, may still be stable depending on the severity and location of the fault with respect to the machines. Fouad et al. described a technique to identify the controlling UEP among several candidates having similar energy levels according to this concept. In the work presented in this section, the TEF was applied to 17-generator system (reduced Iowa network). A recent publication [77] showed that the TEF method has been applied successfully to large-scale power systems of up to 228 generators and 1644 buses. The results presented in [77] indicated that the TEF method is faster (taking less CPU time) than the step-by-step method (performed for a three second period) for applications to systems having up to 100 generators. The efficiency of the TEF method has been extended successfully [78] to larger systems by enhancing the computer program of the TEF, specially the routine for network reduction.

2.5.4 The Structure Preserving Model

All the research work described so far has been done based on converting the system loads to constant impedances and reducing the network to the internal nodes of the generators by eliminating all physical buses. Besides the disadvantage of modeling the loads incorrectly, this approach masks the topology of the network, preventing the explicit monitoring and display of voltages, energy and power transfers during the disturbance period. The first step to solve the problem of load modeling was taken by Bergen and Hill [79] who proposed a structure-preserving model where the loads are explicitly

retained. The authors used a frequency dependent load model where the load variation with frequency is taken to be piecewise-linear about the nominal frequency. Although this work has opened the way to solve the problem of load modeling and remove a major obstacle of applying the direct methods to real power systems, it has some drawbacks. This technique is valid only for an unrealistic type of load models in which the bus voltages have to be assumed constant. The mathematical transformation required by this technique may involve considerably more computational efforts than other methods previously used. Moreover, the energy dissipated in the network was neglected in their formulation. However, a further study on the structure-preserving model by Hill and Nai [80] emphasized the role of different types of damping using the Popov stability criterion, but no examples or applications were given. We conclude that the structure-preserving model, in its current state, is not applicable to real power systems where most of the loads are nonlinear (constant power type) and also because of the computational efforts required for large scale applications.

2.5.5 Vector Lyapunov Approach

In previous sections, we have described the direct methods which use different types of scalar Lyapunov functions. Another interesting approach is the so called vector Lyapunov function originally proposed by Bellman [81]. This approach involves decomposition of the entire system into small interconnected subsystems. For each subsystem, a scalar Lyapunov function is constructed and the stability region is

determined by one of the above techniques. Then, in order to assess the stability of the overall system, an aggregate model is constructed by forming a vector Lyapunov function based on the subsystem functions and the stability region of the composite system is determined using the subsystem stability regions and the properties of the interconnections. The concept of vector Lyapunov function was first applied to interconnected dynamic systems by Bailey [82] and was first applied to the transient stability problem of power systems by Pai and Narayana [70]. Since then extensive research has been done in this area. The main advantage in using decomposition-aggregation methods is their ease and effectiveness for the following two reasons: (i) much more sophisticated subsystem modeling may be considered when constructing a Lyapunov function for a 2-machine system, (ii) an analytical expression may be derived for the stability region of the subsystems. On the other hand, decomposition-aggregation methods have the disadvantage that they rely on a mathematical decomposition since the power system is modeled based on reducing the system to the internal nodes of the generators. However, this problem may be solved if the structure preserving model is used. In this case the physical decomposition can be performed.

2.6 Conclusion

Lyapunov direct methods are faster and more reliable techniques to analyze the transient stability problem as compared to the conventional step-by-step method. Moreover, they can be used for on-line

purposes (security assessment). In this chapter, the Lyapunov criterion and the associated mathematical models of multimachine power systems have been described. Different techniques to apply the Lyapunov direct method to the stability analysis of multimachine power systems have been reviewed with emphasis on the disadvantages and the potentialities of each. From this review, we conclude that the power system stability analysis, at the present state-of-the art, seeks a method which has the advantages of the TEF (as applied to large-scale power systems) and the advantage of including different load models explicitly. In addition, it should be faster than those currently available to be more suitable for on-line security assessment. All these advantages are gained by the Sparse Formulation of the TEF method described in this thesis.

CHAPTER 3

SPARSE TEF FORMULATION

3.1 Introduction

Currently, in the application of the Transient Energy Function (TEF) method, the power network is reduced by eliminating all buses and retaining only the internal nodes of the generators. This Reduced Network Formulation (RNF) may consume significant computational time, especially in applications to large power networks. The Sparse Formulation (SF) described in this chapter has many advantages: the network reduction is avoided completely. All matrices used in the calculation of the Stable Equilibrium Point (SEP) and the Unstable Equilibrium Point (UEP), which are the main steps to calculate the Energy Margin (EM) (the stability index), are very sparse. Therefore, the computational time is reduced significantly as compared to the RNF. The conventional load flow Jacobian matrix (already formulated and available from the load flow solution) is a major part of the main Jacobian matrix used to calculate the SEP and UEP. Both constant impedance and constant power type loads can be handled explicitly. Hence, more accurate results (very close to the time domain results) can be obtained. The TEF method using the proposed technique can handle very large scale power systems so that a better design of transmission network may be obtained by modeling the network in more detail.

The scope of this chapter can be summarized as follows:

(i) Problem formulation.

(ii) A computerized algorithm to calculate the SEP and the UEP and hence the energy margin.

3.2 System Equations

In the analysis, all angles (bus voltage angles and generator internal voltage angles) are referred to the centre of inertia or Centre Of Angle (COA) frame of reference. The COA, denoted by δ_0 , as described in Chapter 2, is defined as [33,34,35]:

$$\delta_0 = \frac{1}{M_0} \sum_{g=1}^{N_g} M_g \delta_g \quad (3.1)$$

$$\text{where } M_0 = \sum_{g=1}^{N_g} M_g \quad (3.2)$$

M_g is the inertia constant of generator g , δ_g is the internal voltage angle of generator g in the synchronous frame of reference, and N_g is the number of generators.

In the COA frame of reference, we can write the system equations as follows (see Appendix B):

$$V_l \sum_{j=1}^{N_l} [V_j Y_{lj} \cos (\gamma_{lj} - \phi_l + \phi_j)] = P_l \quad \text{for all } l \quad (3.3)$$

$$V_g \sum_{j=1}^N [V_j Y_{gj} \cos (\gamma_{gj} - \phi_g + \phi_j)] - P_{G_g} = P_g \quad \text{for all } g \quad (3.4)$$

$$-V_l \sum_{j=1}^N [V_j Y_{lj} \sin(\gamma_{lj} - \phi_l + \phi_j)] = Q_l \quad \text{for all } l \quad (3.5)$$

$$-V_g \sum_{j=1}^N [V_j Y_{gj} \sin(\gamma_{gj} - \phi_g + \phi_j)] - B_g [E_g V_g \cos(\theta_g - \phi_g) - V_g^2] = Q_g \quad \text{for all } g \quad (3.6)$$

$$B_g E_g V_g \sin(\theta_g - \phi_g) - P_{G_g} = 0 \quad \text{for all } g \quad (3.7)$$

$$\frac{P_{G_g}}{M_g} - \frac{P_{G_{g+1}}}{M_{g+1}} = \frac{P_{m_g}}{M_g} - \frac{P_{m_{g+1}}}{M_{g+1}} \quad \text{for all } g \neq N_g \quad (3.8)$$

$$\sum_{g=1}^{N_g} M_g \theta_g = 0 \quad (3.9)$$

where:

N is the total number of buses,

N_l is the number of load buses,

N_g is the number of generator buses,

l is an index for the load buses: $1, 2, \dots, N_l$,

g is an index for the generator buses: $1, 2, \dots, N_g$,

V_i is the magnitude of bus voltage,

ϕ_i is the angle of bus voltage in COA,

θ_g is the angle of generator internal voltage in COA,

Y_{ij} is the magnitude of element ij of the bus admittance matrix,

γ_{ij} is the angle of element ij of the bus admittance matrix,

P_i is the real load power injected at bus i ,

- Q_i is the imaginary load power injected at bus i ,
 P_{G_g} is the generator electrical output power of generator g ,
 X'_{dg} is the direct-axis transient reactance of generator g ,
 B_g is the reciprocal of X'_{dg} , and
 P_{mg} is the mechanical input power of generator g .

The previous equations represent six sets of nonlinear equations in six sets of variables. These sets of variables are ϕ_i , ϕ_g , V_i , V_g , P_{G_g} and θ_g . These sets of equations are used to calculate the SEP and the UEP using a Newton-Raphson (NR) approach. The details of how a proper initial point is obtained will be described in section 3.4. The set of equations can be expressed in a general form as:

$$\underline{f}(\underline{x}) = \underline{b} \quad (3.10)$$

Equation (3.10) can be rewritten in the perturbed form as follows:

$$J^k \cdot \Delta \underline{x}^k = \Delta \underline{b}^k \quad (3.11)$$

where J^k , \underline{b}^k are the Jacobian matrix, and mismatch vector at iteration k . Figure 3.1 shows a tableau form of equation (3.11). Notice that the upper-left block of J is almost the Jacobian used in the load flow calculation. This Jacobian is very sparse. Also the $-I$ block represents a negative unity matrix, D_i represents a diagonal matrix, B represents a bidiagonal matrix, and \underline{m} represents a row vector whose

N_L	N_G	N_L	N_G	N_G	N_G		
J_{11}	J_{12}		<table border="1" style="border-collapse: collapse; width: 100%; height: 100%;"> <tr> <td style="width: 50%; height: 50%; vertical-align: middle;">$-I$</td> <td style="width: 50%;"></td> </tr> </table>			$-I$	
$-I$							
J_{21}	J_{22}						
J_{31}	J_{32}				D_1		
D_2		D_3		$-I$	D_4		
				B			
					m		

$\Delta \phi_L$	=	$\Delta \tilde{b}$
$\Delta \phi_G$		
$\Delta \tilde{V}_L$		
$\Delta \tilde{V}_G$		
ΔPG_G		
$\Delta \theta_G$		

Fig. 3.1 A tableau form of equation (3.11).

i^{th} element is the moment of inertia of the i^{th} generator. The elements of the Jacobian are described in detail in Appendix C.

3.3 Transient Energy Margin

The transient energy function, $V(\underline{\theta}, \underline{\omega})$, is formulated as [66,67]:

$$V(\underline{\theta}, \underline{\omega}) = \sum_{g=1}^{N_g} \int_{\theta_g^s}^{\theta_g} [M_g \omega_g^2 - (P_{m_g} - P_{G_g} - \frac{M_g}{M_0} P_{COA})] d\theta_g ,$$

$$P_{COA} = \sum_{g=1}^{N_g} (P_{m_g} - P_{G_g}) \quad (3.12)$$

where θ^s denotes the post-fault SEP, and ω (for convenience, the " ω ", used in Chapter 2, has been dropped) is the rotor speed in COA. Performing the integration, we get the following expression for V :

$$V(\underline{\theta}, \underline{\omega}) = 0.5 \sum_{g=1}^{N_g} M_g \omega_g^2 - \sum_{g=1}^{N_g} P_{m_g} (\theta_g - \theta_g^s) + \sum_{g=1}^{N_g} \int_{\theta_g^s}^{\theta_g} P_{G_g} d\theta_g \quad (3.13)$$

This energy function is equivalent to that of equation (2.25) of Chapter 2. The three terms of equation (3.13) represent the kinetic energy, positional energy, and magnetic and dissipation energy of the system respectively. To calculate the energy margin, the previous equation will be applied twice; once at clearing to get:

$$V_{cl} = V(\underline{\theta}^{cl}, \underline{\omega}^{cl}) \quad (3.14)$$

where cl denotes clearing values. $\underline{\theta}^{cl}$ and $\underline{\omega}^{cl}$ can be calculated using either the step-by-step method or directly, assuming constant acceleration. Then equation (3.13) is applied at the unstable equilibrium point to get the critical transient energy:

$$V_{cr} = V(\underline{\theta}^u, \underline{0}) \quad (3.15)$$

where cr denotes critical values, and $\underline{\theta}^u$ is the unstable equilibrium point. Notice that the speeds at UEP are zero. The Energy Margin (EM) can be calculated using the following equation:

$$EM = V_{cr} - V_{cl} \quad (3.16)$$

3.3.1 Practical Considerations

As described in section 2.5.3.3 of Chapter 2, equation (3.16) needs to be corrected since the potential energy, the second and the third terms of equation (3.13), at clearing is calculated w.r.t. the pre-fault SEP while that at the UEP is calculated w.r.t. the post-fault SEP. The correction term is the potential energy from the pre-fault SEP to the post-fault SEP. To reduce the required computations, the energy margin can be calculated directly using the following expression:

$$EM = - \sum_{g=1}^{N_g} P_{m_g} (\theta_g^u - \theta_g^{cl}) + \sum_{g=1}^{N_g} \int_{\theta_g^{cl}}^{\theta_g^u} P_{G_g} d\theta_g - 0.5 \sum_{g=1}^{N_g} M_g (\omega_g^{cl})^2 \quad (3.17)$$

Using the concept of Kinetic Energy (KE) correction described in [73,75], only that part of the transient KE which contributes to system separation should be considered in determining transient stability. The KE corresponding to one group of machines (advanced machines) separating from the rest is given by:

$$KE = 0.5 M_{eq} \omega_{eq}^2 \quad (3.18)$$

where $M_{eq} = \frac{M_{adv} \cdot M_{rest}}{M_{adv} + M_{rest}}$, $\omega_{eq} = \omega_{adv} - \omega_{rest}$,

$M_{adv} = \sum_i M_i$, $i \in C$ which contains all advanced machines,

$M_{rest} = \sum_i M_i$, $i \in C'$ which contains the remaining machines,

$\omega_{adv} = \frac{1}{M_{adv}} \sum_i M_i \omega_i$, $i \in C$

and $\omega_{rest} = \frac{1}{M_{rest}} \sum_i M_i \omega_i$, $i \in C'$

Now, the energy margin has the following final form:

$$EM = - \sum_{g=1}^{N_g} P_{mg} (\theta_g^u - \theta_g^{cl}) + \sum_{g=1}^{N_g} \int_{\theta_g^{cl}}^{\theta_g^u} P_{Gg} d\theta_g - 0.5 M_{eq} \omega_{eq}^2 \quad (3.19)$$

The integral term (the second term) will be evaluated assuming a linear trajectory between the clearing point and the UEP. The energy margin can be normalized with respect to the kinetic energy at clearing to give a more meaningful index for system stability.

3.4 Algorithm

In this section, we describe a straightforward algorithm to calculate the SEP, UEP and EM. The following steps are used:

- (1) Having the pre-fault load flow solution, calculate the generator internal emf using

$$\bar{E}_g = \bar{V}_g + \bar{I}_g \cdot j X_{dg}' \quad (3.20)$$

where \bar{E}_g , \bar{V}_g and \bar{I}_g are the generator internal emf, bus voltage and bus current phasors respectively.

- (2) Calculate the COA using equation (3.1).
- (3) Calculate the voltage and emf angles in the COA frame of reference (i.e. subtract COA from those angles).
- (4) Calculate the clearing angles and speeds using either a step-by-step

method (using a suitable numerical integration technique like modified Euler or Runge Kutta) or assuming constant acceleration.

(5) After modifying the bus admittance matrix to represent the post-fault conditions, use equations (3.10) and (3.11) to calculate the post-fault SEP using load flow solution and the emf angles calculated in step 2 as initial values.

(6) Find the initial values x^0 for the UEP calculation using the following steps:

(i) Specify (or, otherwise, use other available computational algorithms to determine) the mode of instability, i.e. those machines tending to separate from the system (the advanced machines) due to the specified fault.

(ii) Calculate the "corner point", described in Chapter 2 [70,71], at which the angles of the advanced machines are set ($\pi - \theta^B$). The angles of the remaining machines are set to their SEP values.

(iii) Calculate the so called "corrected corner point" [11] at which the corner point is corrected to account for the motion of the inertial center from the SEP to the UEP points.

(iv) Calculate the so called "ray point" [84] at which the potential energy of the post-fault system reaches its maximum value along the ray between the SEP point and the corrected corner point. This is a simple one-dimensional maximization as illustrated in [84]. The use of this ray point as initial value for the UEP calculation improves the overall efficiency of the procedure.

- (v) The initial bus voltages are obtained by solving the following sparse nodal equations

$$Y_{bus} \cdot \underline{V}_{bus} = \underline{I}_{bus} \quad (3.21)$$

where Y_{bus} is the bus admittance matrix after adding jX'_{dg} to the diagonal element corresponding to the g^{th} generator, and \underline{I}_{bus} is a vector of zero elements for load buses and elements \bar{E}_g / jX'_{dg} (complex quantities) for generator buses.

- (vi) Calculate the initial guesses of the generator output powers using:

$$PG_g = \text{Re} \{ \bar{E}_g \cdot \bar{I}_g^* \} \quad (3.22)$$

where $\bar{I}_g = [\bar{E}_g - \bar{V}_g] / jX'_{dg}$ and * stands for the conjugate.

- (7) Calculate the UEP by solving equations (3.10) and (3.11) using the modified Newton-Raphson technique [85]. This technique has the advantage of incorporating a cubic interpolation in each iteration of Newton-Raphson to get an optimal step.
- (8) Calculate the energy margin using equation (3.19). To evaluate the integral term in equation (3.19), we use the following steps.
- (i) Assuming a linear trajectory between θ^{cl} and θ^u in angle space, divide the angle path between the end points into a number of equidistant points.

- (ii) Solve the network at each point to obtain the bus voltages and the generator output powers following the procedures described in step 6.
- (iii) Evaluate the integral term using the trapezoidal rule.

3.5 Conclusion

A novel formulation of the TEF method retaining the original sparse network structure has been presented and the associated computerized algorithm has been described. The sparse TEF technique has several advantages over the conventional reduced network formulation: the time consuming network reduction is avoided completely. All matrices used in calculating the SEP and UEP are very sparse. Therefore, the computational time is reduced significantly as compared to the RNF (Chapter 4). The conventional load flow Jacobian matrix (already formulated and available from the load flow solution) is a major part of the main Jacobian matrix used to calculate the SEP and UEP. The TEF method using the proposed technique can handle very large scale power systems, so that a better design of transmission networks can be obtained by modeling the network in more detail (Chapter 4). Moreover, both constant impedance and constant power type loads can be handled explicitly, so, accurate results (very close to the time domain results) can be obtained (Chapter 6).

CHAPTER 4
APPLICATIONS TO LARGE SCALE POWER SYSTEMS
(CONSTANT IMPEDANCE LOADS)

4.1 Introduction

The Sparse Formulation (SF) of the TEF method described in Chapter 3 to assess the transient stability leads to a significant saving in the computational time as compared with the currently used Reduced Network Formulation (RNF) approach. It also allows the TEF to be applied to very large scale power systems which are beyond the scope of RNF approach. The SF technique enables an improved design methodology for transmission networks by including provision for modeling the network in more detail. Moreover, the SF makes the implementation of medium-size transient stability studies on microcomputers feasible. In this chapter, the technique is applied to four different practical systems of up to 300 generators and 1724 buses [81]. Since the RNF is applicable only to systems with loads modeled as constant impedance loads, we devote this chapter to applications of the SF to constant impedance load systems. Appropriate comparisons can then be made between the two techniques. In all comparisons in this chapter, the program version TEF15 (October 1986) of the RNF, developed jointly by Ontario Hydro and Iowa State University, is used. It is important to note here that both of this program and the SF program have since then been modified and upgraded. The comparison results presented in this chapter

were obtained prior to Fall 1986.

For each system, the most important indices for transient stability assessment, namely the critical clearing time and the stability limit, are calculated. The computational time taken by both the SF and RNF are shown. The detailed results, namely the clearing angles and speeds, the SEP, UEP and the energy margin, will be given for the first system only for the purpose of demonstration. The calculations have been performed on a VAX-785 computer. At the end of the chapter, an application on a microcomputer [82] using a multi-stage TEF algorithm (STAFP-1) is presented.

4.2 Application to a 50-Generator, 145-Bus System

4.2.1 System Description

This system represents a reduced 50-generator version of a practical power utility network. Table 4.1 shows the main data of this system. A 3-phase fault is applied on bus 101. The fault is cleared at 0.108 second by tripping out two lines connected to the faulted bus. The mode of instability is chosen such that all station B machines (those connected to buses 1771 and 1793) plus the machine of station D (which is connected to bus 1853) are the advanced machines. Figure 4.1 shows the sparsity pattern of the Jacobian matrix for SEP and UEP calculations.

Description	Number
Total number of generator buses	50
Number of generators out of service	0
Number of generators in service	50
Total number of load buses	95
Total number of buses	145
Total number of lines	647
Number of transformers	63
Number of phase shifters	0
Dimension of the [Y] matrix	145
Number of non-zero elements of the [Y] matrix	985
Dimension of the [J] matrix	390
Number of non-zero elements of the [J] matrix	4390
Sparsity ratio	2.886 %

Table 4.1 The main data of the 50-generator system.

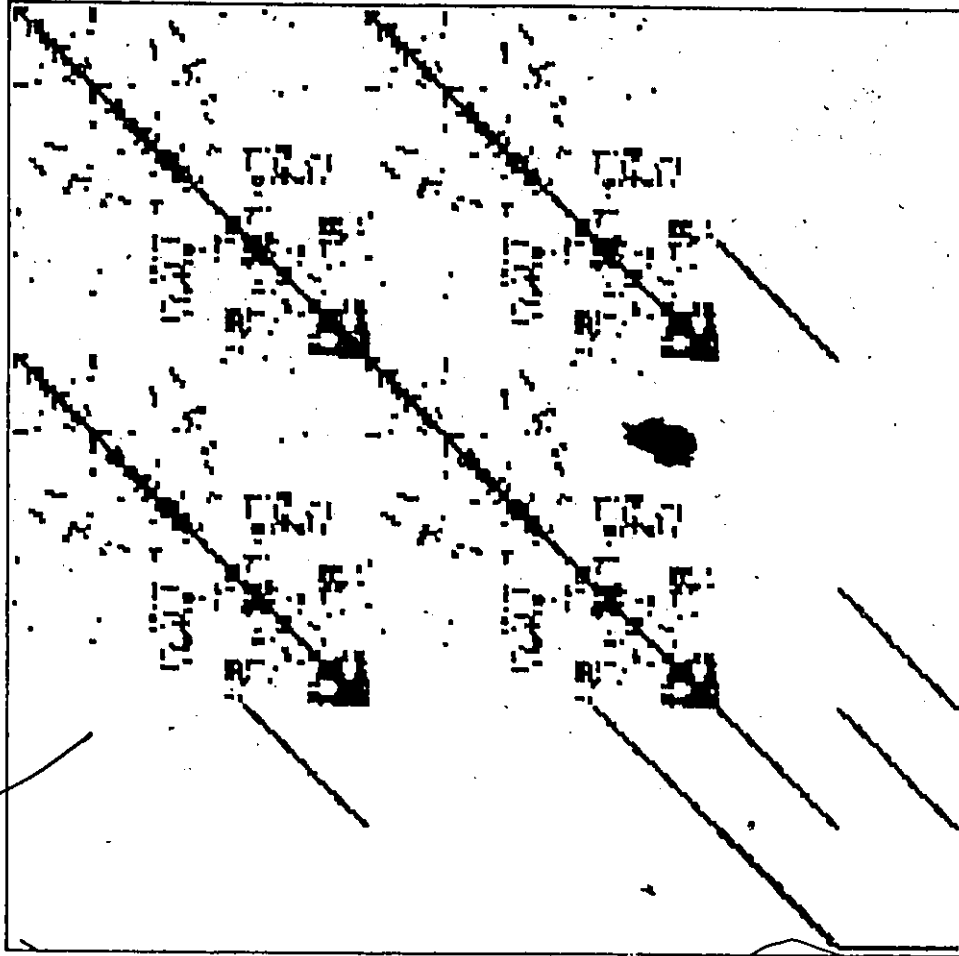


Fig. 4.1 The sparsity pattern of the Jacobian matrix for the 50-generator system (matrix of order 390.).

4.2.2 TEF Results

For this system only, the detailed results corresponding to different steps of the algorithm described in Chapter 3 are presented. Table 4.2 shows the clearing angles and speeds in the COA frame of reference for the fault conditions described in the previous section. The UEP and SEP are given in table 4.3. The ray point (the point of maximum potential energy) has been used as the initial value for the UEP. The final results comprising the values of energy components, the energy margin and the normalized energy margin, are shown in table 4.4. For the system conditions simulated, the system is stable with an energy margin of 0.030691 per unit and normalized energy margin of 0.034892. That is, the system is very close to instability or, in other words, the system is critically stable. The calculation of the energy margin is affected by the number of divisions used to evaluate the integral term as described in step 8 of the algorithm of section 3.4. Figure 4.2 shows the energy margin as a function of the number of divisions. As shown, the value of the energy margin saturates after almost 15 divisions. Based on the experience gained so far, it is found that 20 divisions give satisfactory results for all systems. All the results given in this thesis have been obtained using 20 divisions.

Since, all the network buses are explicitly modeled, the bus voltages can be monitored. Table 4.5 shows voltage magnitudes at some buses and the corresponding angles in degrees (in COA). Table 4.6 gives the detailed CPU times taken by the SF technique and the corresponding times taken by the RNF technique. It should be noted that

Bus No.	θ_{cl}	ω_{cl}	Bus No.	θ_{cl}	ω_{cl}
187	13.117	-0.01418	1856	-21.189	-0.01910
287	-24.390	-0.03270	1863	-21.431	0.08801
1032	-14.022	0.19633	2007	-3.457	-0.02235
1036	11.502	0.08824	2016	-9.479	-0.02195
1262	-30.490	-0.02002	2051	-12.762	-0.01479
1751	-20.386	-0.02340	2079	-11.870	-0.02059
1752	23.613	-0.01995	2152	-58.758	-0.02265
1754	-25.654	-0.01792	2184	-29.622	-0.02243
1771	-11.431	-0.01410	2203	-9.644	-0.02214
1776	21.025	-0.01911	2264	-16.656	-0.02090
1777	48.921	-0.02180	2459	-42.672	-0.02263
1780	-29.965	-0.01975	2601	-46.486	-0.02262
1782	-16.119	-0.01771	2609	-17.301	-0.02262
1783	-15.512	-0.01714	2616	-3.250	-0.02251
1793	10.369	2.25010	2651	9.441	-0.02263
1796	-19.363	-0.01915	2652	47.040	-0.02262
1806	-29.948	-0.02211	2654	21.813	-0.02262
1807	4.906	0.09129	2655	-49.754	-0.02263
1815	-20.088	-0.02072	2666	10.908	-0.02262
1820	-25.781	-0.02532	2669	-1.895	-0.02263
1825	-14.225	0.08837	2674	4.027	-0.02261
1826	-14.250	0.08783	2679	0.190	-0.02260
1831	-30.921	-0.02182	2699	-2.225	-0.02243
1843	-33.481	-0.02095	2719	2.512	-0.02262
1853	11.966	2.14627	2739	42.077	-0.02263

Table 4.2 The clearing angles and speeds in the COA frame
of reference for the 50-generator system,
clearing time = 0.108 second.

Bus No.	SEP	UEP	Bus No.	SEP	UEP
187	14.684	19.440	1856	-18.987	-10.229
287	-22.798	-16.379	1863	-18.491	-8.596
1032	-11.099	-2.309	2007	-3.812	-4.634
1036	14.340	22.952	2016	-9.559	-9.023
1262	-28.187	-20.526	2051	-12.590	-10.782
1751	-16.879	-6.540	2079	-11.850	-10.851
1752	25.456	31.073	2152	-58.594	-57.844
1754	-23.166	-14.885	2184	-28.461	-24.224
1771	11.936	80.108	2203	-8.605	-4.366
1776	22.599	27.366	2264	-15.212	-9.359
1777	49.485	51.156	2459	-42.323	-40.956
1780	-27.141	-17.796	2601	-46.522	-46.458
1782	-14.446	-7.690	2609	-17.497	-17.964
1783	-11.642	-0.389	2616	-3.183	-2.574
1793	29.733	102.630	2651	8.766	6.423
1796	-15.672	-4.837	2652	46.365	43.989
1806	-27.076	-17.520	2654	21.110	18.666
1807	5.389	8.806	2655	-50.911	-55.339
1815	-16.456	-5.772	2666	10.086	7.136
1820	-23.294	-14.300	2669	-2.847	-6.358
1825	-11.172	-0.893	2674	3.511	1.899
1826	-11.212	-1.004	2679	-0.158	-1.113
1831	-29.106	-22.951	2699	-2.387	-2.442
1843	-31.171	-23.502	2719	2.149	1.068
1853	32.570	106.391	2739	41.312	38.607

Table 4.3 The SEP and UEP for the 50-generator system.

Description	Value (p.u.)
Corrected kinetic energy	0.8796
Magnetic and dissipation energy at UEP	-83.608
Positional energy at UEP	84.518
Total energy at UEP	0.9103
Energy margin with KE correction	0.0307
Normalized energy margin with KE correction	0.0349

Table 4.4 The final results of the 50-generator system.

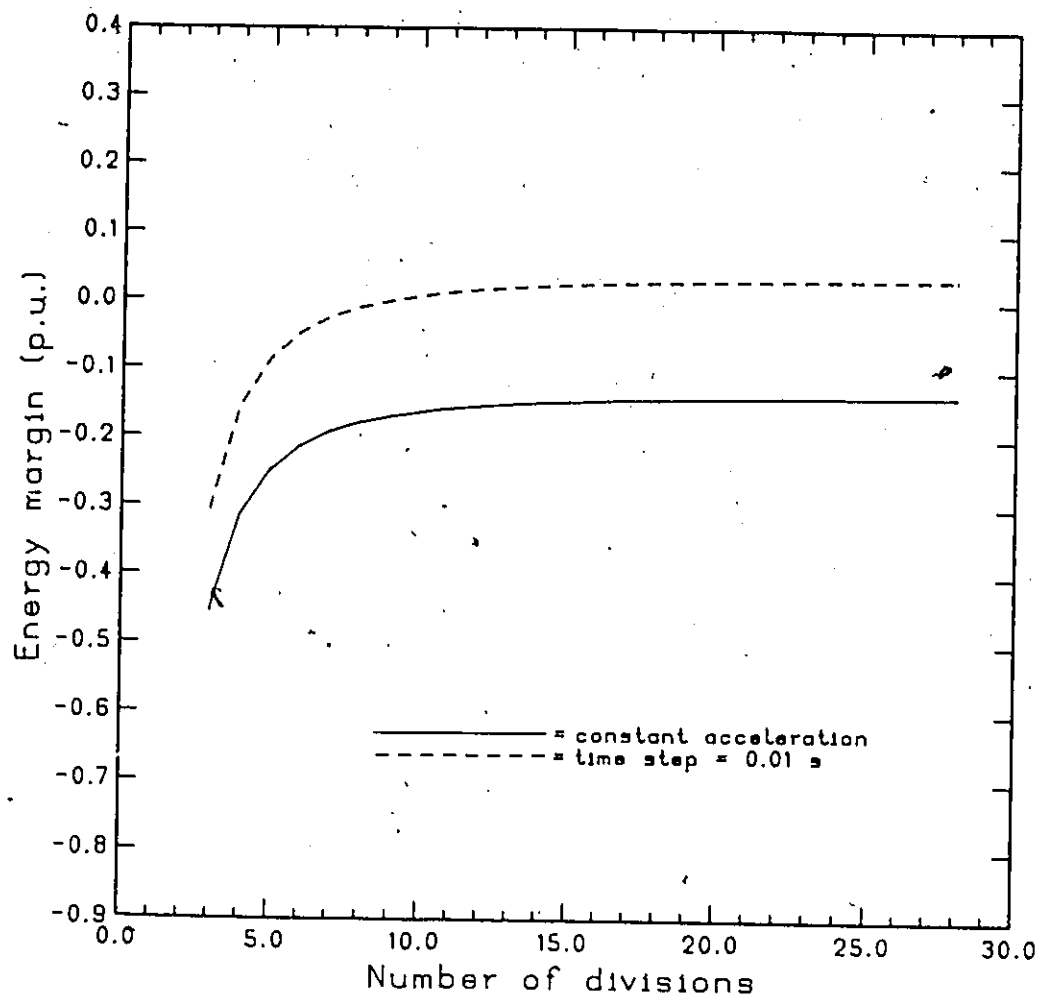


Fig. 4.2 The effect of the number of divisions in the energy margin calculation on the energy margin of the 50-generator system, clearing time = 0.108 s.

Bus No.	at SEP		at UEP	
	V	ϕ	V	ϕ
113	1.051	4.670	0.745	68.45
127	1.025	-1.639	0.623	52.14
128	1.025	-1.630	0.623	52.13
129	1.025	-1.625	0.623	52.12
130	1.025	-1.634	0.623	52.13
131	1.024	-23.266	0.736	-8.16
1616	0.988	0.025	0.649	57.77
1628	1.048	4.318	0.779	70.29
1870	0.950	11.021	0.788	79.10
1873	0.950	11.021	0.788	79.10

Table 4.5 Voltage magnitudes at some buses and the corresponding angles in degrees for the the 50-generator system.

Description	RNF	Sparse
Reading of data	6.38	6.10
Formation and reduction of the [Y] matrix	9.94	0.44
E , θ^{cl} and ω^{cl} calculation	----	1.20
SEP calculation	1.63	5.00
Initial point (x^0) calculation	6.70	1.32
UEP calculation	1.59	2.34
Energy margin calculation	0.48	0.59
Total CPU time	26.72 (100%)	16.99 (63.59%)

Table 4.6 The CPU times (seconds) taken by the sparse formulation and the corresponding times taken by the reduced network formulation for the 50-generator system.

that the CPU time corresponding to the clearing angles and speeds calculation, in both techniques, is based on the constant acceleration assumption. As shown, the CPU time has been reduced to 63.59 % when the sparse formulation is used. In calculating the UEP, we utilize the fact that the Jacobian has the same sparsity pattern as that at the SEP. This may explain why the calculation of UEP takes less CPU time than that taken by the SEP, as shown in table 4.6.

4.2.3 Stability Indices

The most important indices for the transient stability assessment are the Critical Clearing Time (CCT) and the Transient Stability Limit (TSL). The CCT is obtained by calculating the energy margin as the clearing time is increased until a negative energy margin occurs. Then, by linear interpolation between the last two values (positive and negative) of the energy margin, the CCT can be calculated (the time corresponding to zero energy margin). The energy margin is also affected by the time step used in calculating the clearing angles and speeds. Heun's algorithm which is also known as the modified Euler's algorithm [83] is used to calculate the clearing angles and speeds. Figure 4.3 shows the energy margin as a function of the clearing time for different time steps. As shown, for constant acceleration, the CCT is 0.101 second compared to 0.1095 second if a time step of 0.01 second (11 steps) is used. The relative error is 0.0085 second which represents 8.416 %.

Similarly, the TSL can be obtained by calculating the energy margin while increasing the generated output power of only one machine

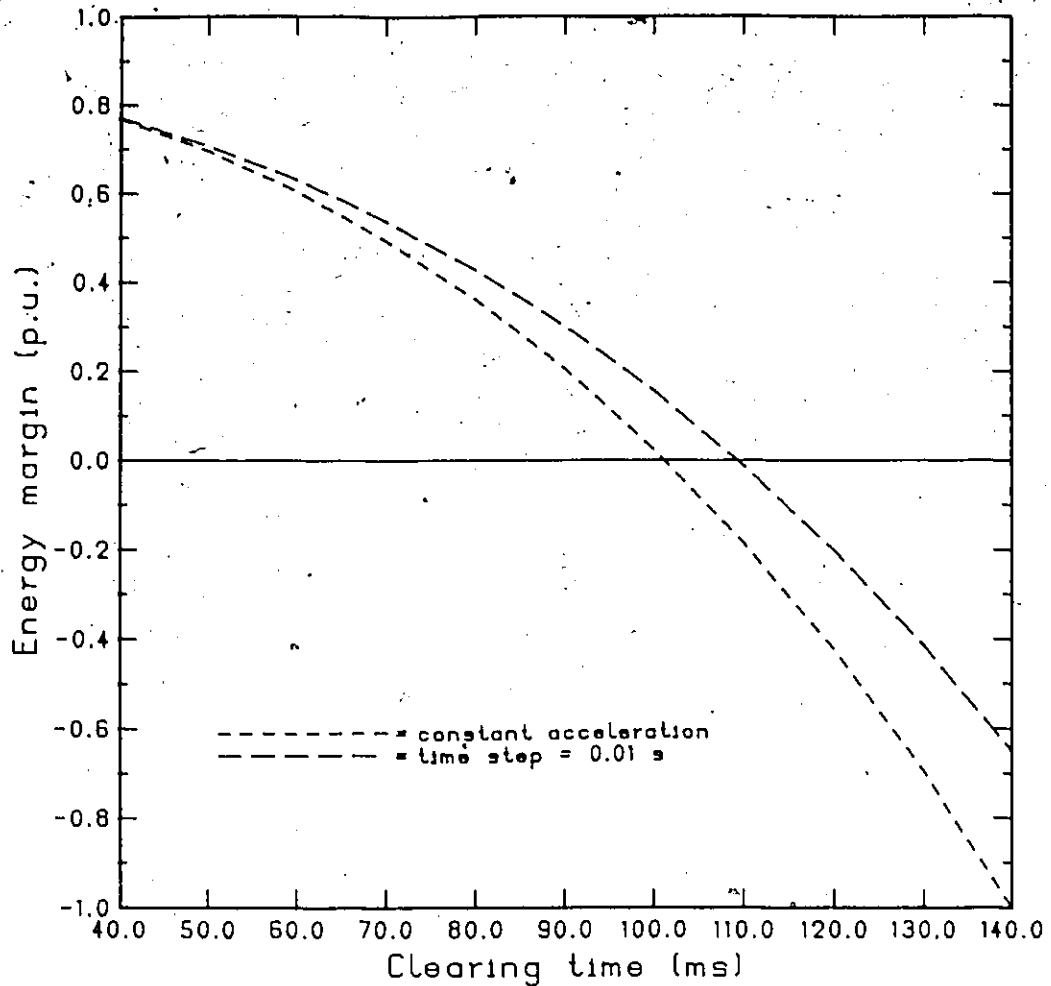


Fig. 4.3 The effect of the number of steps in clearing angles and speeds calculation on the energy margin - clearing time characteristic of the 50-generator system. Station B output = 1380 MW, and loads = constant impedance.

of station B (where the TSL is required) till we get a negative energy margin. Then by linear interpolation between the last two values of the energy margin, the TSL can be calculated. Figure 4.4 shows the energy margin - interface flow characteristics for three different time steps, namely, constant acceleration (1 step), 0.027 second (4 steps) and 0.0135 second (8 steps). The TSL's in the three cases are 1270.5, 1275 and 1277 MW, respectively. The errors in this case are almost negligible. Compromising between the accuracy required and the CPU time needed, it is found that the time step of 0.01 second is quite suitable for both the CCT and TSL calculations and it will be used for all the following applications.

4.3 Application to a 100-Generator, 1095-Bus System

4.3.1 System Description

This system represents another version of the previous system. The main data shown in table 4.7. A 3-phase fault is applied at bus 101. The fault is cleared after 0.068 sec. This system has the same mode of instability as the previous 50-generator system but with the machines of station B connected to buses 1771 and 1855. The sparsity pattern of the Jacobian is shown in figure 4.5.

4.3.2 TEF Results and Stability Indices

To calculate the clearing angles and speeds, Heun's algorithm with a time step of 0.01 second is used. For the fault conditions

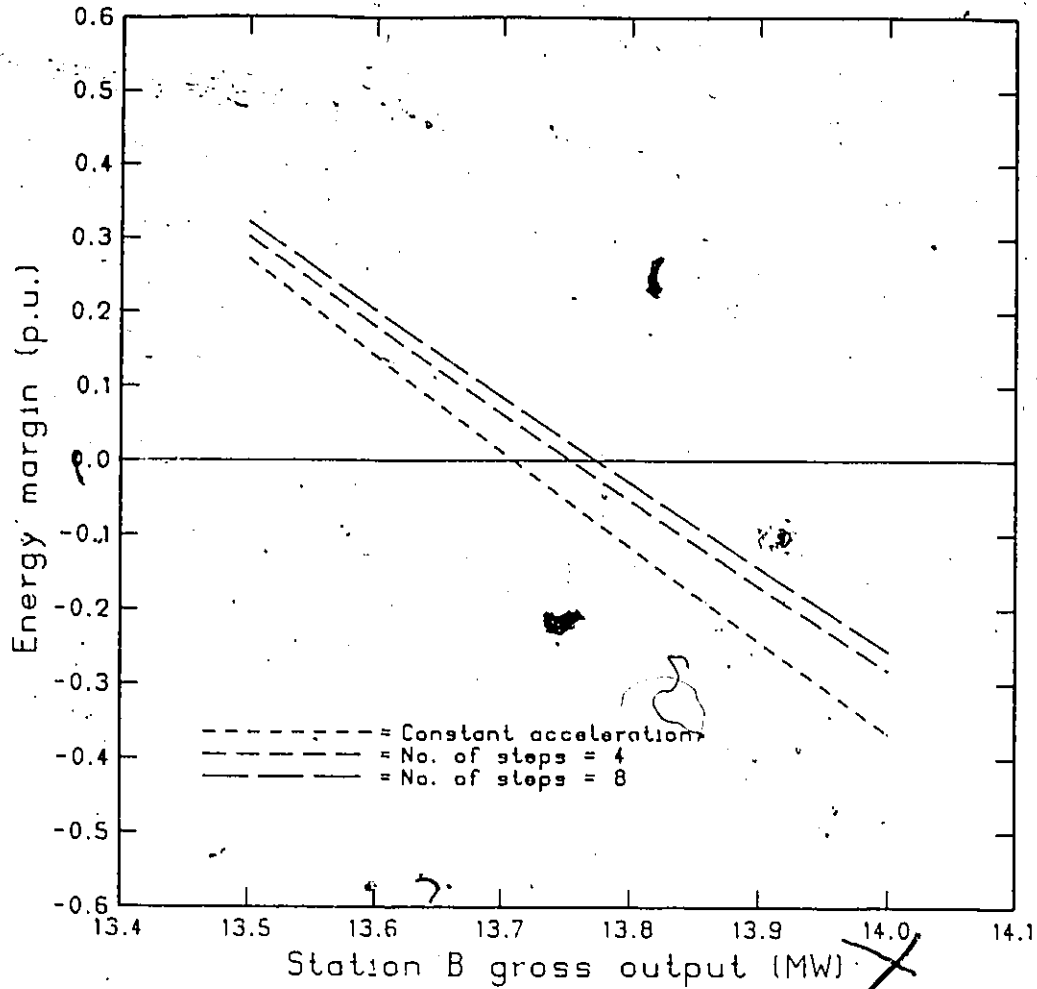
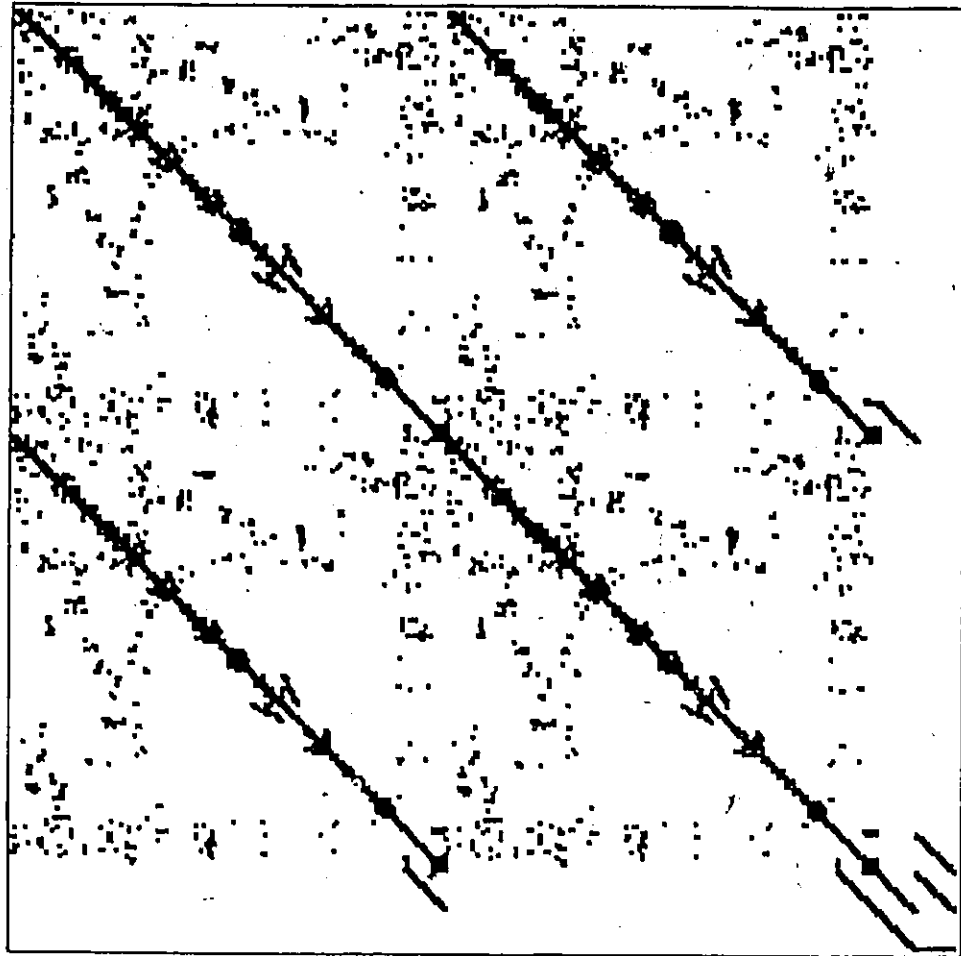


Fig. 4.4 The effect of the number of steps in clearing angles and speeds calculation on the energy margin - station B output characteristic of the 50-generator system. $T_{cl} = 0.108$ s, and loads = constant impedance.

Description	Number
Total number of generator buses	100
Number of generators out of service	2
Number of generators in service	98
Total number of load buses	997
Total number of buses	1095
Total number of lines	2039
Number of transformers	247
Number of phase shifters	2
Dimension of the [Y] matrix	1095
Number of non-zero elements of the [Y] matrix	4277
Dimension of the [J] matrix	2386
Number of non-zero elements of the [J] matrix	1700
Sparsity ratio	0.316 %

Table 4.7 The main data of the 100-generator system.



*Fig. 4.5 The sparsity pattern
of the Jacobian matrix for
the 100-generator system
(matrix of order 2386).*

described above, the system is stable with an energy margin of 1.2166 per unit and a normalized energy margin of 1.7128. Table 4.8 gives the CPU times taken by both SF and RNF techniques. As shown, the CPU time has been reduced to 46.07 %, i.e. the larger the system the bigger the CPU reduction. The CCT and TSL are calculated following the procedure described in section 4.2. The energy margin - clearing time characteristic is shown in figure 4.6 which gives a CCT of 0.1105 sec. Figure 4.7 shows the energy margin - station B interface flow characteristic. The TSL is 1485.7 MW.

4.4 Application to a 156-Generator, 1184-Bus System

4.4.1 System Description

The main data of this system are shown in table 4.9. A 3-phase fault is applied on bus 17. The fault is cleared at 0.108 sec. The chosen mode of instability is that 5 machines of station N will be advanced, namely, those connected to buses 1819, 1820, 1821, 1656 and 1857. The sparsity pattern of the Jacobian of this system is quite similar to that of the 100-generator system.

4.4.2 TEF Results and Stability Indices

For this fault, and using a time step of 0.01 second, the system is unstable with an energy margin of -1.7772 per unit and a normalized energy margin of -0.2248. Table 4.10 shows CPU times taken by both techniques. As shown, the CPU time has been reduced to 38.66 %.

Description	RNF	Sparse
Reading of data	19.93	21.43
Formation and reduction of the [Y] matrix	80.42	1.62
E , g^{cl} and w^{cl} calculation	—	5.05
SEP calculation	5.88	16.44
Initial point (x^0) calculation	21.31	5.49
UEP calculation	6.24	9.73
Energy margin calculation	1.59	2.61
Total CPU time	135.37 (100%)	62.37 (46.07%)

Table 4.8 The CPU times (seconds) taken by the sparse formulation and the corresponding times taken by the reduced network formulation for the 100-generator system.

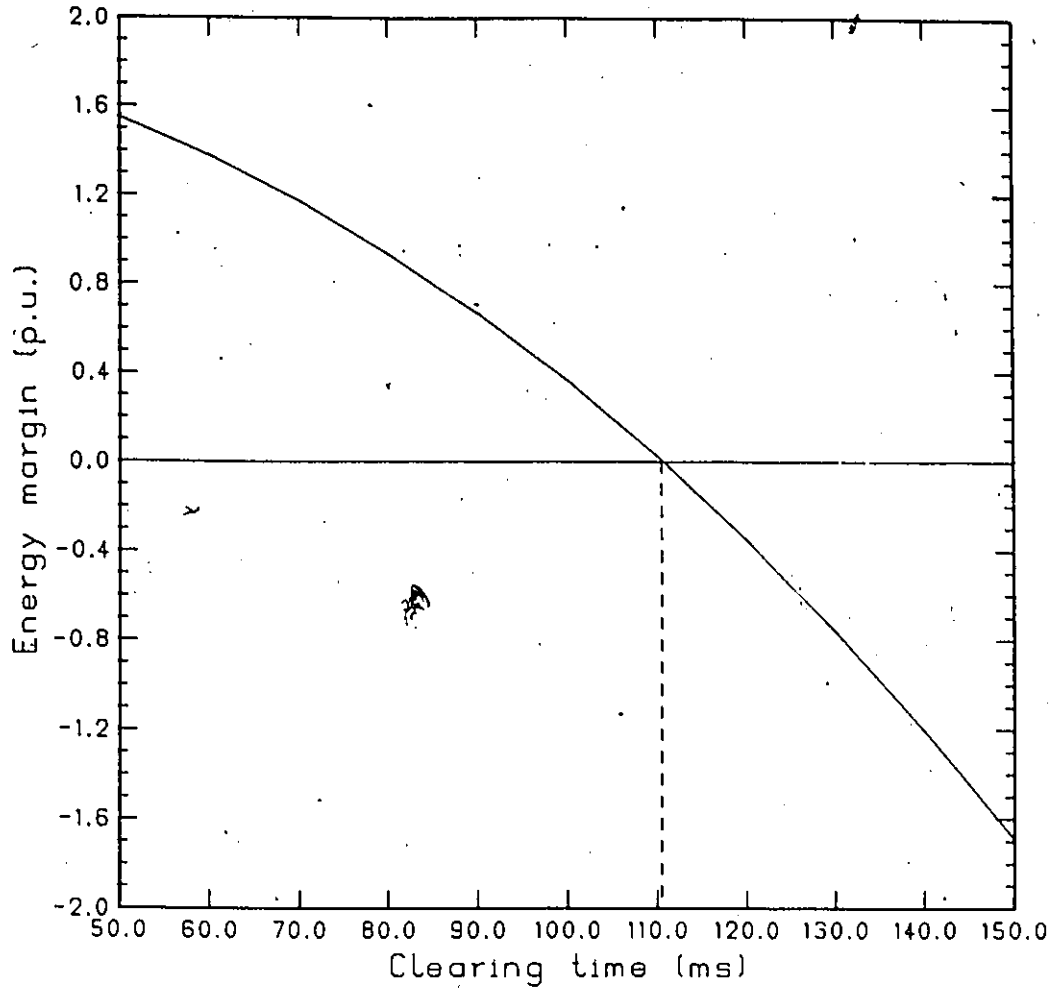


Fig. 4.6 The energy margin of the 100-generator system versus the clearing time for constant impedance loads and station B gross output = 1350 MW (critical $T_{cl} = 0.1105$ s).

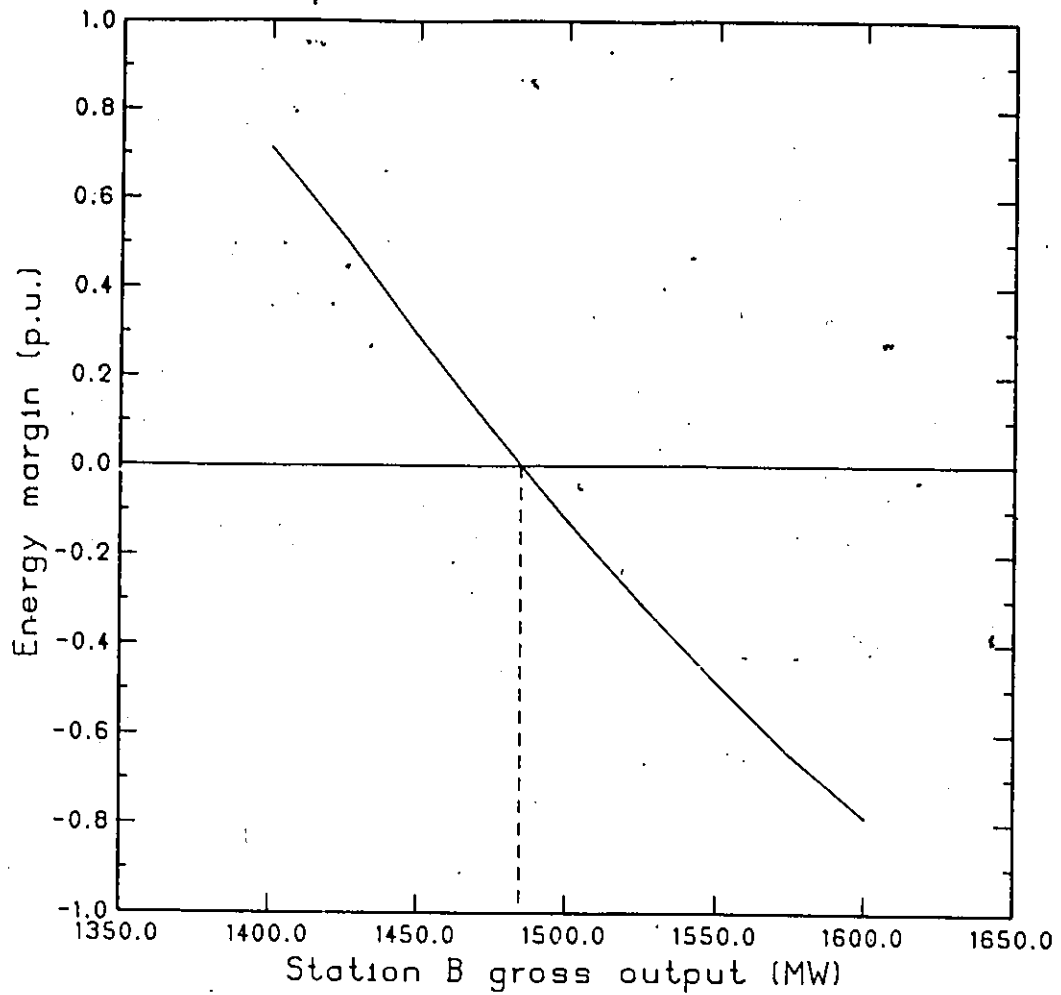


Fig. 4.7 The energy margin of the 100-generator system versus station B interface flow for constant impedance loads and clearing time = 0.068 s (stability limit = 1485.7 MW).

Description	Number
Total number of generator buses	156
Number of generators out of service	3
Number of generators in service	153
Total number of load buses	1031
Total number of buses	1184
Total number of lines	2371
Number of transformers	260
Number of phase shifters	2
Dimension of the [Y] matrix	1184
Number of non-zero elements of the [Y] matrix	5026
Dimension of the [J] matrix	2674
Number of non-zero elements of the [J] matrix	21481
Sparsity ratio	0.301 %

Table 4.9 The main data of the 156-generator system.

Description	RNF	Sparse
Reading of data	24.30	24.56
Formation and reduction of the [Y] matrix	115.58	1.89
E , θ^{cl} and ω^{cl} calculation	-----	6.41
SEP calculation	20.20	29.09
Initial point (x^0) calculation	39.82	6.87
UEP calculation	29.59	18.21
Energy margin calculation	3.44	3.03
Total CPU time	232.93 (100%)	90.06 (38.66%)

Table 4.10 The CPU times (seconds) taken by the sparse formulation and the corresponding times taken by the reduced network formulation for the 156-generator system.

The energy margin - clearing time characteristic is shown in figure 4.8 while figure 4.9 shows the energy margin - station B output characteristic. The CCT is 0.09665 second and the TSL is 3375.7 MW.

4.5 Application to a 300-Generator, 1724-Bus System

4.5.1 System Description

This system represents a base case data used for operations planning studies. The main data is given in table 4.11. The system has exactly the same fault conditions and mode of instability as those of 156-Generator system. Figure 4.10 shows the sparsity pattern of the Jacobian matrix. Table 4.11 illustrates the fact that as the power system becomes larger the sparsity ratio becomes smaller.

4.5.2 TEF Results and Stability Indices

For this fault condition, the system is stable with an energy margin of 1.4036 per unit and a normalized energy margin of 0.1729. Since the RNF technique is not applicable to that size of systems due to storage-related problems, table 4.12 shows CPU times taken by the SF technique only.

From figure 4.11, which shows the energy margin - clearing time characteristic, the CCT is 0.1146 second. Figure 4.12 shows the energy margin - station B output characteristic and the TSL is 3557.2 MW.

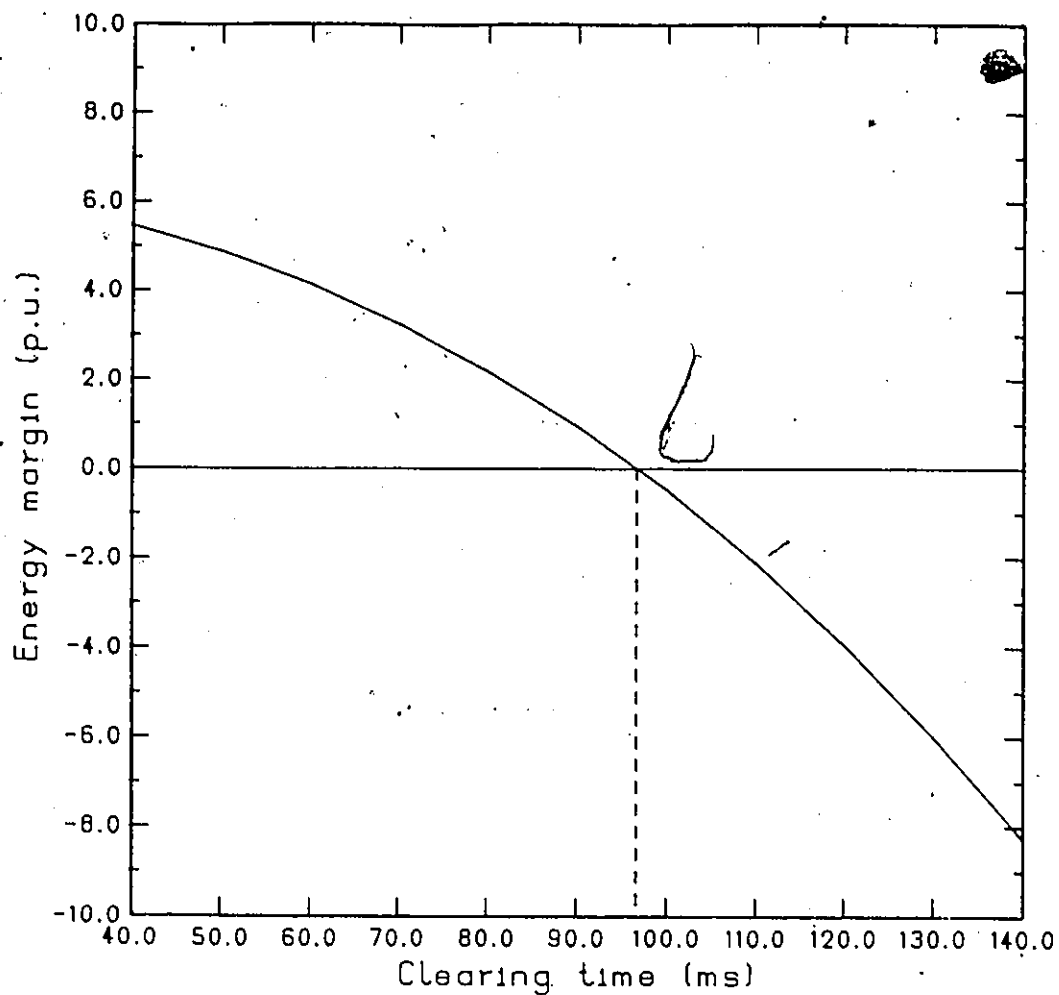


Fig. 4.8 The energy margin of the 156-generator system versus the clearing time for constant impedance loads and station N gross output = 3500 MW (critical $T_{cl} = 0.09665$ s).

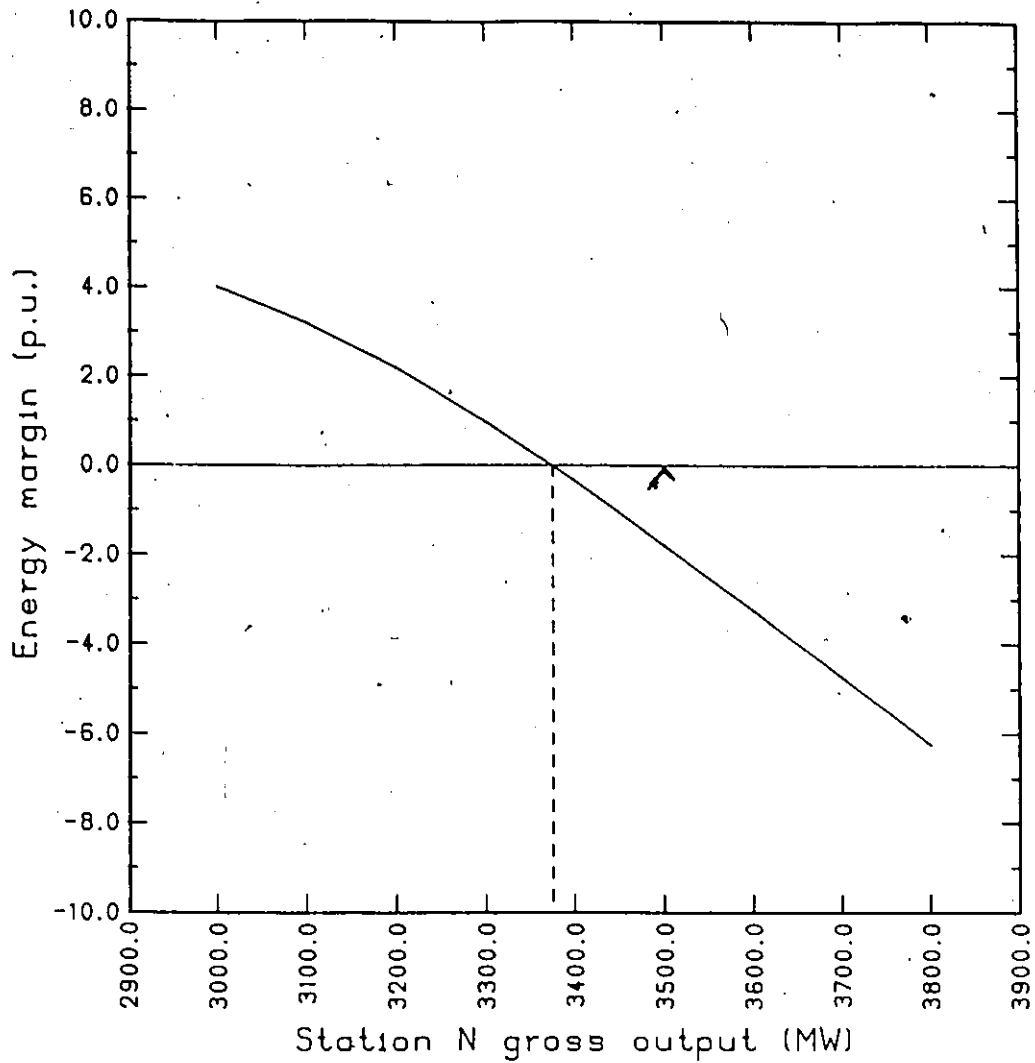


Fig. 4.9 The energy margin of the 156-generator system versus station N interface flow for constant impedance loads and clearing time = 0.108 s (stability limit = 3375.7 MW).

Description	Number
Total number of generator buses	300
Number of generators out of service	11
Number of generators in service	289
Total number of load buses	1435
Total number of buses	1724
Total number of lines	3708
Number of transformers	403
Number of phase shifters	10
Dimension of the [Y] matrix	1724
Number of non-zero elements of the [Y] matrix	8310
Dimension of the [J] matrix	4026
Number of non-zero elements of the [J] matrix	35841
Sparsity ratio	0.221 %

Table 4.11 The main data of the 300-generator system.

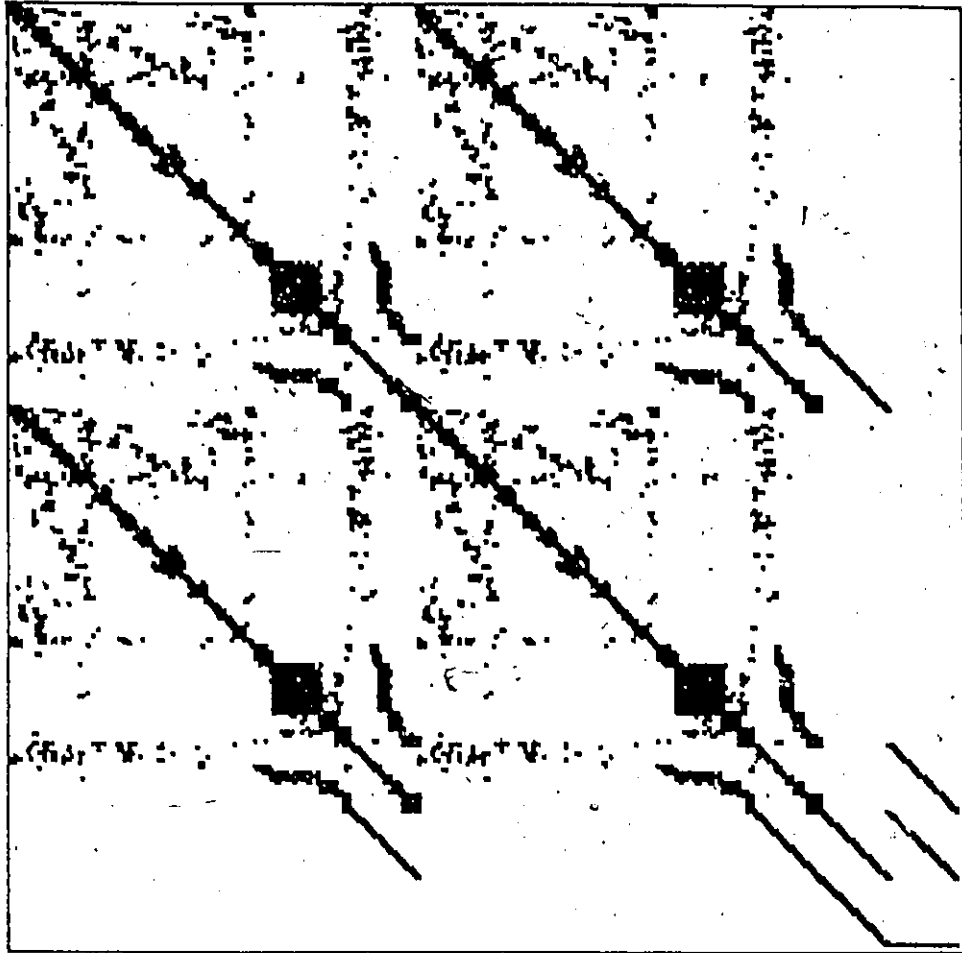


Fig. 4.10 The sparsity pattern of the Jacobian matrix for the 300-generator system (matrix of order 4026).

Description	Sparse
Reading of data	37.67
Formation of the [Y] matrix	3.07
E, θ^{cl} and ω^{cl} calculation	13.85
SEP calculation	83.63
Initial point (x^0) calculation	15.99
UEP calculation	58.20
Energy margin calculation	5.60
Total CPU time	218.01

Table 4.12 The CPU times (seconds) taken by the sparse formulation for the 300-generator system.

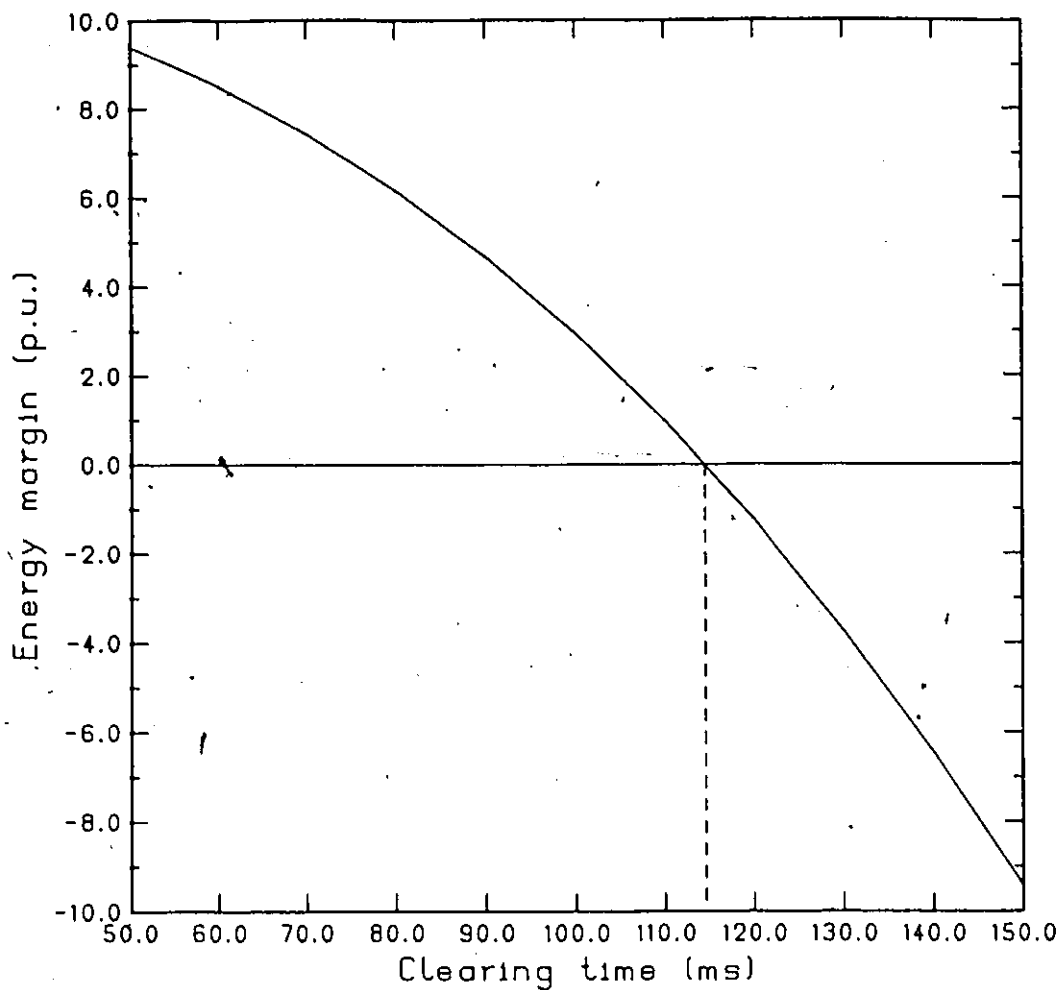


Fig. 4.11 The energy margin of the 300-generator system versus the clearing time for constant impedance loads and station N gross output = 3500 MW (critical $T_{cl} = 0.1146$ s).

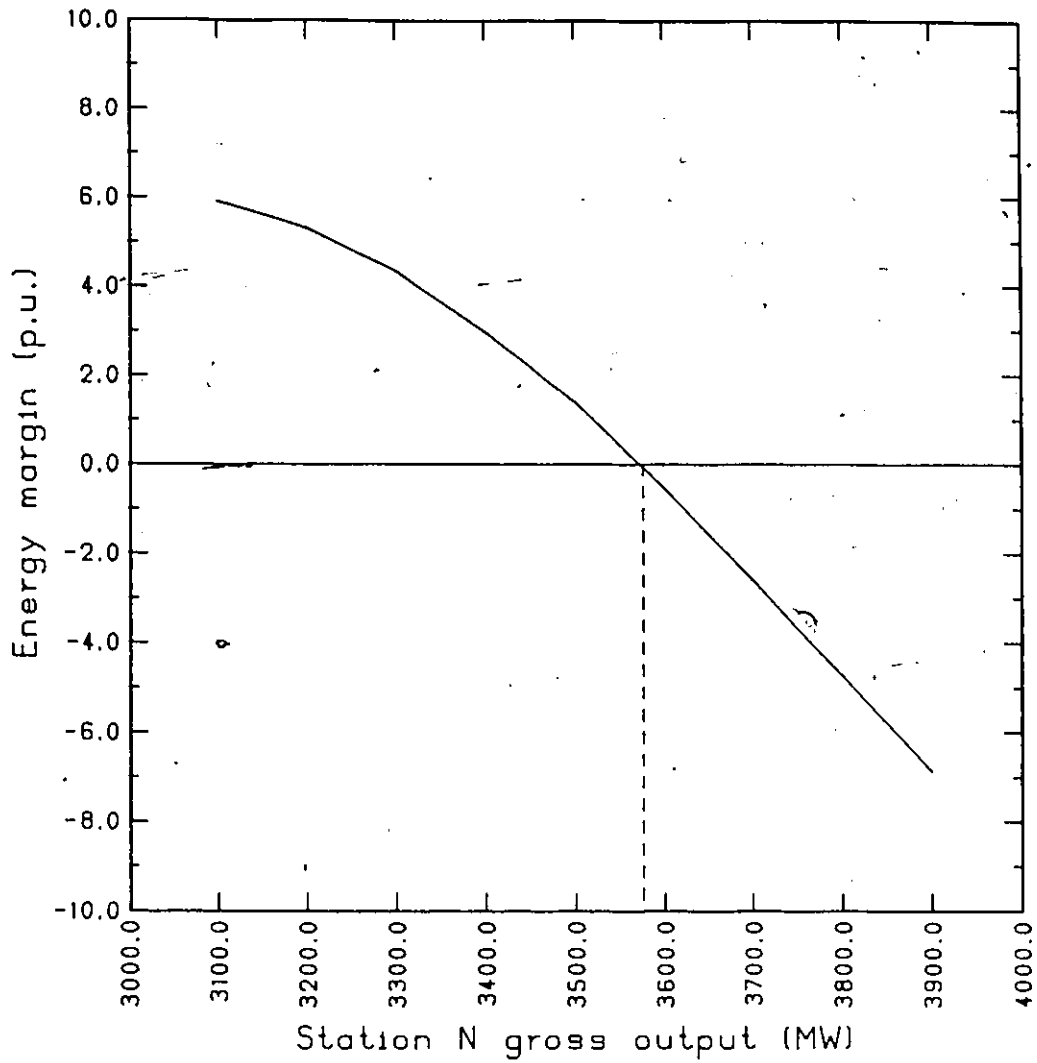


Fig. 4.12 The energy margin of the 300-generator system versus station N interface flow for constant impedance loads and clearing time = 0.108 s (stability limit = 3557.2 MW).

4.6 Application on a microcomputer

Another main advantage of the SF is that it can be performed on microcomputers [82] using systems of moderate size like the 50-generator, 145-Bus system. A multi-stage algorithm (STAFP-1) to perform transient stability calculations, i.e. to calculate the SEP, the UEP and the energy margin using a TI microcomputer (MS-DOS Operating system) is described in detail in Appendix D. An application to a 50-generator, 145-Bus system is also given. The STAFP-1 program is written in Standard Fortran 77 and can easily be transferred to most of other commercial microcomputers currently available. Further enhancements have been introduced to STAFP-1 since it has been described in [82], and the CPU times shown in Appendix D are much less than those previously shown in [82]. For this system, the total CPU time 924.1 second. Here, it is important to mention that the actual computational time is 420.7 second while the rest (503.4 second) has been consumed in I/O operations, i.e. in reading the data for a certain stage (the results produced by the previous stage) and writing the results (the data required by the next stage). It is expected, by the continuing development of microcomputers with large memory, that the time consumed in I/O operations will vanish (except for the first reading of the initial data).

4.7 Conclusion

The successful results of the sparse TEF development have made it possible to perform transient stability assessment with computation time and computer storage comparable to those of the load flow solution (by

Newton-Raphson method). The superiority of the SF technique over RNF approach regarding the computational time has been demonstrated. The SF technique also allows the TEF to be applied to very large scale power systems which are beyond the scope of RNF approach. Consequently, it enables an improved design methodology for transmission networks by including provision for modeling the network in more detail. The SF technique has been applied to four different utility systems of up to 300 generators and 1724 buses. Moreover, the SF has made the implementation of the transient stability studies on microcomputers feasible. A multi-stage algorithm (STAFP-1) for transient stability applications on microcomputers has been described and the output screens associated with each stage of the algorithm have been displayed and discussed.

CHAPTER 5

A ROBUST TECHNIQUE FOR LARGE SCALE ILL-CONDITIONED POWER SYSTEMS

5.1 Introduction

The sparse formulation of the TEF method will be considered as a powerful and useful tool only if it can be applied to practical power systems which are, in most cases, stressed (ill-conditioned) or highly stressed (very ill-conditioned). In such cases, the sparse TEF formulation should be equipped with a mathematically robust technique to solve for the UEP.

In this chapter, a robust computerized technique is described for ill-conditioned SEP and UEP solutions [86]. This technique combines a direct method of Gaussian elimination [87] and a least squares iterative method [88] to calculate the Newton step needed by the Newton-Raphson approach described in Chapter 3. The technique is applied to a 108-generator, 252-bus ill-conditioned system with loads modeled as constant impedance loads. The effect of choosing the modes of instability on the UEP calculation is also discussed. The techniques used in the RNF are described and a comparison is performed between the SF results and those obtained by the RNF method. In this comparison, the program version TEF15 (October 1986) of the RNF is used. The superiority of the sparse formulation to handle large-scale ill-conditioned systems is emphasized.

5.2 Physical Aspects

The analysis of stressed power system is often characterized by ill-conditioned computations. Stressed systems are those of heavily loaded weak transmission. Numerical problems could also arise if generators with very large inertias exist close to the disturbance. Such large inertias may be created by equivalencing techniques. The problem of ill-conditioning is accentuated by the fact that the Potential Energy Boundary Surface (PEBS) around a UEP may be very steep in certain directions and very shallow in other directions. This characteristic makes convergence to the desired UEP a formidable numerical task.

Numerically, this can be explained as follows. Recalling equation (3.11), after dropping " Δ " and " k " (the iteration number):

$$J \underline{x} = \underline{b} \quad (5.1)$$

which represents the system equations in the perturbed form. The solution \underline{x} of the equation (5.1) is not the required UEP but rather it represents the Newton step in a certain iteration to get the UEP. If the system is ill-conditioned, i.e. if the Jacobian is an ill-conditioned matrix, the solution \underline{x} is very sensitive to any small change in either the elements of J or the elements of \underline{b} . Consequently, to get an accurate solution, both J and \underline{b} must be evaluated to a very high degree of accuracy. Depending upon the system and the computer, the required degree of accuracy may not be attainable. J , in this case, is said to have a high condition number.

The condition number (K) is defined as [89]:

$$K(J) = \|J\| \cdot \|J^{-1}\| = \frac{\lambda_{\max}}{\lambda_{\min}} \quad (5.2)$$

where $\| \cdot \|$ represents the Frobenius norm of the matrix and λ_{\max} and λ_{\min} are the maximum and minimum eigenvalues of J respectively. To examine the range of K for power systems, let us consider the 11-generator, 55-bus system which will be described in detail in Chapter 6. The Jacobian matrix is of order 132, λ_{\max} and λ_{\min} are 17447.814453 and 0.057448, respectively and K is 303715.44. This value of K is reasonable and the Jacobian matrix of this system is said to be well-conditioned. In general, we expect higher condition numbers (of the order of 10^8 or higher) for ill-conditioned systems. Another property of the ill-conditioned system is that the solution vector x (the Newton step) at each iteration is very large. This can be explained by the tendency of the small eigenvalue(s) to pull the solution towards infinity (the system, in this case, is near singularity).

5.3 Techniques Used in the RNF for Ill-Conditioned Systems

Because the RNF uses dense (non-sparse) matrices, there are many methods available in the literature to solve the problem of the ill-conditioning. Two methods are now in use in the practical applications, namely, the Davidon Fletcher Powell (DFP) method [90-92] and the Corrected Gauss Newton (CGN) method [93].

5.3.1 The Davidon Fletcher Powell Method

This method combines some of the more desirable features of the steepest descent and the Newton-Raphson method. It is an extension of Davidon's variable metric method [92]. The DFP method has been used for systems of a small dimension and found to be reliable and efficient. However, as the system size increases, the method becomes computationally inefficient and unreliable.

5.3.2 The Corrected Gauss Newton Method

After a careful search of the various methods available to solve the minimization problem and in consideration of the practical system sizes, the CGN method was selected as a suitable alternative to the DFP method. This is a modification of the Gauss-Newton method of solving the nonlinear least squares problem. The method avoids the deficiencies in the Gauss-Newton method by improving, when necessary, the approximation of the Hessian matrix (the second derivatives of the system equations) by removing the singularity of the Jacobian matrix using a singular value decomposition technique. The CGN method is safeguarded, robust and reliable. It will be used for comparisons with the proposed technique.

5.4 The Proposed Technique

A robust iterative algorithm to solve the problem of ill-conditioning should:

- (a) use a starting point that is as close as possible to the desired UEP, and

(b) prevent the solution, during iterations, from diverging.

The first point is of no concern because the ray point, described in section 3.4 of Chapter 3, can be used as a good starting point which is close enough to the UEP. In addition, the initial user-defined candidate for the mode of instability should be chosen carefully to ensure that the correct UEP is achieved. Inaccurate choice of the candidate advanced machines may also lead to extra computational time in the UEP evaluation.

For the second point, if a direct method of Gaussian elimination such as the MA28 routine [87] is used in each iteration to calculate the Newton step (for ill-conditioned system), the solution will likely diverge. Hence we need a more robust method to solve the system of linear equations (5.1). The method we choose should be an iterative method. It should regulate the Newton step to moderate values. One technique to accomplish this is by suppressing the effect of the small eigenvalue(s). This will result in an approximate solution corresponding to a number of subiterations specified by the user. Examples of such methods are the following.

- (a) The implicit deflation method based on an iterative refinement procedure given by Stewart [94].
- (b) The conjugate-gradient method for least squares systems given by Hestenes and Stiefel [95].
- (c) The least squares method based on the QR transformation given by Paige and Saunders [96].

The first method is based on the idea of projecting the solution vector \underline{x} onto a space orthogonal to the right or left null vectors corresponding to the smallest eigenvalues of the Jacobian matrix, J . Those vectors can be obtained by a variant of the inverse power method [97]. Then, using some form of the iterative refinement procedure [98,99], an approximate solution (called the deflated solution) can be calculated. This method has been implemented and applied to an ill-conditioned power system, but it did not work appropriately and a divergence occurred. The reason (according to our discussion with the author of [94]) is that this method is applicable only to systems which have one singular value that is substantially smaller than the others. It was found that the system which has been tried had more than one small singular value. Due to this limitation, this method will not be used.

The second and the third methods are described as algorithms "CGLS" and "LSQR" respectively in [96]. They have similar qualitative properties, but the latter is likely to obtain a more accurate solution in fewer iterations if the matrix J of equation (5.1) is moderately or severely ill-conditioned. Therefore, it will be adopted in the proposed technique.

5.4.1 The Least Squares Method

The algorithm LSQR solves the following damped least squares problem:

$$\text{minimize} \quad \left\| \begin{bmatrix} J \\ \lambda I \end{bmatrix} \underline{x} - \begin{bmatrix} \underline{b} \\ 0 \end{bmatrix} \right\|_2 \quad (5.3)$$

where λ is a damping factor, specified by the user, to prevent the small singular values from swamping the solution and causing numerical instability. Notice that if λ is set to zero, the problem will lead to the regular linear least squares problem. The algorithm can be summarized in the following two main steps.

- (1) Reduce the matrix J to a lower bidiagonal matrix B_k of order $(k+1, k)$, where k is the number of subiterations specified by the user, using the Golub and Kahan (GK) algorithm [100]. Then the k^{th} approximation to the solution \underline{x} is defined as :

$$\underline{x}_k = V_k \underline{y}_k \quad (5.4)$$

where V_k is the transformation matrix used in the GK algorithm and \underline{y}_k solves the subproblem:

$$\text{minimize} \quad \left\| \begin{bmatrix} B_k \\ \lambda I \end{bmatrix} \underline{y}_k - \begin{bmatrix} \beta \underline{e}_1 \\ 0 \end{bmatrix} \right\|_2 \quad (5.5)$$

where β is the Euclidean norm of \underline{b} and \underline{e}_1 is the 1st principle unit vector.

- (2) Solve the subproblem (5.5) for \underline{y} using the QR orthogonal transformation. Then, solve for \underline{x} using equation (5.4).

The QR factorization is an iterative process. Therefore, a termination criterion is needed. The following termination criterion is formulated in terms of three dimensionless quantities (ATOL, CONDLIM and ITERLIM) specified by the user.

$$(a) \text{ Stop if } \frac{\|J \underline{r}_k\|}{\|J\| \|\underline{r}_k\|} < \text{ATOL} \quad (5.6)$$

where \underline{r}_k represents the residual vector at subiteration k

$$(b) \text{ Stop if } K(J) > \text{CONDLIM} \quad (5.7)$$

$$(c) \text{ Stop if } \text{No. of subiterations} > \text{ITERLIM} \quad (5.8)$$

Practical values for the previous parameters are:

$$(a) \text{ ATOL} = 10^{-6}, \quad (b) \text{ CONDLIM} = 10^{+6} \quad \text{and} \quad (c) \text{ ITERLIM} = n$$

where n represents the number of the system equations and is given by

$$n = 2 N_d + 4 N_g \quad (5.9)$$

Although LSQR is a lengthy process and may consume a considerable computational time, it is a powerful algorithm for ill-conditioned systems. On the other hand, direct solution routines such as MA28 are

usually very fast but are not suitable for ill-conditioned cases. Therefore, an optimal technique can be obtained by using both LSQR and MA28 alternatively in the main iterations of the Newton-Raphson procedure.

5.4.2 Fibonacci Search

After calculating the Newton step (using LSQR or MA28) and before updating the variables, an optimal step that minimizes the system mismatch is calculated using a one-dimensional optimization method. The cubic interpolation [85] suggested in Chapter 3 is conditional on the Newton step being calculated exactly, i.e. using a direct method (like the MA28 routine). Another effective method, called the Fibonacci direct elimination method [101-103], can be used with LSQR. The method is based on the Fibonacci sequence of numbers, defined by:

$$N_0 = N_1 = 1$$

$$N_i = N_{i-1} + N_{i-2}, \quad i=2,3,\dots$$

Assume that we obtained an initial interval (x_l^1, x_u^1) which contains the minimum mismatch (the required point). At the j^{th} iteration of the Fibonacci search using m function evaluations ($m \geq 2$ specified by the user) we have:

$$x_a^j = \frac{N_{m-1-j}}{N_{m+1-j}} I^j + x_l^j, \quad j=1,2,\dots, m-1 \quad (5.11)$$

$$x_b^j = \frac{N_{m-j}}{N_{m+1-j}} I^j + x_g^j, \quad j=1,2,\dots, m-1 \quad (5.12)$$

$$\text{where } I^j = x_u^j - x_g^j \quad (5.13)$$

is the interval of the uncertainty at the start of the j^{th} iteration. Observe that each subiteration except the first actually requires only one function evaluation (using either x_a^j or x_b^j) due to symmetry. The interval of the uncertainty after j iterations is

$$I^{j+1} = x_u^j - x_a^j = x_b^j - x_g^j \quad (5.14)$$

Using equations (5.11), (5.12), (5.13) and (5.14), we can show that the total reduction ratio of the interval of the uncertainty after $m-1$ iterations is equal to N_m . For example, for $m=11$, the reduction ratio is equal to 144.

5.4.3 Algorithm

The proposed technique has the following steps.

- (1) Calculate the starting point (the ray point described in section 3.4 of Chapter 3).
- (2) Evaluate the initial mismatch F_0 using

$$F_0 = \sum_{i=1}^n f_i^2 \quad (5.15)$$

where n is given by equation (5.9) and f_i represents the left hand side of equation i of the system equations.

- (3) Calculate the Newton step using LSQR, calculate the optimal step using the Fibonacci search technique: update the variables.
- (4) Evaluate the mismatch F : check if F is less than the required tolerance.
- (5) Calculate the Newton step using MA28, calculate the optimal step using the Fibonacci search or the cubic interpolation and update the variables.
- (6) Evaluate the mismatch F : check if F is less than the required tolerance.
- (7) Using a parameter NILL (specified by the user according to the severity of the system ill-conditioning, e.g. for moderately ill-conditioned systems specify $NILL=5$ and for severely ill-conditioned systems specify $NILL>10$), check:
 - (i) if $F > F_0 / NILL$ go to step 3.
 - (ii) if $F < F_0 / NILL$ go to step 5.

5.5 Application to a 108-Generator, 252-Bus Ill-Conditioned System

5.5.1 System Description

This system represents another reduced version of a practical, highly stressed power network. Table 5.1 shows the main data of this system. A 3-phase fault is applied at bus 53. The fault is cleared at

Description	Number
Total number of generator buses	108
Number of generators out of service	0
Number of generators in service	108
Total number of load buses	144
Total number of buses	252
Total number of lines	1296
Number of transformers	0
Number of phase shifters	0
Dimension of the [Y] matrix	252
Number of non-zero elements of the [Y] matrix	2016
Dimension of the [J] matrix	720
Number of non-zero elements of the [J] matrix	9036
Sparsity ratio	1.743 %

Table 5.1 The main data of the 108-generator ill-conditioned system.

0.04 second by tripping one line connected to the faulted bus. The estimated mode of instability is that 10 machines (those connected to buses 61, 88, 95, 96, 100, 217, 222, 223, 224 and 225) are the advanced machines.

5.5.2 TEF Results

For this system, the detailed results corresponding to different steps of the algorithm described in Chapter 3 are presented. Table 5.2 shows the clearing angles and speeds in the COA frame of reference for the fault conditions described in the previous section. The ray point (the point of maximum potential energy) is used as an initial value for the UEP. Then, the proposed algorithm is applied using the following parameters:

- (a) ATOL = 10^{-6}
- (b) CONDLIM = 10^{+6}
- (c) ITERLIM = n = 720
- (d) NILL = 20

The UEP and SEP are given in table 5.3 and, as shown, the estimated mode of instability (10 machines are advanced) has led to the actual mode in which 19 machines are advanced. This mode is called an interarea mode because the system is split into two subsystems (two areas) in each of which machines are running together in synchronism. Note that the modes described in the different applications of Chapter 4 are called local modes because only the machines near the disturbance are advanced.

Bus	θ_{cl}	ω_{cl}	Bus	θ_{cl}	ω_{cl}	Bus	θ_{cl}	ω_{cl}
1	-66.459	-0.1464	118	0.132	-0.1095	177	11.413	-0.0738
2	-74.329	-0.0837	122	-8.033	-0.2586	178	17.671	-0.0738
8	-35.126	-0.1224	124	-3.579	-0.1510	179	-25.720	-0.0738
9	-43.228	-0.1378	125	-1.187	-0.0500	180	27.671	-0.0738
11	5.983	0.0011	127	-8.652	-0.3714	181	3.101	-0.0737
12	10.584	0.0878	128	9.796	0.4473	182	9.970	-0.0738
17	-8.064	-0.0754	129	4.484	0.0551	187	21.267	0.0340
18	-8.915	-0.0782	131	2.381	0.1630	188	22.331	0.0309
25	-75.930	-0.0921	132	-12.603	-0.3353	217	34.990	1.0441
26	-76.376	-0.0864	134	-27.577	-0.1195	222	43.759	0.7310
27	-3.776	-0.0648	147	-4.377	-0.0661	223	34.359	0.4638
37	-14.197	-0.0833	148	-58.584	-0.0793	224	24.504	1.6960
39	-62.412	-0.0845	149	-60.738	-0.0790	225	23.970	1.3694
40	-56.257	-0.0770	150	-50.859	-0.0752	227	6.793	-0.0107
41	-66.700	-0.0779	151	-80.543	-0.0930	229	-96.413	-0.0829
43	-63.181	-0.1074	153	-29.986	-0.0736	230	14.030	0.1496
44	-47.595	-0.0758	154	-70.693	-0.0744	231	-31.301	-0.1496
45	-65.926	-0.0789	155	-48.460	-0.0740	232	-22.791	-0.1045
46	-63.279	-0.0744	159	-5.028	-0.0738	234	-19.717	-0.0801
47	-46.723	-0.0743	160	12.917	-0.0738	235	-64.703	-0.1685
58	30.396	1.4286	161	-6.497	-0.0733	237	14.462	0.0185
61	46.739	0.6486	162	28.014	-0.0738	238	-48.419	-0.1185
67	13.787	0.2378	163	35.647	-0.0738	239	0.956	0.0394
78	14.787	0.2911	164	57.384	-0.0738	240	14.256	0.1032
82	12.671	0.4640	165	13.609	-0.0738	241	2.091	-0.0727
88	47.152	0.6194	166	-4.068	-0.0738	242	-27.578	-0.0737
95	22.107	0.6104	167	-2.839	-0.0738	243	3.673	-0.0589
96	35.892	1.0290	168	4.657	-0.0704	244	28.339	-0.0655
100	26.226	0.6120	169	4.741	-0.0714	245	-31.561	-0.0747
102	25.756	1.6066	170	-3.128	-0.0437	246	-12.604	-0.0736
105	32.570	1.1218	171	3.564	-0.0732	247	5.157	0.0470
107	27.359	0.5543	172	7.353	-0.0701	248	5.839	-0.0116
108	10.895	0.3369	173	11.218	-0.0640	249	20.144	0.0080
114	24.160	0.6066	174	30.132	-0.0726	250	2.283	-0.0627
115	25.861	0.4183	175	16.263	-0.0735	251	7.734	-0.0597
117	11.810	0.2796	176	4.063	-0.0733	252	-16.412	-0.0503

Table 5.2 The clearing angles and speeds in COA frame
of reference for the 108-generator ill-conditioned system,
clearing time = 0.04 second.

Bus	SEP	UEP	Bus	SEP	UEP	Bus	SEP	UEP
1	-65.924	-52.398	118	1.391	40.538	177	11.157	-1.762
2	-73.961	-64.062	122	-6.615	32.211	178	17.400	3.911
8	-34.295	-2.889	124	-2.275	36.768	179	-26.079	-43.276
9	-42.511	-17.676	125	-0.001	38.882	180	27.410	14.353
11	6.599	32.506	127	-7.101	31.870	181	2.947	-5.635
12	11.351	46.300	128	10.432	49.774	182	9.775	-0.579
17	-7.123	36.344	129	5.554	44.575	187	22.338	87.025
18	-7.976	34.897	131	3.323	42.152	188	23.442	92.595
25	-75.557	-65.928	132	-11.110	27.159	217	35.013	79.015
26	-75.999	-65.934	134	-26.389	9.553	222	44.105	83.928
27	-2.836	41.531	147	-3.892	13.378	223	35.022	75.790
37	-13.238	25.513	148	-58.402	-54.657	224	23.742	64.179
39	-61.883	-44.688	149	-60.938	-56.211	225	23.584	64.034
40	-55.742	-38.681	150	-50.741	-48.990	227	7.243	22.975
41	-66.163	-48.064	151	-80.243	-73.233	229	-95.991	-83.691
43	-62.562	-42.939	153	-29.985	-32.363	230	14.798	53.659
44	-47.063	-29.090	154	-70.549	-67.968	231	-30.185	17.611
45	-65.389	-47.452	155	-48.348	-46.773	232	-21.846	18.933
46	-62.770	-45.735	159	-5.234	-16.043	234	-18.570	35.619
47	-46.208	-28.868	160	12.638	-1.208	235	-63.989	-43.141
58	29.894	69.188	161	-6.608	-13.743	237	15.596	76.151
61	47.184	87.046	162	27.685	11.816	238	-47.774	-26.959
67	14.174	38.010	163	35.324	19.697	239	2.035	59.833
78	15.426	53.016	164	57.032	40.248	240	15.054	51.548
82	13.139	51.132	165	13.287	-2.299	241	2.146	1.965
88	47.634	87.544	166	-4.392	-20.102	242	-27.474	-26.084
95	22.583	62.806	167	-3.184	-19.768	243	3.855	9.707
96	35.923	76.963	168	4.658	2.313	244	28.534	35.303
100	26.731	75.149	169	4.732	1.952	245	-31.422	-28.819
102	25.124	68.871	170	-2.986	0.636	246	-12.583	-14.200
105	32.503	76.481	171	3.450	-3.729	247	5.536	21.171
107	27.921	69.558	172	7.303	2.860	248	6.073	14.320
108	11.698	53.232	173	11.201	8.191	249	20.596	37.550
114	24.667	68.708	174	30.079	25.430	250	2.410	4.575
115	26.583	70.516	175	16.165	9.638	251	7.774	7.033
117	12.637	52.134	176	3.992	-1.169	252	-16.119	-7.664

Table 5.3 The SEP and UEP for the 108-generator

ill-conditioned system.

The final results including the values of different types of energy, the energy margin and the normalized energy margin, are shown in table 5.4. The system is unstable with an energy margin of -0.3374 perunit and normalized energy margin of -0.1768 . Table 5.5 gives the detailed CPU times taken by the SF technique and the corresponding times taken by the RNF technique (the clearing angles and speeds have been calculated, in both techniques, using constant accelerations). As shown, the CPU time has been reduced to 31.03 % of that taken by the RNF technique .

It has been found that (for this system) termination criteria (a) and (b) were not used. Only the iterations limit given by (c) was in effect. Also, it has been found that ITERLIM and NILL have a strong effect on the number of times that LSQR, whose computational time is dominant, is used, i.e. on the total CPU taken by the sparse formulation. Table 5.6 shows the effect of choosing ITERLIM = 1000 and NILL=10 on the convergence behaviour of the UEP and consequently on the total computational time taken. In this case, LSQR has been used just once and the total CPU time has been reduced further to 248.93 seconds. This represents 23.84 % of the time taken by the RNF.

5.5.3 The Effect of the Mode of Instability on the Speed of Calculation

Three different choices of the candidate advanced machines for determining the mode of instability are tried to show the effect of the choice of these candidates on the speed of the calculation (the number of iterations needed for the UEP calculation). These choices are

Description	Value (p.u.)
The corrected kinetic energy	1.9087
The magnetic and dissipation energy at UEP	-169.71
The positional energy at UEP	171.28
The total energy at UEP	1.5712
The energy margin with K.E. correction	-0.3374
The Normalized energy margin with K.E. correction	-0.1768

Table 5.4 The final results of the 108-generator
ill-conditioned system.

Description	RNF	Sparse
Reading of data	11.60	11.42
Formation and reduction of [Y] matrix	80.25	0.42
E , g^{cl} and w^{cl} calculation	—	2.88
SEP calculation	8.90	9.24
Initial point (x^0) calculation	28.67	3.17
UEP Calculation	912.65	294.81
Energy margin calculation	1.90	1.97
Total CPU time	1043.97 (100%)	323.91 (31.03%)

Table 5.5 The CPU times (seconds) taken by the sparse formulation and the corresponding times taken by the RNF for the 108-generator ill-conditioned system.

Iteration No.	ITERLIM=1000, NILL=10	ITERLIM=720, NILL=20
0	1016.49	1016.49
1	77.653 LSQR	69.481 LSQR
2	59.796 MA28	60.664 MA28
3	53.490 MA28	30.291 LSQR
4	50.104 MA28	24.088 MA28
5	48.171 MA28	20.707 MA28
6	44.299 MA28	17.717 MA28
7	37.107 MA28	13.158 MA28
8	20.890 MA28	6.7356 MA28
9	7.2936 MA28	3.1508 MA28
10	1.7370 MA28	0.7769 MA28
11	0.0850 MA28	0.0715 MA28
12	0.0004 MA28	0.0001 MA28
CPU for UEP (sec.)	219.83	294.81
Total CPU (sec.)	248.93	323.91
Total CPU %	23.84 %	31.03 %

Table 5.6 The total mismatch, the method used in each iteration and total CPU time for different values of ITERLIM and NILL to calculate the UEP for the 108-generator ill-conditioned system.

shown in table 5.7. For this purpose, we use $ITERLIM=1000$ and $NILL=5$. Table 5.8 gives the number of iterations needed to calculate the UEP in each case, and the corresponding computational time. It should be noted that in all cases convergence was attained to the correct UEP. It is clear that as the estimated mode of instability (the candidate advanced machines) comes closer to the correct mode, the number of iterations needed to calculate the UEP decreases and more computational time can be saved. It should be noticed that the CPU time is not proportional to the number of iterations in each case because all three cases used LSQR (for which the CPU is dominant) equal numbers of times (one time in this case). The saving in time occurred only for those iterations for which MA28 was used.

5.7 Conclusion

A very robust technique to compute the SEP and/or UEP for large-scale ill-conditioned power systems has been described. This technique combines the direct method of Gaussian elimination and the least squares method. The technique has been applied to a 108-generator, 252-bus ill-conditioned system with loads modeled as constant impedance loads. The effect of the proper choice of the mode of instability on the computational time taken in the UEP calculation has been demonstrated. The various techniques used in the RNF have also been discussed. The comparison between the computational time taken by both the SF and RNF has demonstrated the superiority of the sparse formulation to handle large-scale ill-conditioned systems.

Mode 1 (11 machines) Machine No.	Mode 2 (16 machines) Machine No.	Mode 3 (19 machines) Machine No.
58	58	58
61	61	61
88	88	88
95	95	95
96	96	96
100	100	100
217	102	102
222	105	105
223	107	107
224	114	114
225	115	115
	217	187
	222	188
	223	217
	224	222
	225	223
		224
		225

Table 5.7 The three modes of instability used to calculate the UEP for the 108-generator ill-conditioned system.

Iteration No.	Mode 1 (13 iterations) F_T , method	Mode 2 (8 iterations) F_T , method	Mode 3 (6 iterations) F_T , method
0	1016.49	961.01	995.34
1	77.653 LSQR	137.56 LSQR	108.37 LSQR
2	59.796 MA28	83.628 MA28	102.34 MA28
3	53.490 MA28	65.858 MA28	34.068 MA28
4	50.104 MA28	44.892 MA28	3.1627 MA28
5	48.171 MA28	8.4260 MA28	0.1131 MA28
6	44.299 MA28	1.1197 MA28	0.0002 MA28
7	37.107 MA28	0.0193 MA28	
8	20.890 MA28	0.0000 MA28	
9	7.2936 MA28		
10	1.7370 MA28		
11	0.0850 MA28		
12	0.0004 MA28		
CPU (sec.)	219.83	210.69	206.23

Table 5.8 The total mismatch, the method used in each iteration and CPU time consumed in the UEP calculation for different modes of instability for the 108-generator ill-conditioned system.

CHAPTER 6

SPARSE TEF METHOD INCLUDING LOAD MODELS

6.1 Introduction

This chapter discusses the inclusion of load modeling in the TEF, which is the second main advantage of the Sparse Formulation (SF). To apply the Reduced Network Formulation (RNF) of the TEF, all system loads are modeled in the conventional approaches as constant impedance loads in order to be able to reduce the network to the internal nodes of the generators. In practice, most industrial loads consist of induction motor type loads. They represent the majority of system loads, in the nature of constant power type. Neglecting these types of load modeling in transient stability analysis is a conservative feature of the RNF. In the SF, the loads can be represented more accurately (constant impedance, constant power or any combination thereof) [104]. This, as will be shown in this chapter, gives correct and accurate results (matching with those of the time domain solutions). The scope of this chapter can be summarized as follows :

- (i) Applications to a 11-generator, 55-bus system which show :
 - (a) The effect of load modeling on the critical clearing time with a comparison with that obtained by the time domain.
 - (b) The effect of load modeling on the energy margin.
- (ii) Applications to a 50-generator, 145-bus system which show :
 - (a) The effect of load modeling on the stability limit with

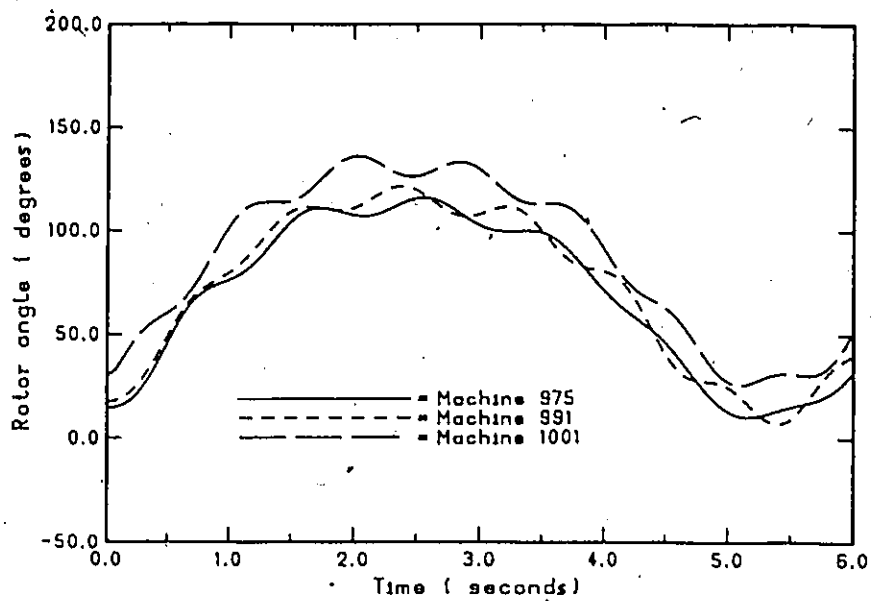
a comparison with that obtained by the time domain solutions.

6.2 Applications to a 11-Generator, 55-Bus System

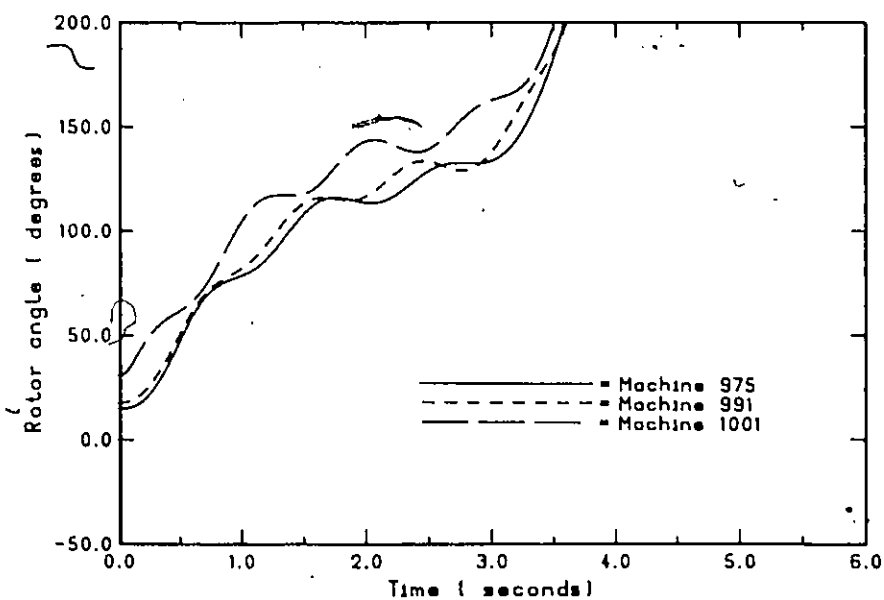
The SF is applied through the algorithm described in Chapter 3 to a 11-generator system (a reduced version of a practical system) using different load models. In this system, a three phase fault occurs at bus number 226 (Station B) and the fault is cleared in 0.068 second by tripping out four lines connected to the faulted bus. The mode of instability for this specified fault is that Station B machines, those which are connected to buses 975, 991 and 1001, are the advanced machines. Two important effects of load modeling are discussed in the following sections.

6.2.1 The Effect of Load Modeling on the Critical Clearing Time

The critical clearing time is the clearing time before which if the fault is cleared the system is stable and after which if the fault is cleared the system is unstable. The critical clearing time is calculated using both time domain and the SF of the TEF method for three main load models; 100% constant impedance, 50% constant impedance + 50% constant power and 100% constant power load models. This comparison will be offered as a proof of the validity of the SF for different load models applications. To calculate the clearing angles and speeds needed by the SF, the Heun's algorithm [82] is used with time step of 0.01 second. This yields sufficient accuracy (as described in Chapter 4). For 100% constant impedance load models, figure 6.1 shows the rotor angles.



(a) Critically stable case, $T_{cl} = 0.0986$ s.



(b) Critically unstable case, $T_{cl} = 0.0988$ s.

Fig. 6.1 The rotor angles of the advanced machines in time domain for 100 % constant impedance load models for the 11-generator system.

of the advanced machines in the time domain for both critically stable and unstable cases. The clearing times are 0.0986 and 0.0988 second respectively, i.e. the critical clearing time is 0.0987 second. Figure 6.2 shows the energy margin versus clearing time using the SF for the same load model. As shown, the critical clearing time (time corresponding to zero energy margin) is 0.0956 second with a difference of 0.0031 second (3.14 %). For 50% constant impedance + 50% constant power load models, figure 6.3 shows the time domain results from which the critical clearing time is 0.1417 second. From figure 6.4, the critical clearing time using the SF is 0.1347 second with a difference of 0.0070 second (4.94 %). For 100% constant power load models, the difference is 0.0169 second (8.44 %). Figures 6.5 and 6.6 show the results obtained from both methods. Figure 6.7 shows the critical clearing times for other load models using both time domain and the SF while figure 6.8 gives the percentage relative errors. As shown, the results of the SF match with those of the time domain with acceptable errors. From the previous results, we conclude that neglecting load modeling may lead to a significant relative error (more than 45 % in the previous case) in the critical clearing time calculation.

Now, we present some other useful results. Figures 6.9 and 6.10 show the effect of changing the clearing time on the energy at the UEP and the energy at clearing respectively for different load models. As the clearing time increases, the energy at the UEP decreases while that at clearing increases. This can be explained very simply using the well known Equal Area Criterion (EAC) [6]. Figure 6.11 shows the EAC

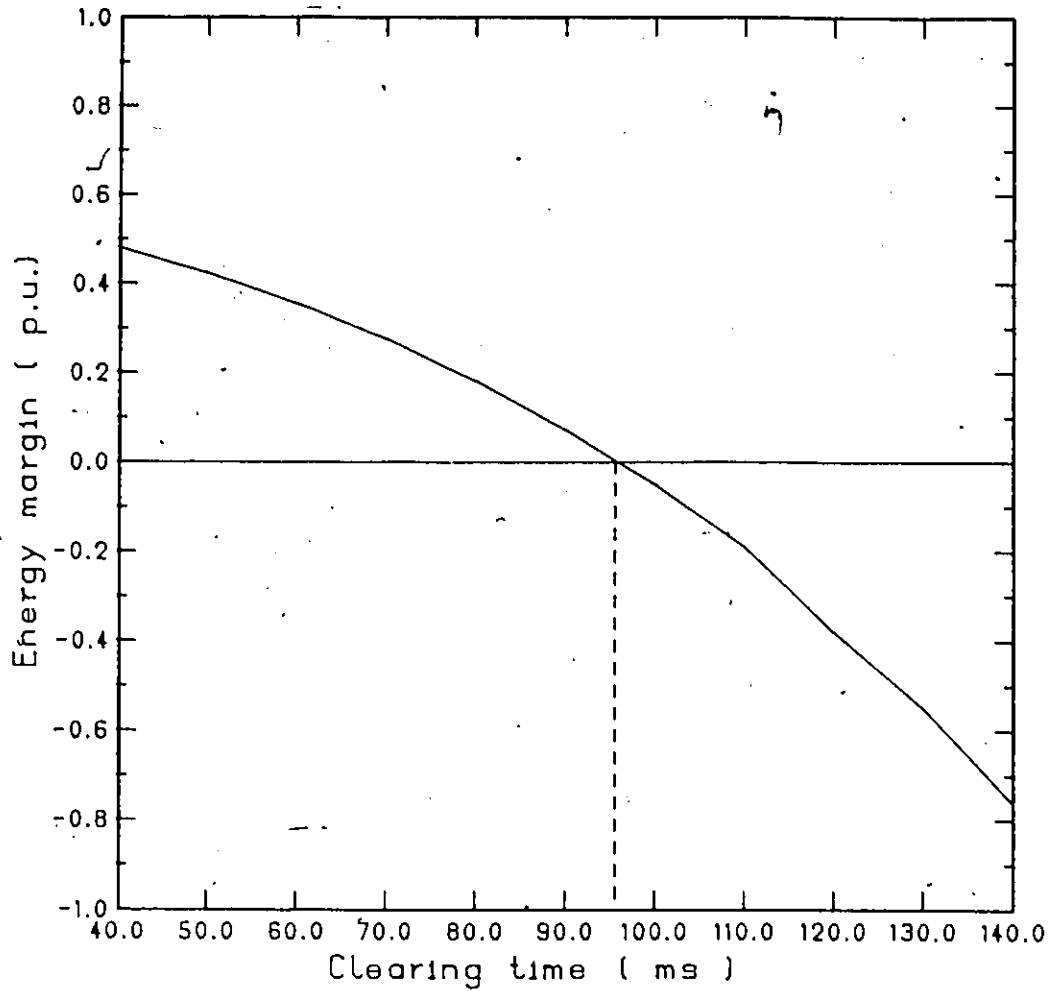
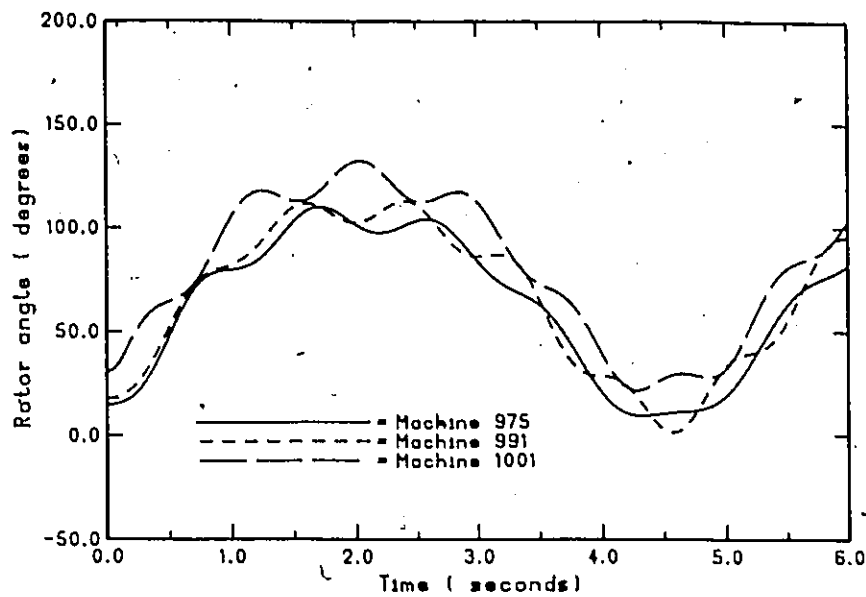
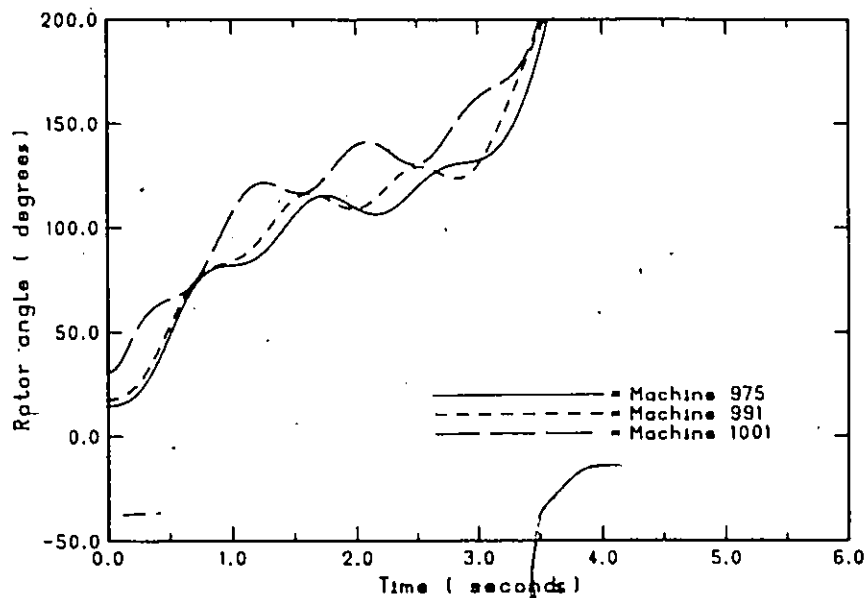


Fig. 6.2 The energy margin of the 11-generator system versus the clearing time for 100 % constant impedance loads (critical $T_{cl} = 0.0956$ s).



(a) Critically stable case, $T_{cl} = 0.1416$ s.



(b) Critically unstable case, $T_{cl} = 0.1418$ s.

Fig. 6.3 The rotor angles of the advanced machines in time domain for 50% constant impedance and 50% constant power load models for the 11-generator system.

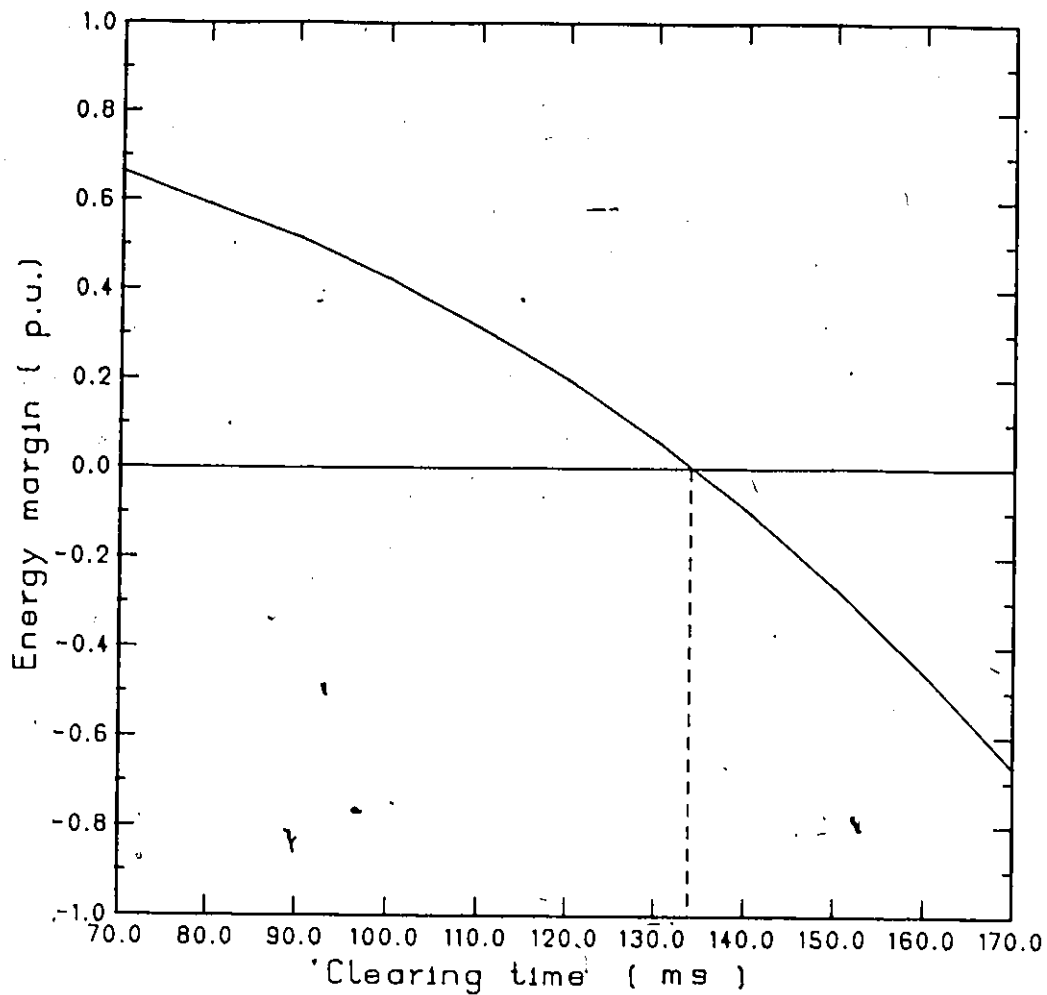
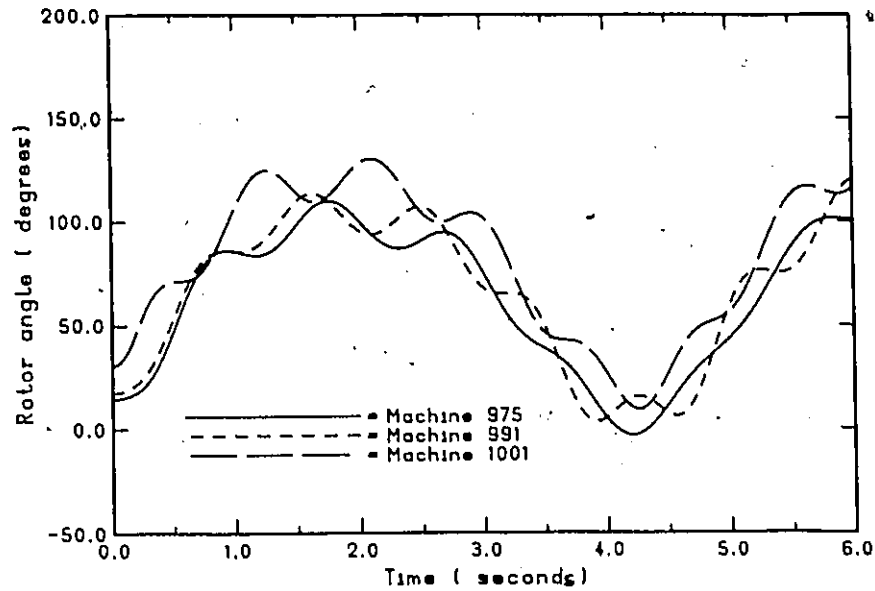
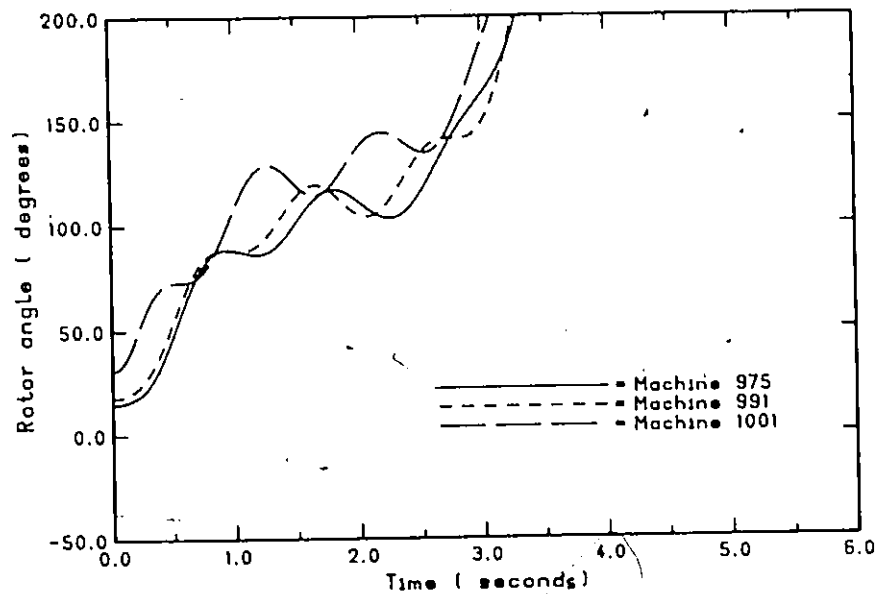


Fig. 6.4 The energy margin of the 11-generator system versus the clearing time for 50 % constant impedance + 50 % constant power loads (critical $T_{cl} = 0.1347$ s).



(a) Critically stable case, $T_{cl} = 0.1995$ s.



(b) Critically unstable case, $T_{cl} = 0.201$ s.

Fig. 6.5 The rotor angles of the advanced machines in time domain for 100 % constant power load models for the 11-generator system.

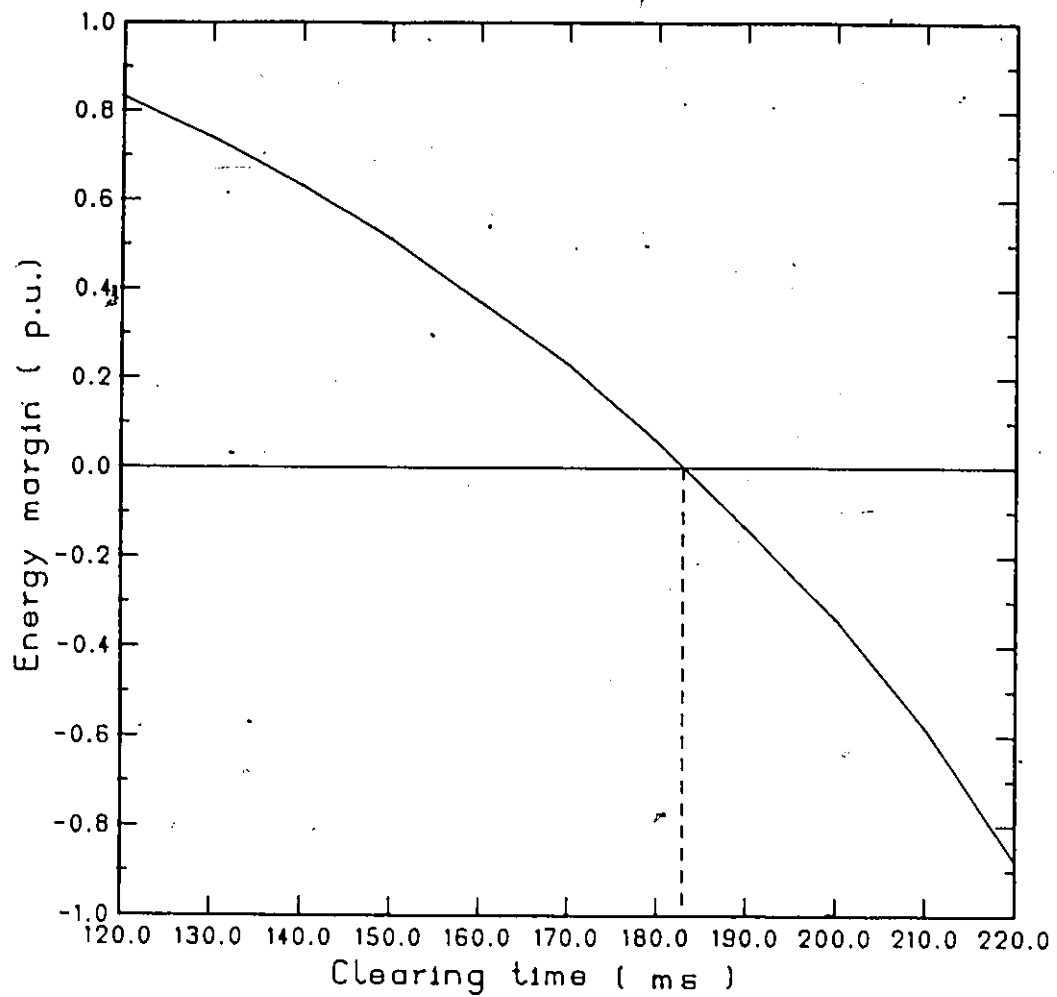


Fig. 6.6 The energy margin of the 11-generator system versus the clearing time for 100 % constant power loads (critical $T_{cl} = 0.1833$ s).

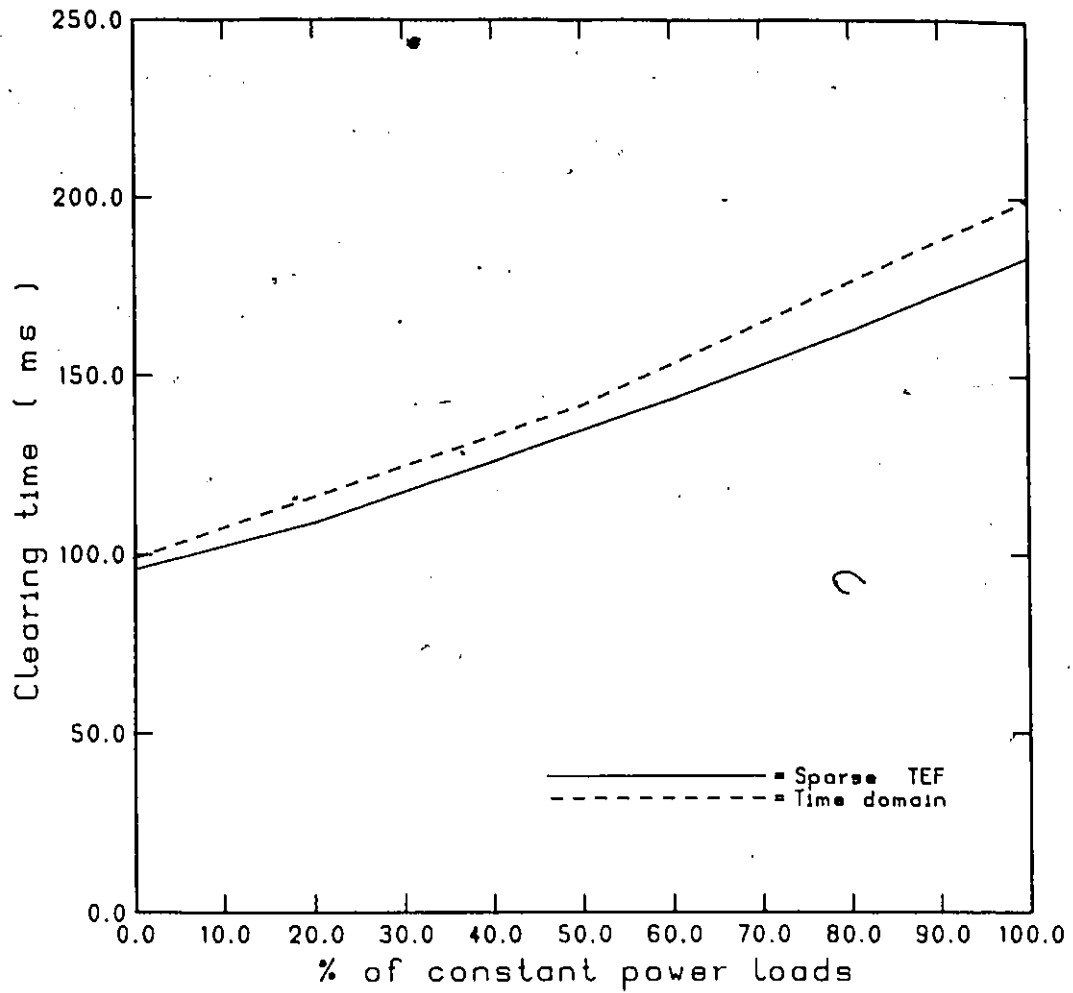


Fig. 6.7 The critical clearing times of the 11-generator system for different load models using the sparse formulation of the TEF and the time domain.

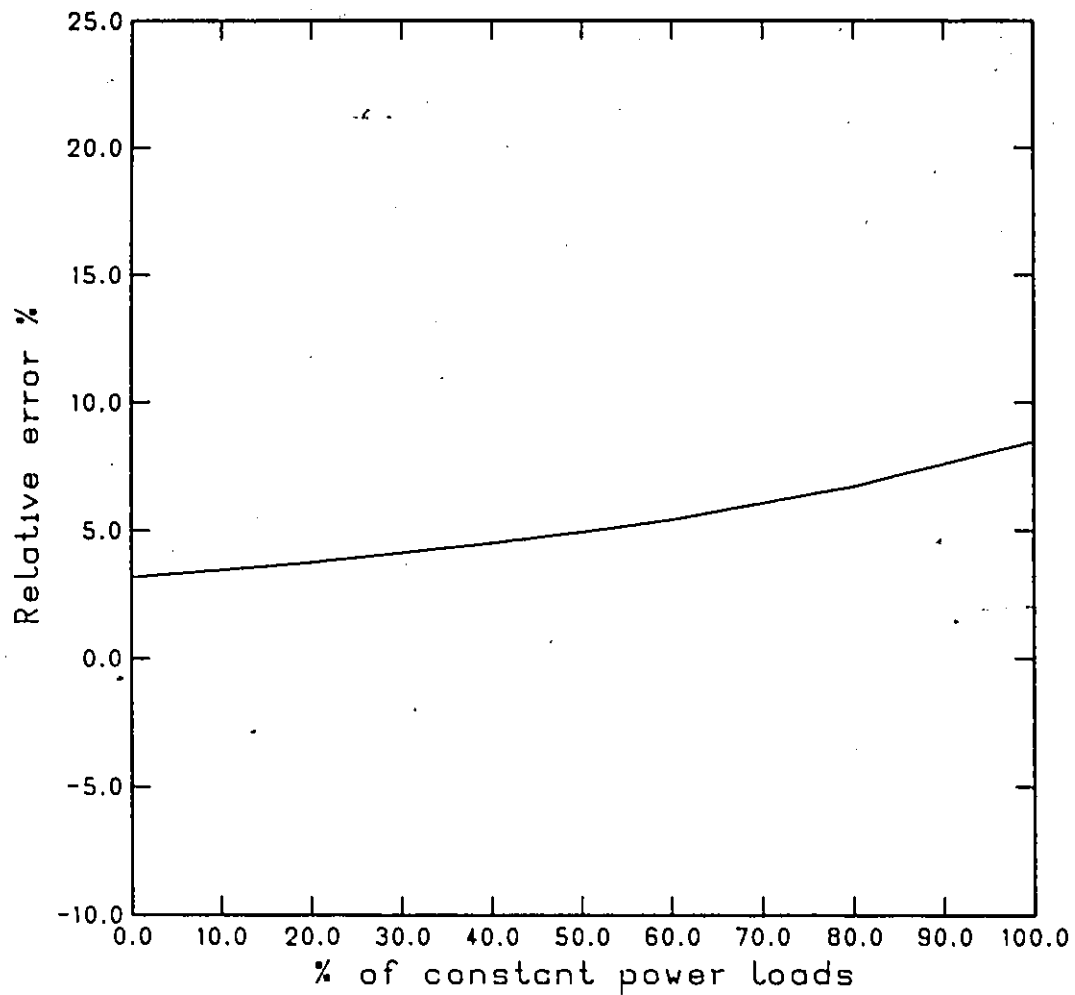


Fig. 6.8 The percentage relative error in the critical clearing time calculation of the 11-Generator system for different load models.

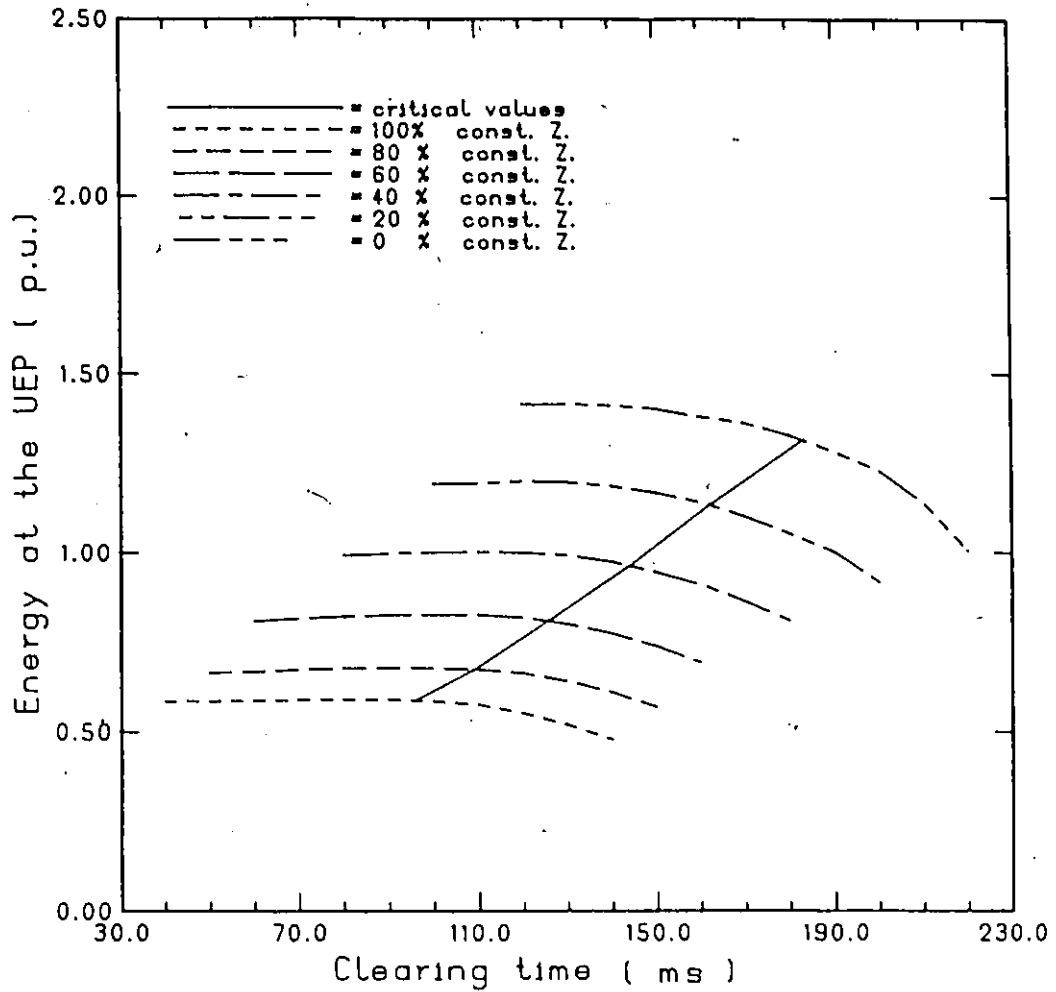


Fig. 6.9 The energy at the UEP of the 11-generator system versus the clearing time for different load models (different % of constant impedance loads).

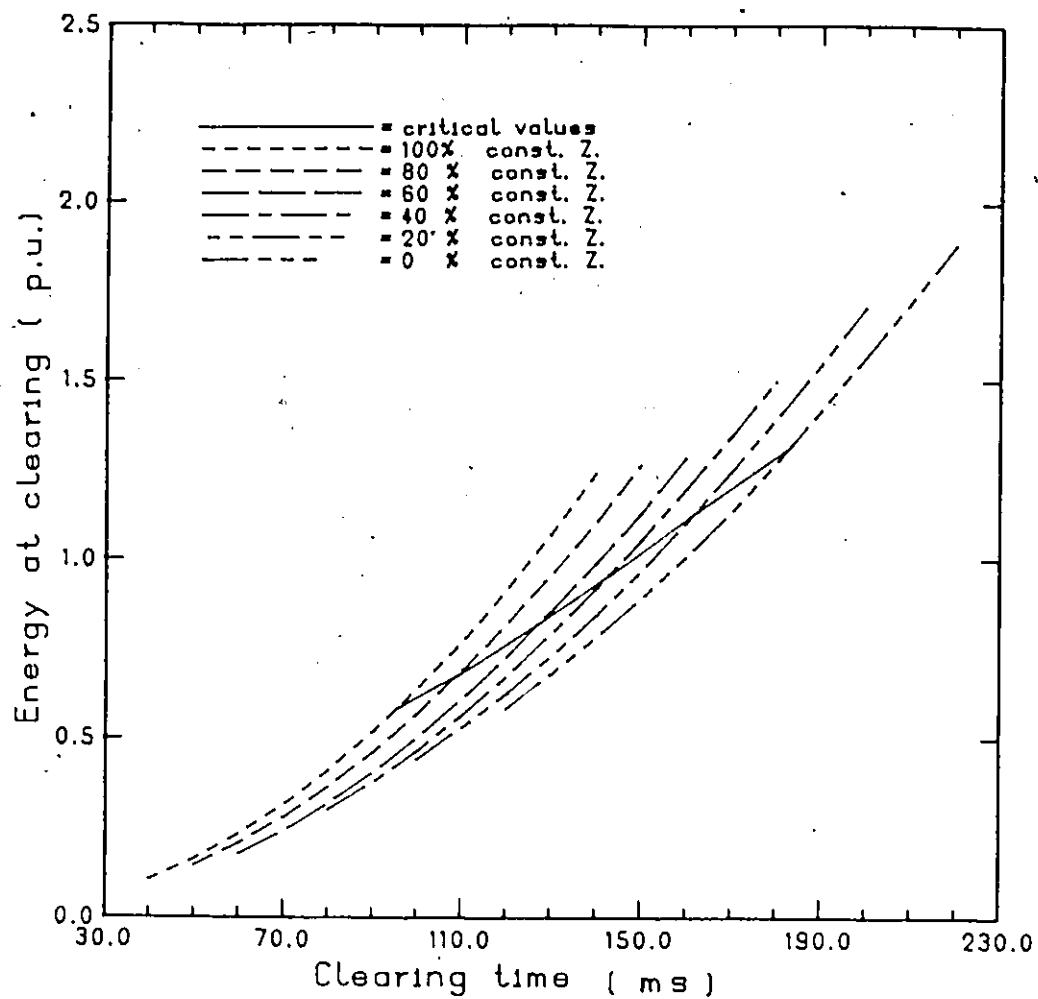


Fig. 6.10 The energy at clearing of the 11-generator system versus the clearing time for different load models (different % of constant impedance loads).

of a single generator - infinite bus system for two values of the clearing time. In each case, the area A1 represents the energy at clearing while the area A2 represents the energy at the UEP. It is clear that as we increase the clearing time, i.e. as we increase the clearing angle, A1 increases and A2 decreases. It should also be noticed that, in figures 6.9 and 6.10, the curves for different load models have the same shape but they move to the right (the direction of increasing the clearing time) as the load models change from constant impedance to constant power loads. Notice also that the solid line in each figure represents those values corresponding to the critical clearing time in each case of the load modeling. Since it corresponds to zero energy margin which is the difference between the energy at the UEP and the energy at clearing, the points of intersections of the solid line and the energy lines in each figure should have the same values. Figures 6.12 and 6.13 show the energy margin and the normalized energy margin respectively for different clearing times. The intersection of the energy margin line of each case with the zero reference gives the critical clearing time of that case.

6.2.2 The Effect of Load Modeling on the Energy Margin

The energy margin, as described in Chapter 3, is the difference between the energy at the UEP and the energy at fault clearing. Figure 6.14 shows these two types of energies and the energy margin as we change the models of all system loads from constant impedance to

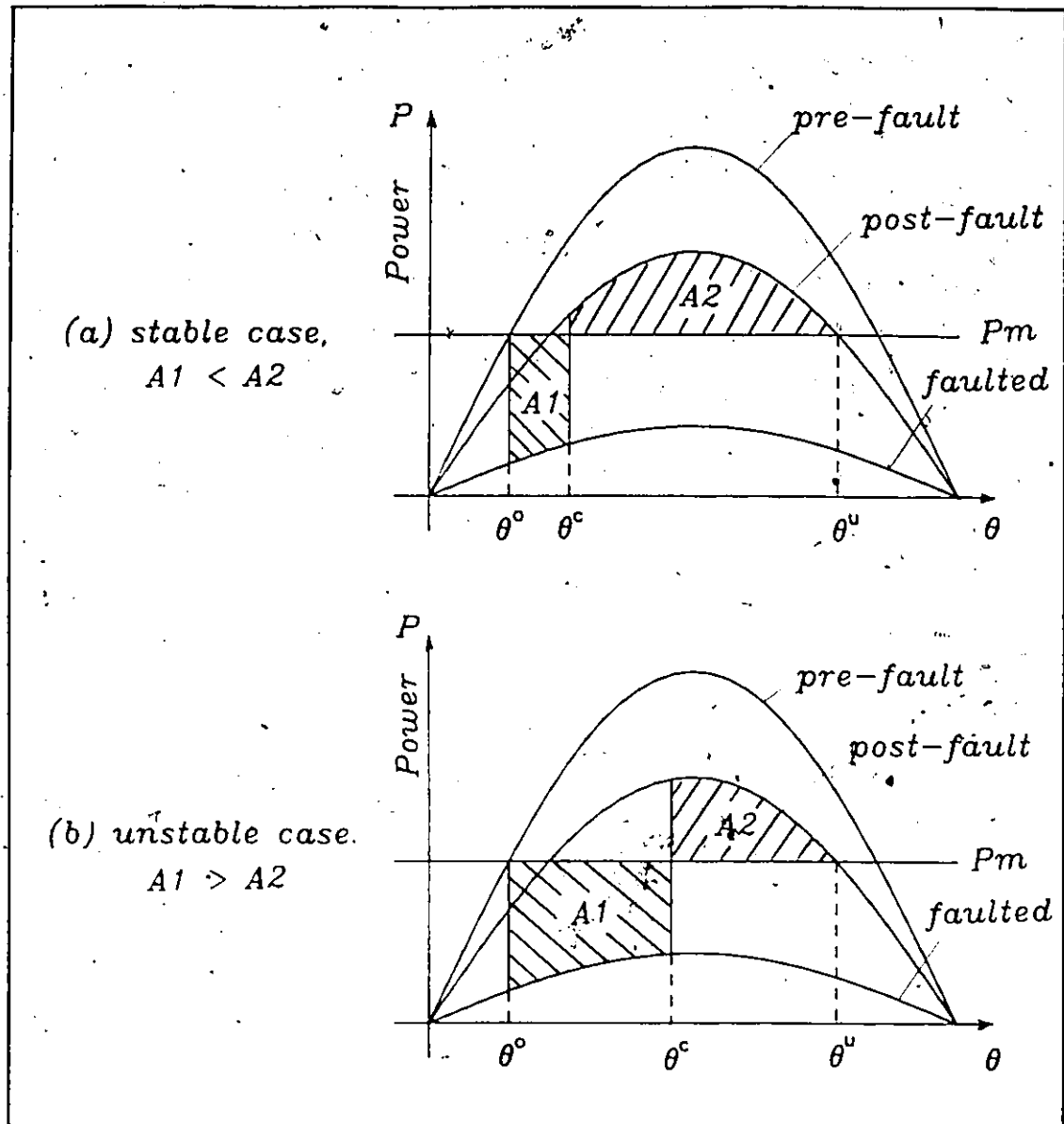


Fig. 6.11 The EAC criterion for 1 machine-infinite bus system;
(a) stable case,
(b) unstable case.

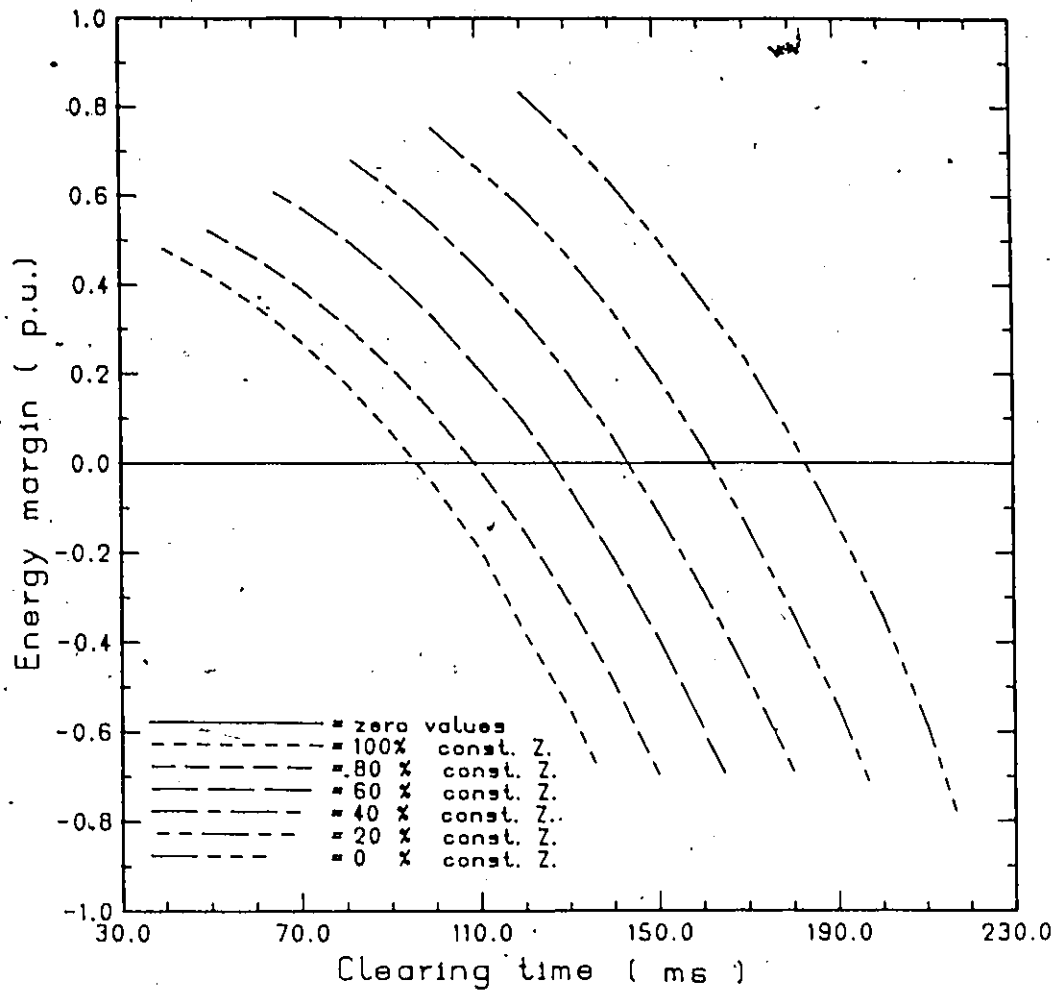


Fig. 6.12 The energy margin of the 11-generator versus the clearing time for different load models (different % of constant impedance loads).

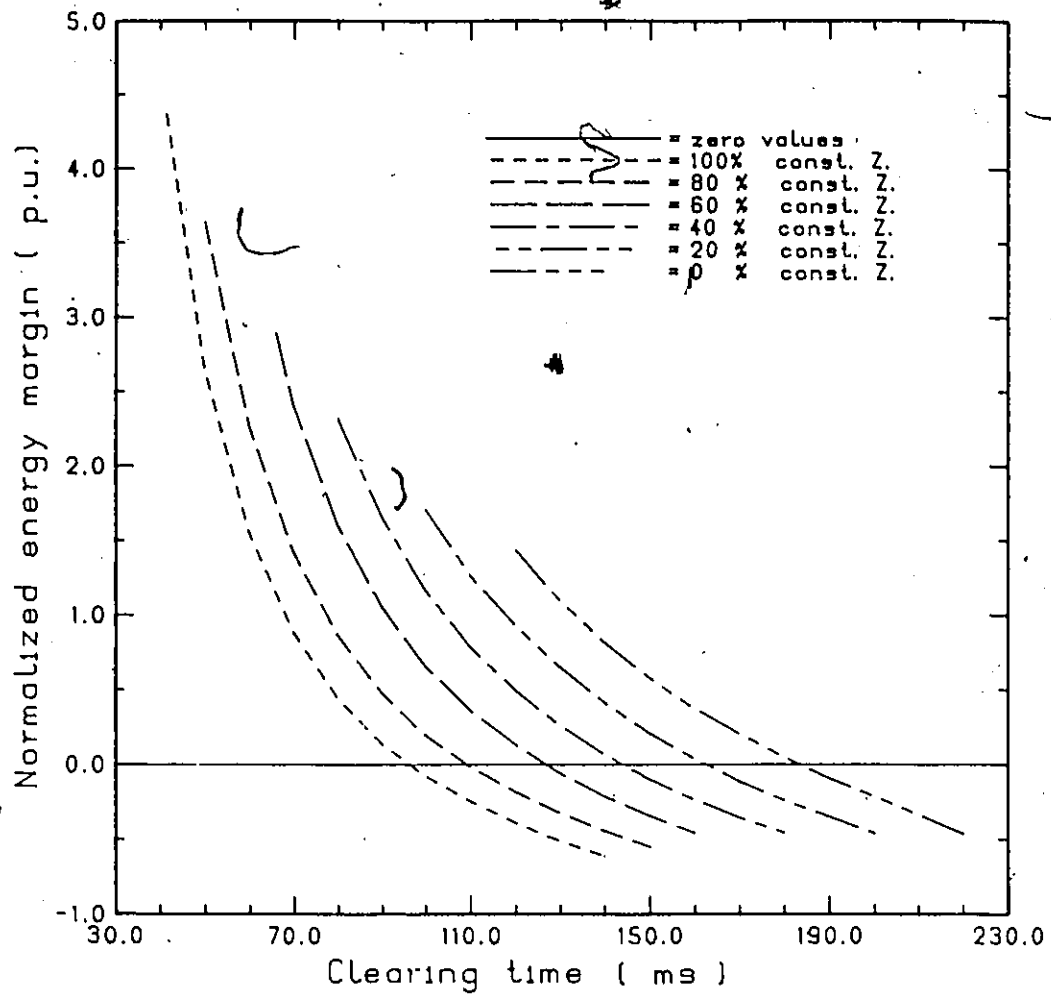


Fig. 6.13 The normalized energy margin of the 11-generator system versus the clearing time for different load models (different % of constant impedance loads).

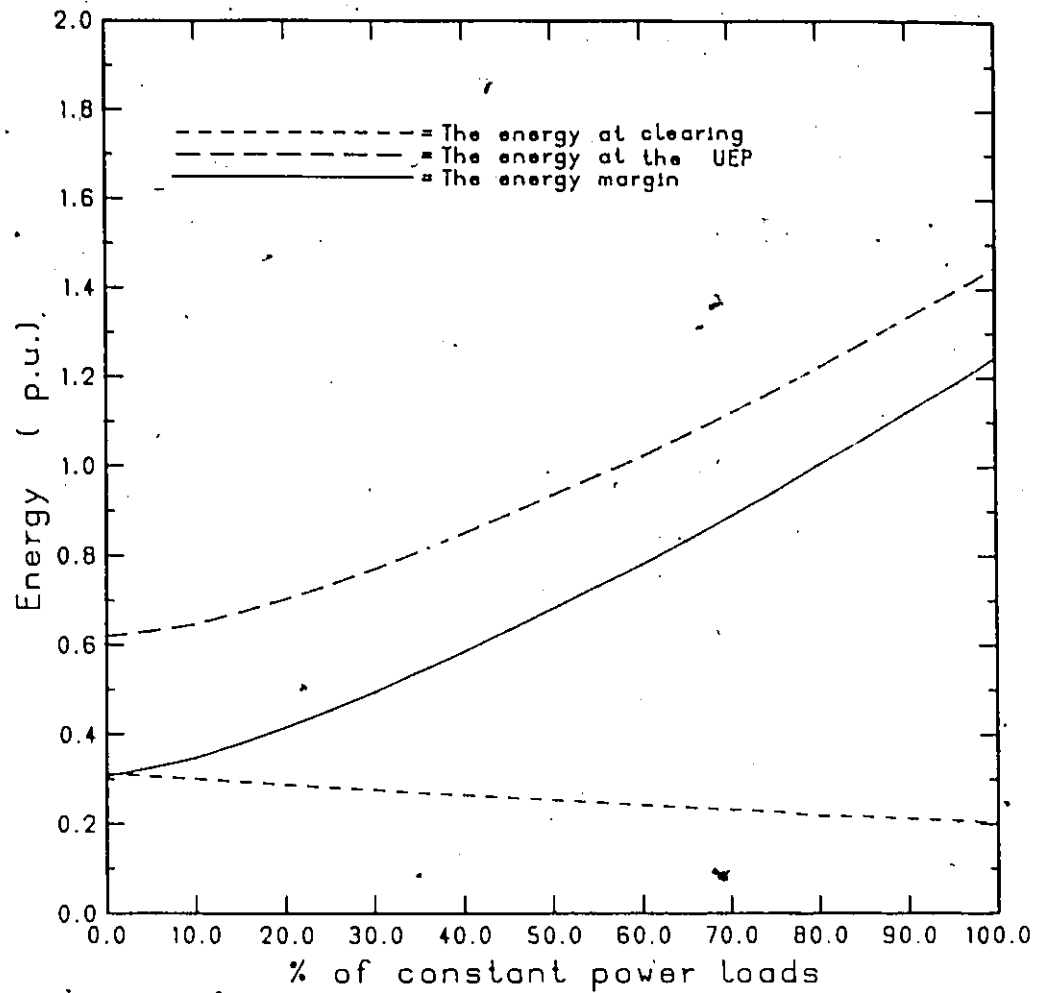


Fig. 6.14 The energy at clearing, the energy at the UEP and the energy margin of the 11-generator system versus the clearing time for different load models, clearing time = 0.068 s.

constant power loads. The clearing angles and speeds are calculated assuming constant acceleration because the clearing time (0.068 second) is small enough. As shown in figure 6.14, as the loads change from constant impedance to constant power, the energy margin increases from 0.3042 p.u. to 1.2452 or by 409.34 %. The difference between these two values is 0.9410 p.u. , i.e. 94.10 MJ, a relatively large value. The relative robustness of the system can be evaluated by the normalized energy margin as shown in figure 6.15. The normalized energy margin increases from 0.9713 to 6.1355, an increase of 631.68 %. This percentage shows that the system is actually much more robust if we consider the loads as constant power than constant impedance. This means that neglecting the true load modeling may lead to a false judgement on the system stability. Recalling equation 3.19, the energy margin depends on three terms as follows. The first term is the positional energy. The second term is the magnetic and dissipated energy. They depend on the clearing angles and the UEP. The third term is the kinetic energy at clearing. This term depends on the speeds at clearing, i.e. the behaviour of the energy margin shown in figure 6.14 can be explained by investigating the values of the clearing angles and speeds and the UEP point as the load models are changed.

6.2.2.1 The Effect of Load Modeling on the Clearing and UEP Points

The most effective machines on the energy margin are the advanced machines and what we call the reference machine. When a detailed large scale power system is required to be reduced to another version of,

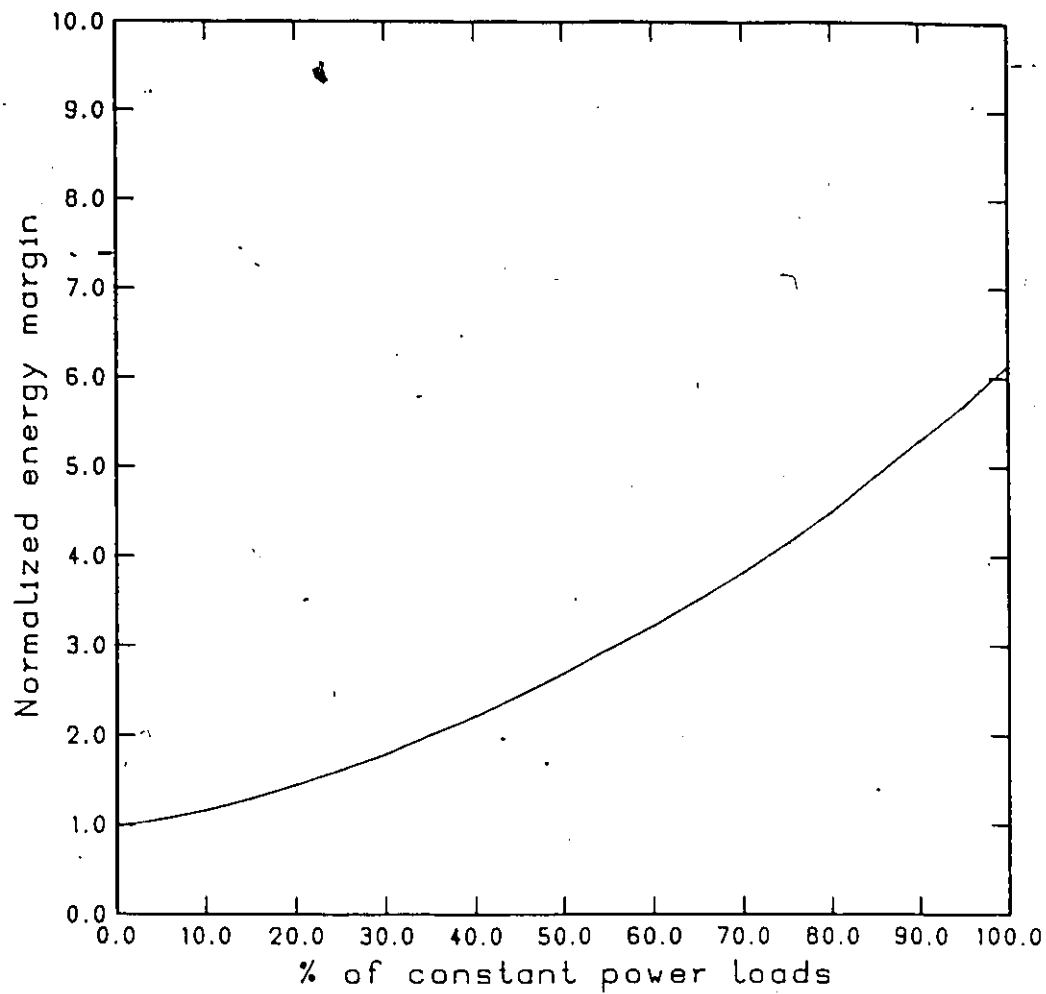


Fig. 6.15 The normalized energy margin of the 11-generator system for different load models, clearing time = 0.068 s.

smaller size (keeping the load models as they are), usually that part of interest of the large system is kept unchanged while the rest of the system is reduced to an equivalent machine with some local load. This equivalent machine is called the reference machine because its parameters (rotor angle and speed) are considered to be not affected much by any fault which occurs some where else. Figure 6.16 shows the first two terms of the energy margin expression, the positional energy and the magnetic and dissipated energy for different load models. The difference between these two curves is the energy at the UEP shown in figure 6.14. Figure 6.17 shows the UEP of the advanced machines and the reference machine as well for different load models. The UEP of the advanced machines (975, 991 and 1001) decrease (by 5.761, 5.382 and 4.801 degrees) as the loads are changed from constant impedance to constant power loads while the UEP of the reference machine increases (just by 1.490 degrees). As shown in figure 6.18, the changes of the clearing angles (-0.113, -0.200, -0.525 and +0.0512 degrees) are very small. From the previous values, we conclude that the integration span (the distance between the UEP and the clearing points in the angle domain) is decreasing for both the advanced machines and the reference machine resulting in decreasing energies as they shown in figure 6.16. But because the mechanical input powers of the advanced machines are 1.0, 2.0 and 13.0 p.u. and that of the reference machine is 2418.8 p.u. and because the electrical output powers are of the same ranges, the reference machine is dominant and the signs of the calculated energies shown in figure 6.16 are different from those shown in equation 3.19.

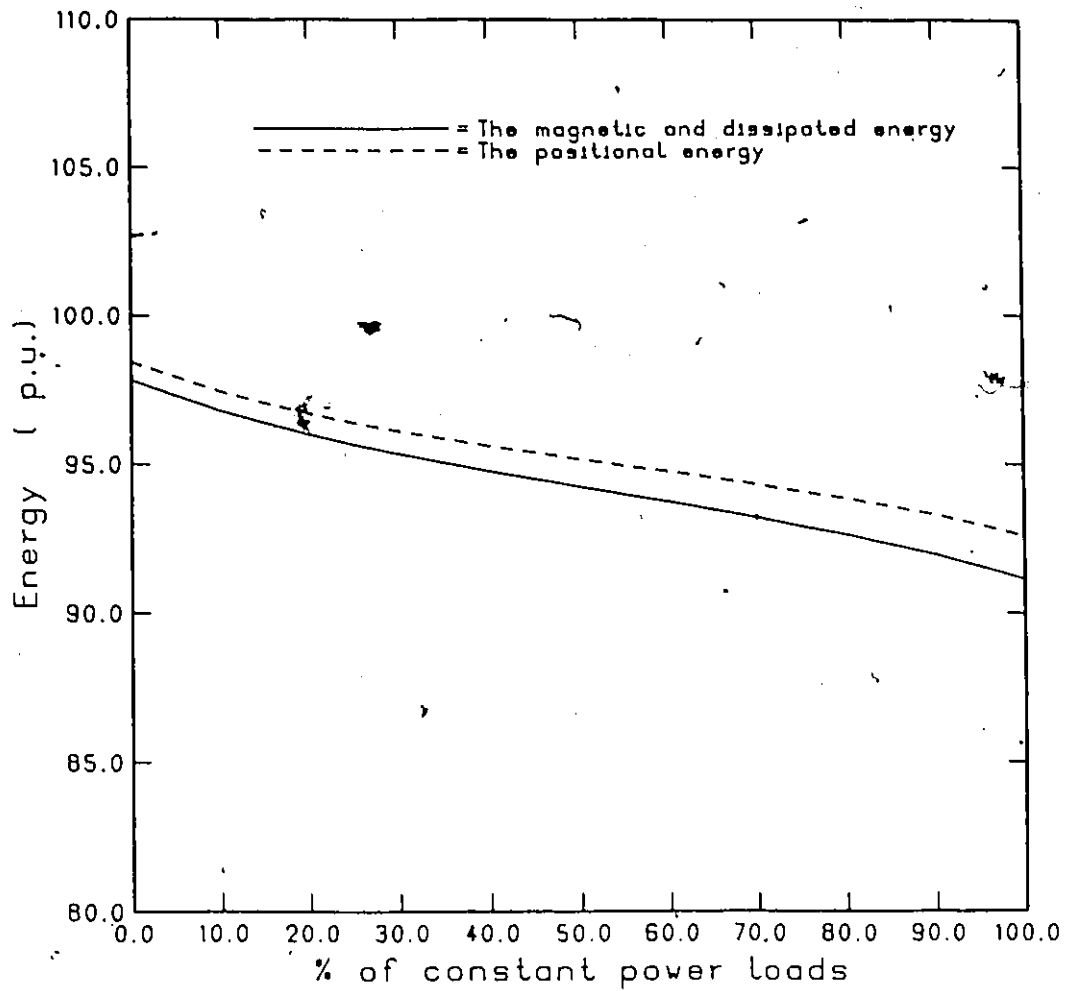


Fig. 6.16 The magnetic and dissipated energy and the positional energy of the 11-generator system for different load models, clearing time = 0.068 s.

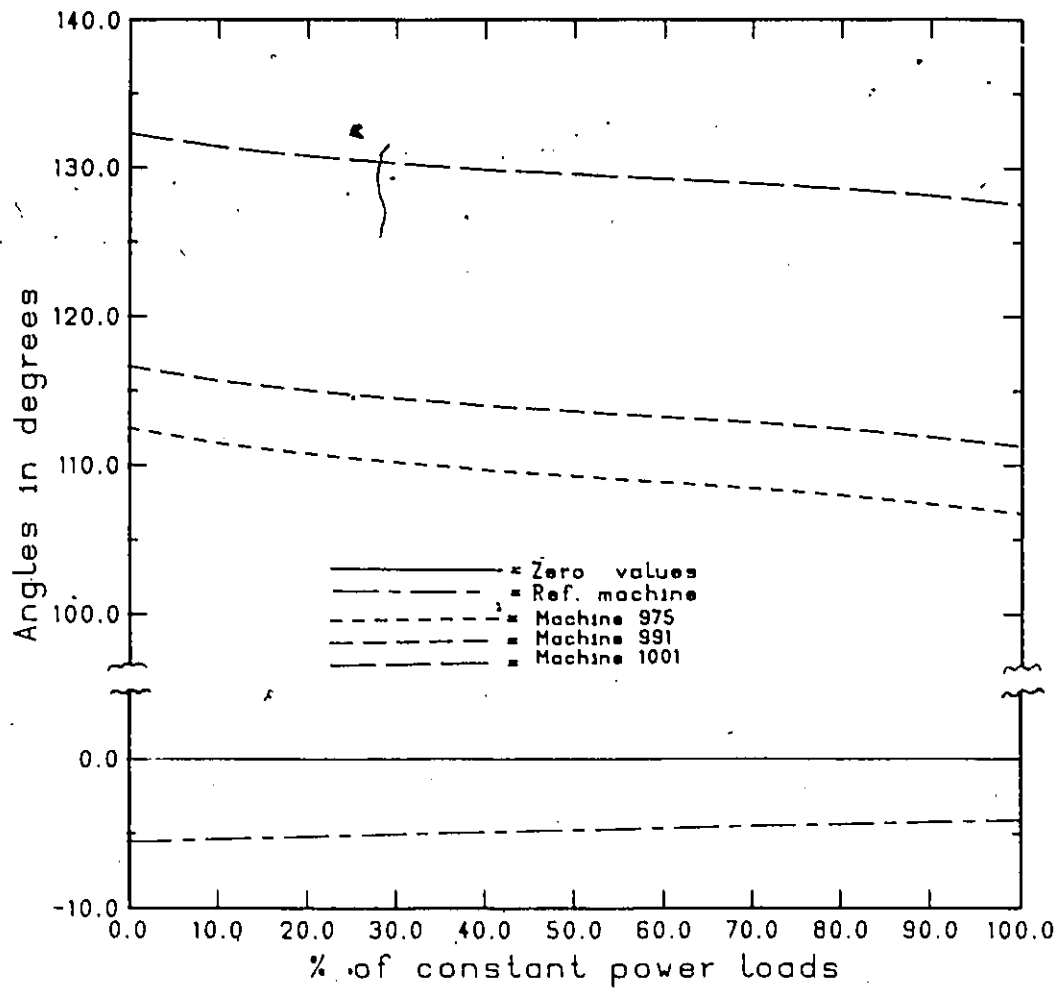


Fig. 6.17 The UEP of the advanced machines and the reference machine of the 11-generator system for different load models, clearing time = 0.068 s.

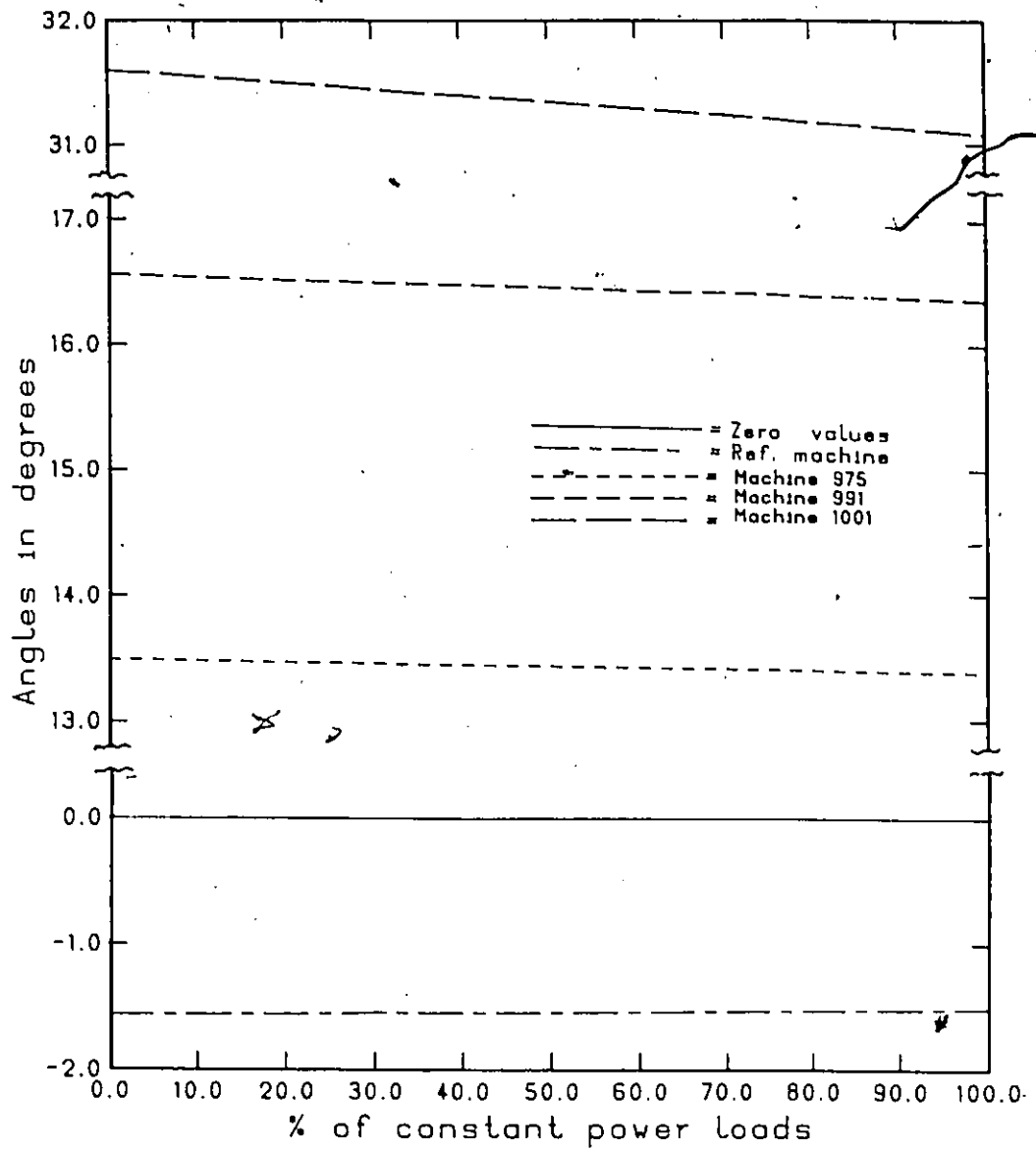


Fig. 6.18 The clearing angles of the advanced machines and the reference machine of the 11-generator system for different load models, clearing time = 0.068 s.

6.2.2.2 The Effect of Load Modeling on the Clearing Speed

Figure 6.19 shows the clearing speeds of the advanced machines as well as the speed of the reference machine for different load models. The speeds of the advanced machines decrease by 0.0267, 0.0709 and 0.2381 rad/s while that of the reference machine increases by 0.0227 rad/s. The situation here is slightly more complex since the kinetic energy is equal to the speed square times the inertia constant. Therefore, although the inertia constants of the advanced machines are 57.52, 115.04 and 105.79 p.u. while that of the reference machine is 9344.17 p.u., the advanced machines are dominant because the speed of the reference machine is a small fraction. Here, it should be noted that the "speed square" term makes both the reference and advanced machines causing the kinetic energy to decrease as shown in figure 6.14. Since the energy at the UEP (according to the previous section) increases and the kinetic energy at clearing decreases, the energy margin increases as the load models change from constant impedance to constant power loads.

6.3 Applications to a 50-Generator, 145-Bus System

The effect of load modeling on the stability limit is discussed through applications of the SF to the 50-generator, 145-bus system described in Chapter 4. In this system, a three phase fault occurs at bus number 101 (Station B) and the fault is cleared in 0.068 second by tripping out two lines connected to the faulted bus. The mode of instability for this specified fault is that Station B machines, those which are connected to buses 1771 and 1853, plus Station D machine,

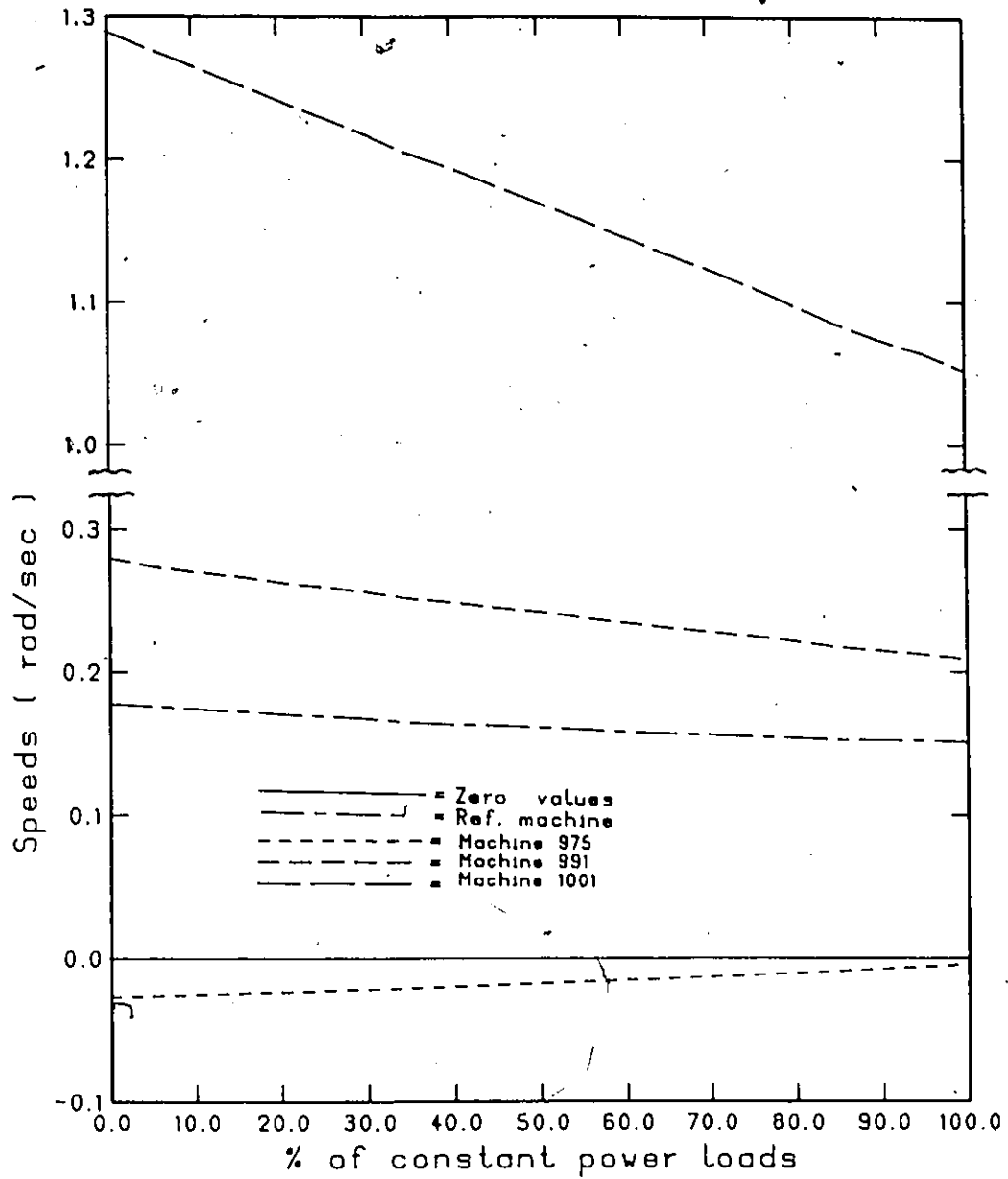
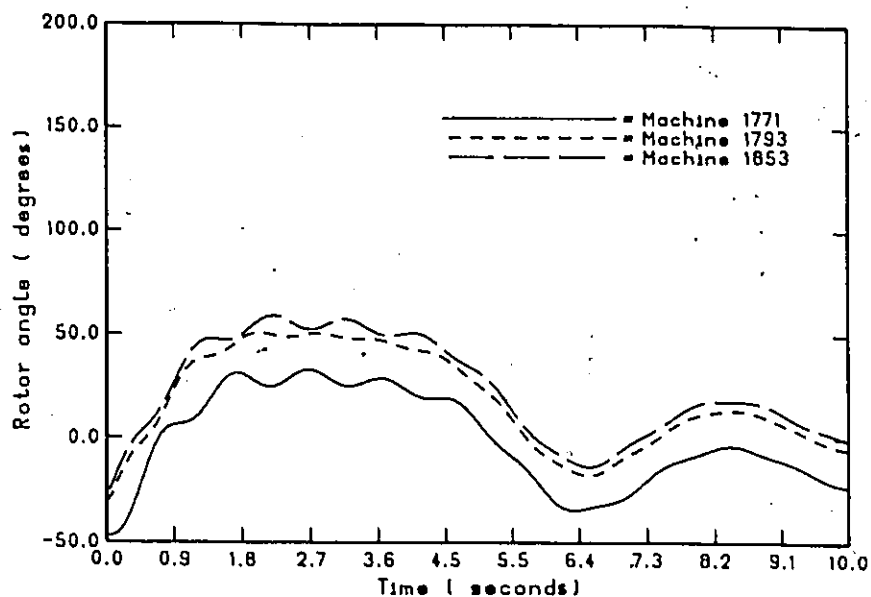


Fig. 6.19 The clearing speeds of the advanced machines and the reference machine of the 11-generator system for different load models, clearing time = 0.068 s.

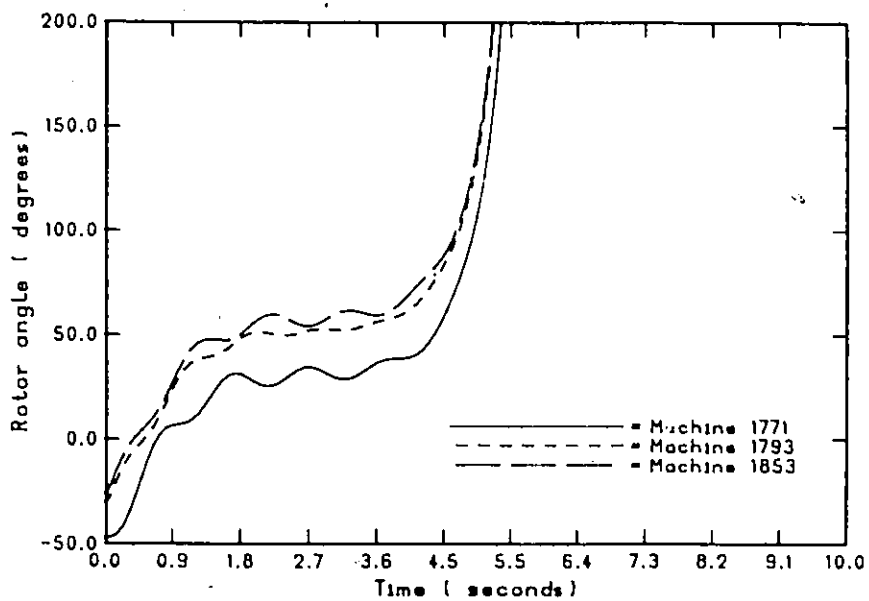
which is connected to bus 1793, are the advanced machines. A comparison between the Sparse TEF results and those obtained using the time domain is presented, which confirms the accuracy of the SF for different load models application.

6.3.1 The Effect of Load Modeling on the Stability Limit

The stability limit is calculated using first the time domain by increasing the gross output of Station B (by increasing the generated output power of the machine connected to bus number 1853 and keeping all other outputs constant) while watching the rotor angles of the advanced machines. Similar to section 6.2.1, the time domain results of the three main load models; 100% constant impedance, 50% constant impedance + 50% constant power, 100% constant power load models, are presented. Figure 6.20 shows the critically stable and unstable cases of the first load model, from which the stability limit is 1514 MW. Using the SF, the stability limit is the interface flow at zero energy margin. Figure 6.21 gives a stability limit of 1423.5 MW for the same load model. The difference is 90.5 MW, representing 5.98%. Figures 6.22 to 6.25 show the results of the second and third load models using both the time domain and the SF of TEF methods. The results are summarized in table 6.1. The stability limits for some other load models are shown in figure 6.26 while the corresponding relative errors are shown in figure 6.27. As shown, the results of the SF of the TEF are close to those of the time domain with acceptable errors. Figure 6.28 shows the effect of load modeling on the energy margin - interface flow characteristics. The



(a) Critically stable case, interface flow = 1414 MW.



(b) Critically unstable case, interface flow = 1415 MW.

Fig. 6.20 The rotor angles of the advanced machines in time domain for 100 % constant impedance load models for the 50-generator system.

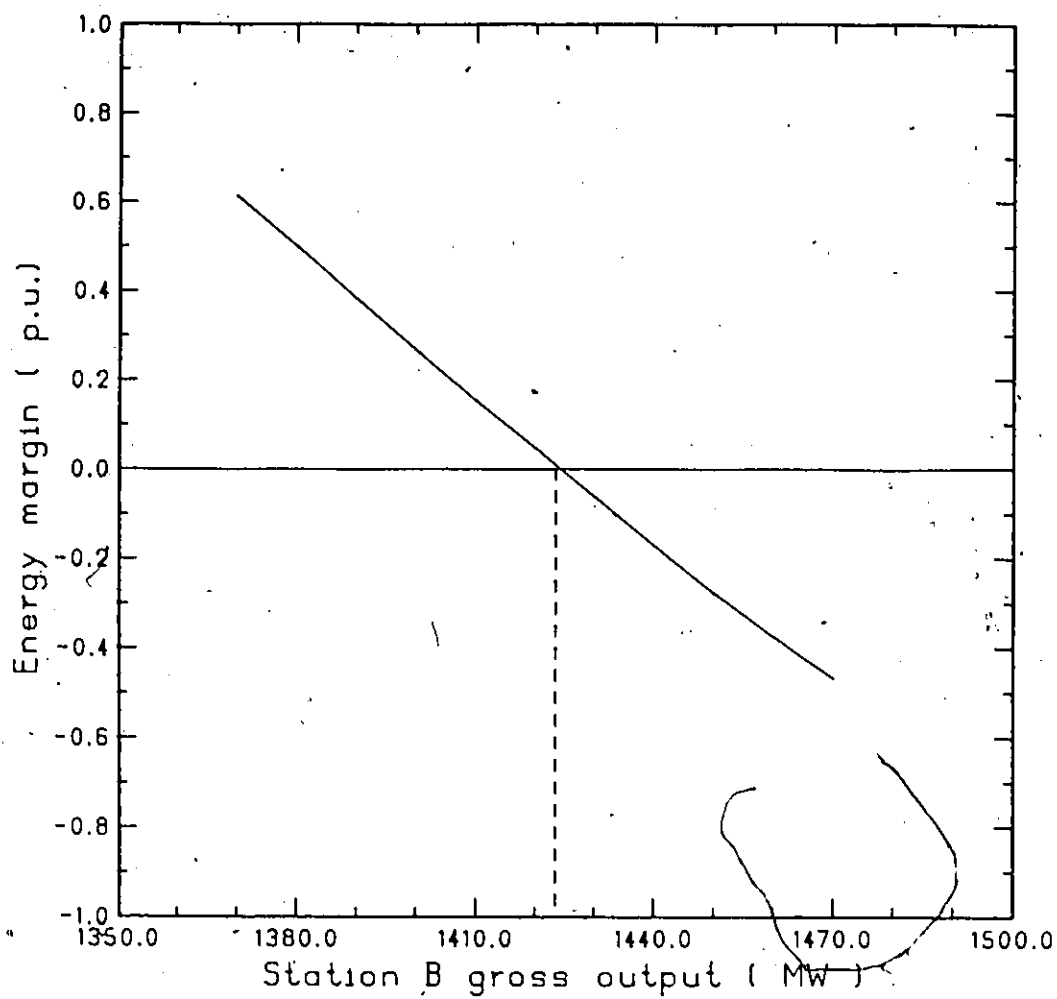
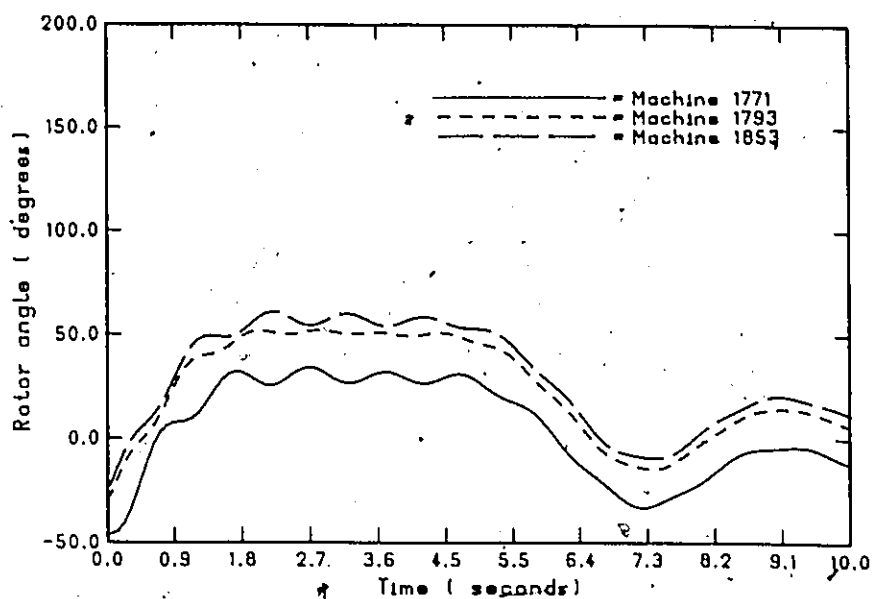
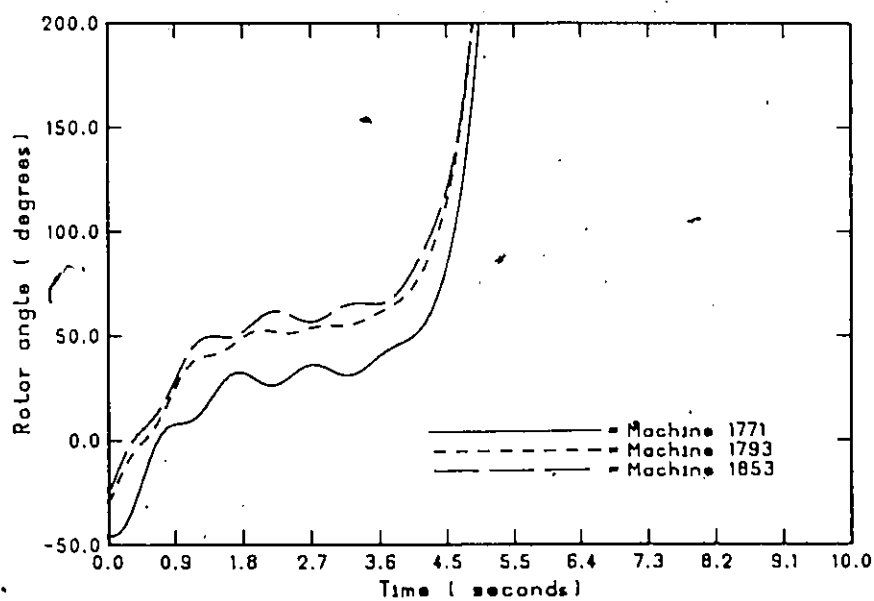


Fig. 6.21 The energy margin of the 50-generator system versus station B interface flow for 100 % constant impedance loads (stability limit = 1426.5 MW)



(a) Critically stable case, interface flow = 1441 MW.



(b) Critically unstable case, interface flow = 1442 MW.

Fig. 6.22 The rotor angles of the advanced machines in time domain for 50% constant impedance and 50% constant power load models for the 50-generator system.

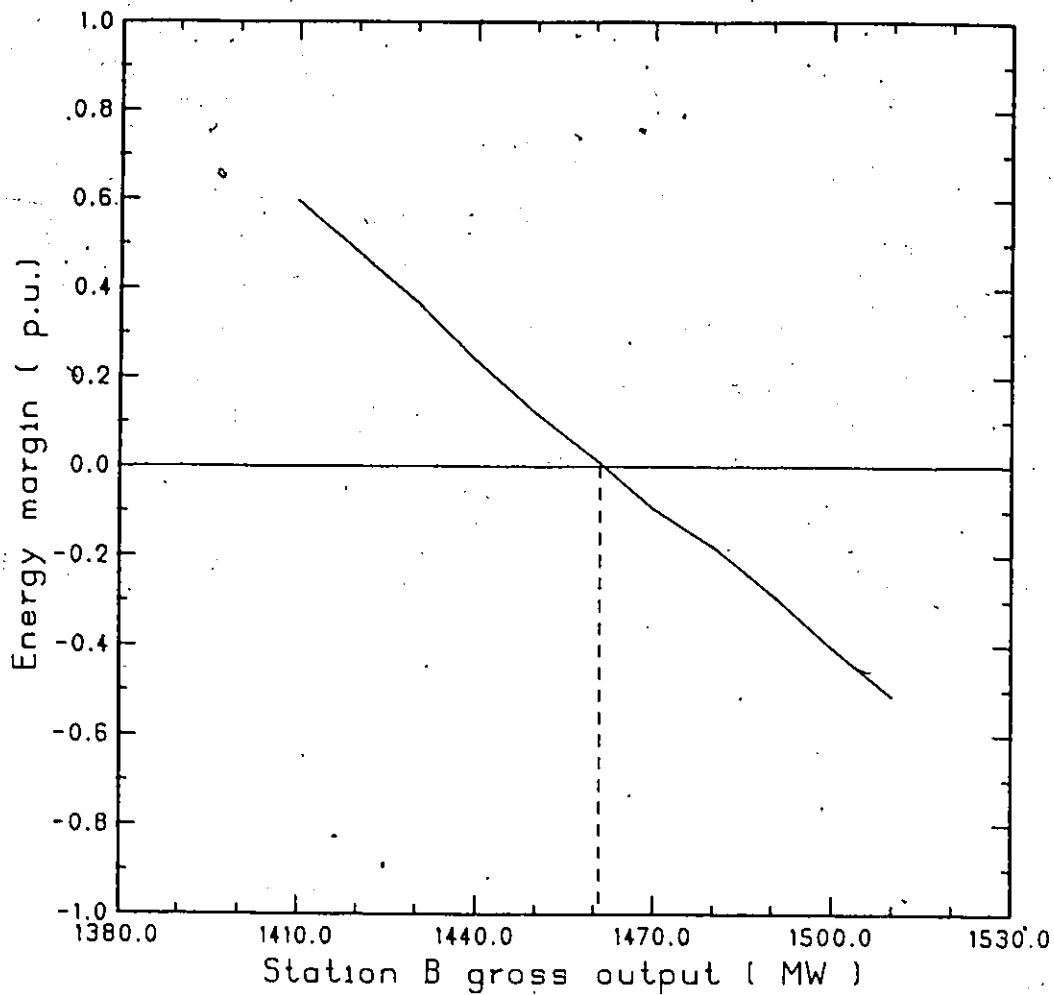
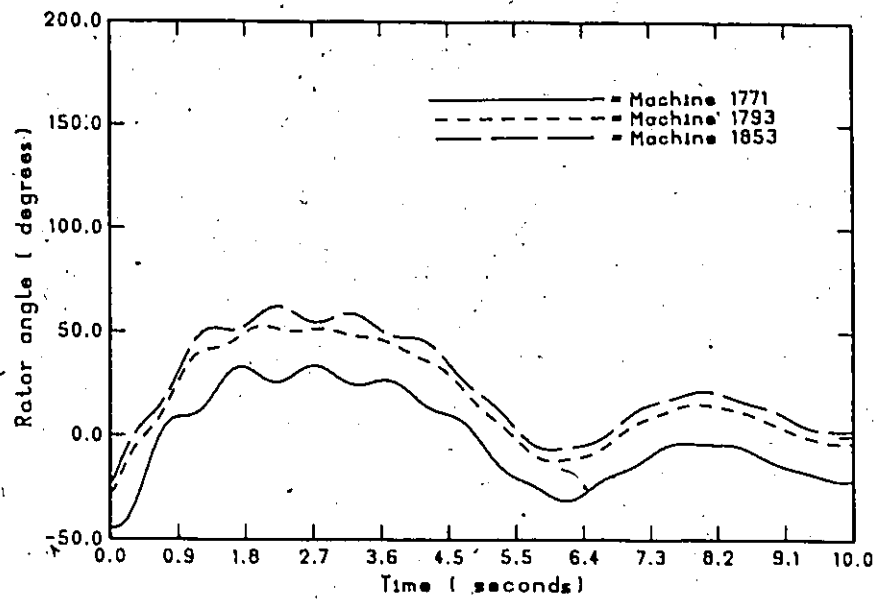
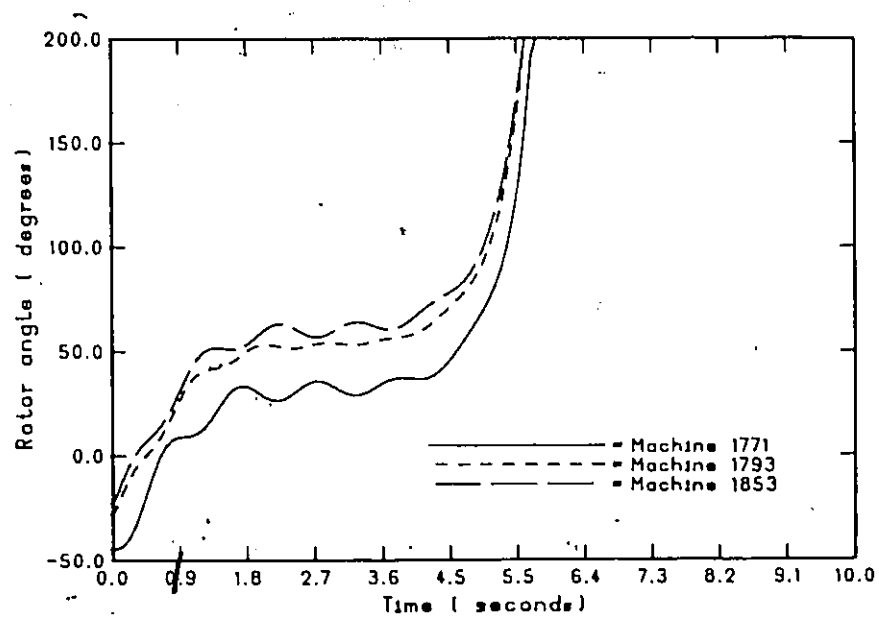


Fig. 6.23 The energy margin of the 50-generator system versus station B interface flow for 50 % constant impedance + 50 % constant power loads (stability limit = 1462.5 MW)



(a) Critically stable case, interface flow = 1469 MW.



(b) Critically unstable case, interface flow = 1470 MW.

Fig. 6.24 The rotor angles of the advanced machines in time domain for 100% constant power load models for the 50-generator system.

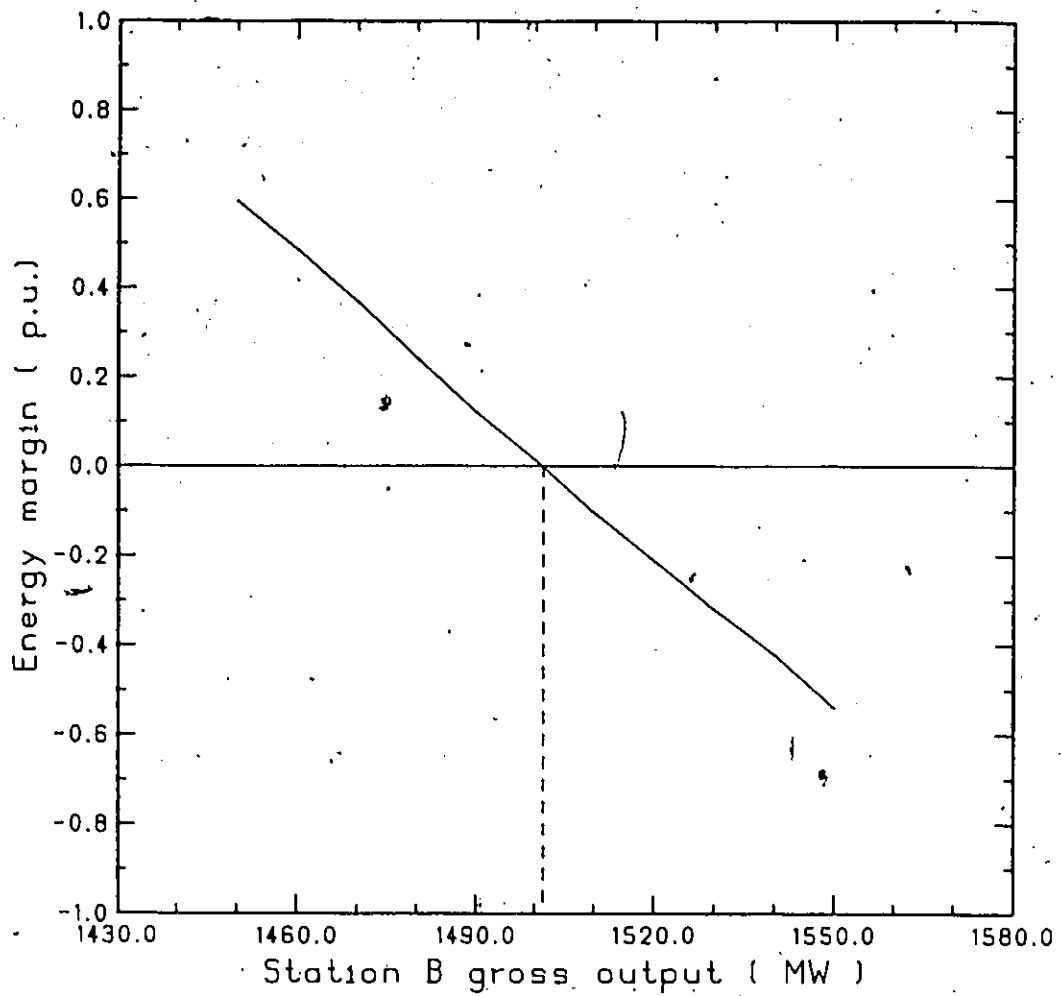


Fig. 6.25 The energy margin of the 50-generator system versus station B interface flow for 100 % constant power loads (stability limit = 1502.0 MW)

Load model	Time domain	Sparse TEF	Difference %
100 % constant impedance	1514	1426.5	5.98
50 % constant impedance +50 % constant power	1541	1462.5	5.19
100 % constant power	1569	1502.0	4.37

Table 6.1 The stability limits (MW) of different load models using time domain and sparse TEF methods for the 50-generator system.

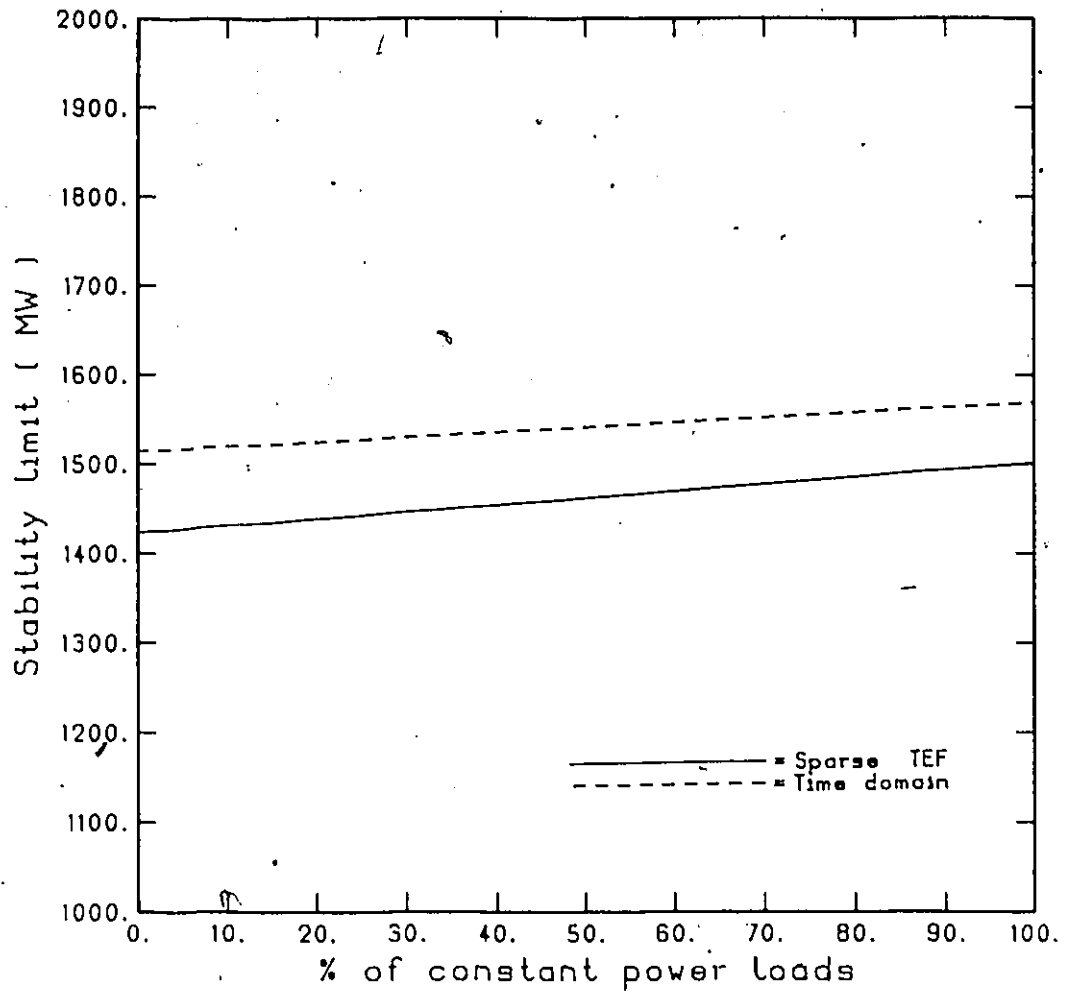


Fig. 6.26 The stability limit of the 50-generator system for different load models using the sparse formulation of the TEF and the time domain.

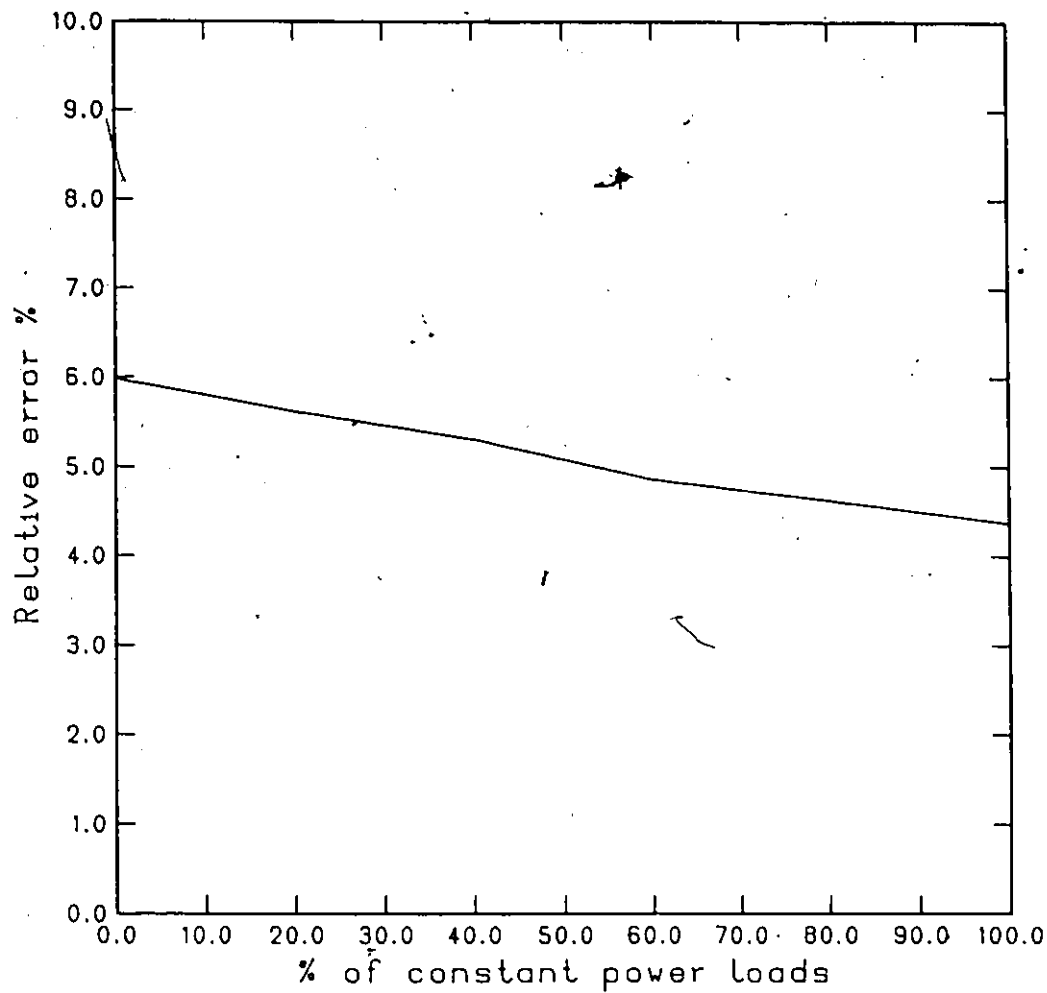


Fig. 6.27 The percentage relative error in the stability limit calculation of the 50-Generator system for different load models.

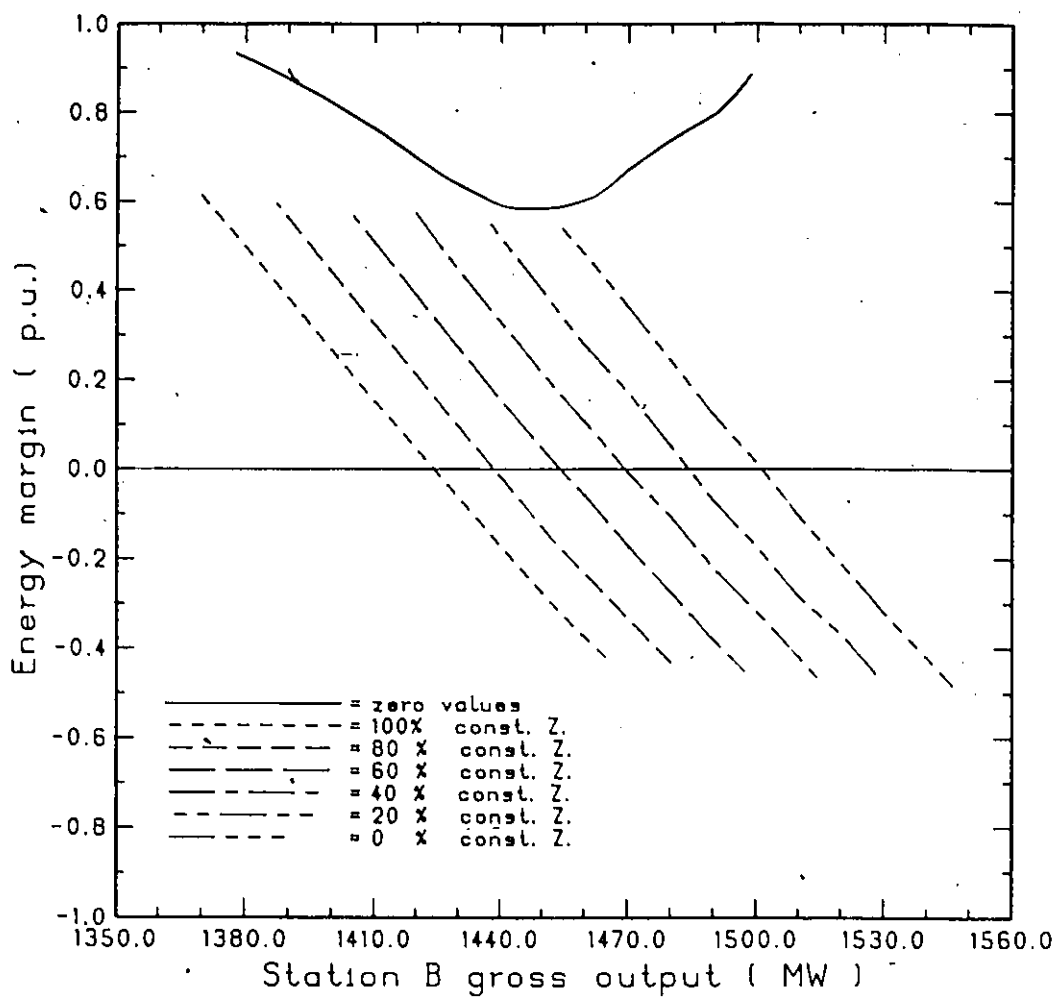


Fig. 6.28 The energy margin of the 50-generator versus station B interface flow for different load models (different % of constant impedance loads).

normalized energy margins, which give good measure of the system robustness, are shown in figure 6.29 for different load models. The characteristics shown in figures 6.28 and 6.29 are of great importance because for a certain Station B gross output, which can be represented in both figures as a vertical line, we can establish the status of the system for different load model. For example, for 1460 MW gross output, the status of the system for different load models is shown in table 6.2. This shows us how much important the consideration of load modeling in the transient stability analysis is.

6.4 Conclusion

The capability to include load modeling which is one of the main advantages of the SF has been demonstrated in this chapter. The strong effect of load modeling on both the critical clearing time and the stability limit has been emphasized and the accuracy of the SF results for different load models application has been proved by comparisons with time domain solutions. Most of the industrial loads, which represent the majority of system loads, are in the nature of constant power type because they use large induction motors. Neglecting these types of load modeling in transient stability analysis may lead to significant errors in the critical clearing time calculation (as in the case of the 11-generator system power). Also, in one of the applications shown, the incorrect load modeling has resulted in wasting more than 70 MW in the stability limit calculation (the case of the 50-generator system). That is, the SF gives more accurate and correct results

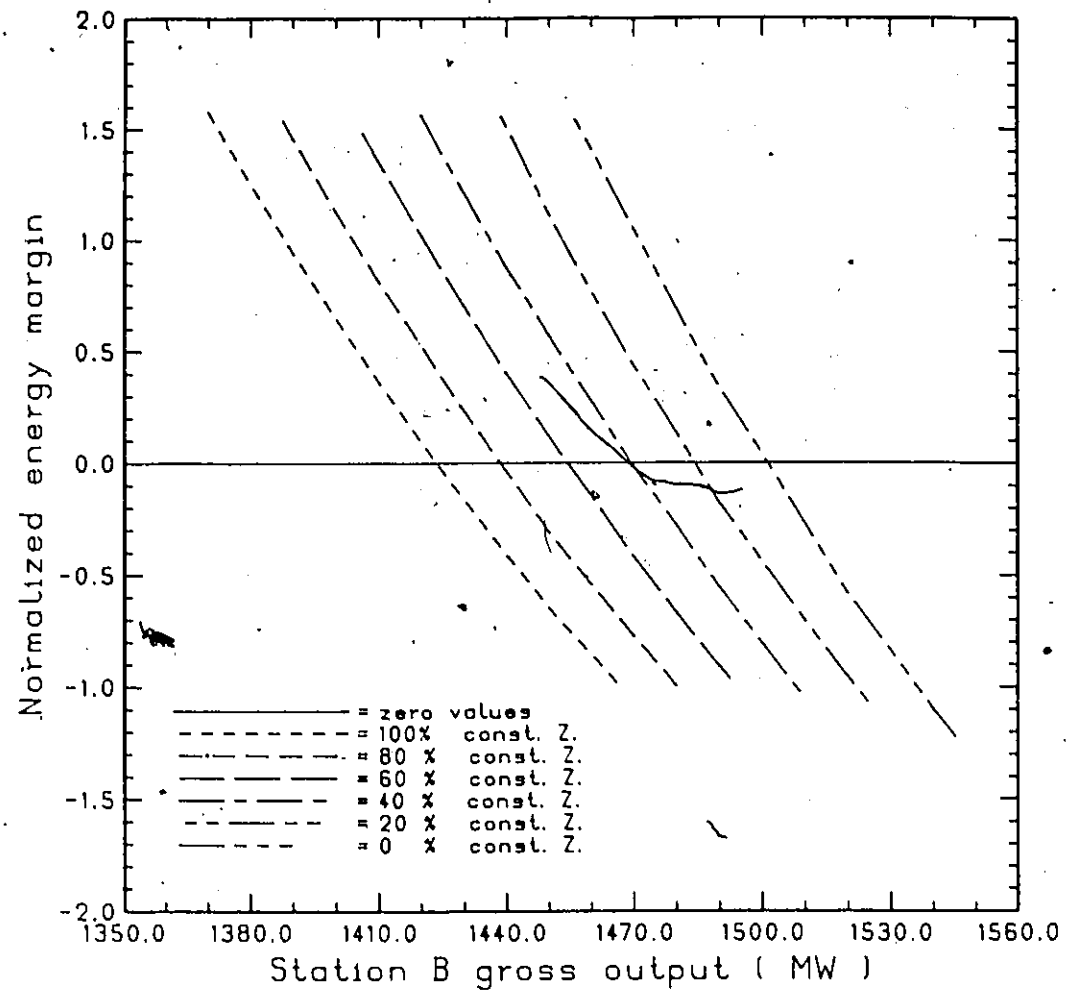


Fig. 6.29 The normalized energy margin of the 50-generator versus station B interface flow for different load models (different % of constant impedance loads).

Load model	EM	norm. EM	status
100% const. Z + 00% const. P	-0.3795	-0.8556	unstable
80% const. Z + 20% const. P	-0.2324	-0.5426	unstable
60% const. Z + 40% const. P	-0.0582	-0.1468	unstable
40% const. Z + 20% const. P	0.1064	0.2782	stable
20% const. Z + 80% const. P	0.2869	0.7678	stable
00% const. Z + 100% const. P	0.4815	1.4083	stable

Table 6.2 The effect of load modeling on the status
of the 50-generator system, $T_{cl} = 0.068$ s,
station B gross output = 1460 MW.

(compared with those of the RNF) because it can represent the loads by models realistically, as they occur in practice.

CHAPTER 7

CONCLUSION

The TEF method represents a powerful technique to analyze the transient stability of large-scale power systems. In current applications of the TEF method, the power network is reduced by eliminating all buses and retaining only the internal nodes of the generators. This Reduced Network Formulation (RNF) yields dense (non-sparse) matrices in the computations and consumes significant computational time. This represents a serious drawback of the RNF, especially in applications to large power networks. Also, all system loads are conventionally modeled as constant impedance loads in order to be able to reduce the network to the internal nodes of the generators. Other types of loads (e.g. constant power loads), which represent a majority in all practical power systems, are approximated as constant impedance type based on the pre-fault conditions. Consequently, accurate results may not be obtained. Moreover, the RNF of the TEF is not applicable to very large-scale power systems (e.g. 300-generator system) due to computer storage-related problems (e.g. file paging).

A novel formulation of the TEF method retaining the original structure of the system network has been presented and the associated computerized algorithm has been described. All the above-mentioned

problems have been solved using the proposed Sparse Formulation (SF) of the TEF method.

7.1 Research contribution

The contribution of this research work can be summarized in the following :

(1) The sparse formulation avoids completely the network reduction. All matrices used in the calculation of the SEP and UEP, for which the computational times are dominant in the calculation process of the energy margin (the stability index), are very sparse. This leads to a significant saving in computational time as compared with the RNF approach. This saving increases with the size of the system, as it has been shown in chapter 4, and it may reach more than 60% as in the case of the 156-generator system. The sparse formulation technique has been applied to different (realistic) utility systems up to a 300-generator, 1724-bus system. Such a system represents one of the base cases of Ontario Hydro. A comparison with the results obtained by the RNF technique has been given in each case (except the base case) regarding the CPU time and storage, and the superiority of the sparse formulation has been emphasized.

(2) Either constant impedance or constant power load models (or any combination thereof) can be handled explicitly. Considering these actual load models, the stability indices (the critical clearing time and the transient stability limit) can be calculated accurately.

Neglecting the true load models may lead to a critical error of more than 45% in the critical clearing time calculation (as in the case of considering the load models of the 11-Generator system as constant power loads).

(3) The proposed technique can handle very large-scale power systems which are beyond the scope of the RNF approach. Consequently, it enables an improved design methodology of transmission networks by including provision for modeling the network in more detail.

(4) Using the sparse formulation, it is possible to perform a transient stability analysis on a microcomputer. This will render cost-effective the use of such analysis.

(5) A very powerful and robust numerical technique to deal with ill-conditioned power systems is described. Therefore, practical (stressed) power systems can be handled, retaining the efficient sparse formulation of the TEF method.

We conclude that the sparse formulation has proved to be more efficient, more accurate and more reliable as compared with the RNF technique. The author claims that the research described in this thesis constitutes a useful contribution to the area of the transient stability analysis of large-scale power systems.

7.2 Recommendations for further research

This research has contributed to the effective removal of several major difficulties that have seriously limited the application of the TEF method to the power system transient stability problem. Considering the problems that have been faced during the investigation of this research, the following areas of future research are recommended:

1. Using more enhanced mathematical algorithms to deal with the ill-conditioned systems, e.g. the corrected Gauss Newton algorithm utilizing sparse eigenvalues techniques.
2. Investigating the effect of relaxing the tolerance in the SEP and UEP calculations on the computational time.
3. Enhancing existing techniques to reduce the computational time such that it can be used in the area of transient security monitoring. That is by using the updated commercial packages for solving systems of linear equations (for SEP and UEP solutions).
4. Further improvements and refinements are required for the direct method to be able to handle the cases of multiwing instability by including the effect of the post-fault network on the system transient behaviour.
5. Implementation of the automatic determination of the mode of instability, currently used in the RNF, in the sparse formulation. Also, further developments are needed to extend this implementation for the applications to stressed systems.

6. Using a more complex model to represent the system generating units; to represent the exciter and the governor (if possible). This will make the direct method suitable for power system planning, or at least it will complement the simulation method in planning studies by selecting those cases which require more detailed investigation.

7. Modeling of special controls which include :

- (i) load rejection, and
- (ii) generation rejection.

APPENDIX A

STABILITY DEFINITIONS AND LYAPUNOV STABILITY THEORY

Stability Definitions of Lyapunov [10]

Consider a dynamic system described by:

$$\dot{\underline{x}} = \underline{f}(\underline{x}, t) \quad (\text{A.1})$$

and assume that the system has a unique solution starting at a given initial condition \underline{x}_0 . If we denote the solution by $\Omega(t; \underline{x}_0, t_0)$ then

$$\Omega(t_0; \underline{x}_0, t_0) = \underline{x}_0 \quad (\text{A.2})$$

In the system of equations (A.1), a state \underline{x}_e is called an equilibrium state if

$$\underline{f}(\underline{x}_e, t) = \underline{0} \quad \text{for all } t \quad (\text{A.3})$$

Now let $S(\lambda)$ consists of all points that

$$\| \underline{x}_e - \underline{x}_0 \| \leq \lambda \quad (\text{A.4})$$

where $\| \underline{x} \|$ is the Euclidean norm of \underline{x} and let $S(\epsilon)$ consists of all points that

$$\| \Omega(t; \underline{x}_0, t_0) - \underline{x}_e \| \leq \epsilon \quad \text{for all } t \leq t_0 \quad (\text{A.5})$$

An equilibrium state \underline{x}_e is said to be stable in the sense of Lyapunov if, corresponding to each $S(\varepsilon)$, there is an $S(\lambda)$ such that the trajectories starting in $S(\lambda)$ do not leave $S(\varepsilon)$ as t increases indefinitely.

An equilibrium state \underline{x}_e is said to be asymptotically stable if it is stable in the sense of Lyapunov and if every solution starting within $S(\lambda)$ converges, without leaving $S(\varepsilon)$, to \underline{x}_e as t increases indefinitely.

If the asymptotic stability holds for all states (all points in the state space) from which the trajectories originate, the equilibrium state is said to be asymptotically stable in the large.

The second method of Lyapunov stability theory

Given a dynamic system described by equation (A.1) with the origin as an equilibrium state, then the equilibrium state at the origin is asymptotically stable if there exists a scalar function $V(\underline{x}, t)$ having continuous first partial derivatives and satisfying the following conditions:

- (a) $V(\underline{x}, t)$ is positive definite,
- (b) $\dot{V}(\underline{x}, t)$ is negative definite

The second criterion is relaxed if $\dot{V}(\underline{x}, t)$ is negative semi-definite instead of negative definite. If $\dot{V}(\underline{x}, t)$ is zero, the system can remain in a limit cycle and the equilibrium state at the origin is said to be Lyapunov stable.

For non-linear systems, the stability problem is a local problem in the sense that the equilibrium state at the origin can be locally asymptotically stable without being asymptotically stable in the large. therefore, the concept of boundary of stability, or domain of attraction, is of a great importance.

APPENDIX B.

DERIVATION OF SYSTEM EQUATIONS

Similar to the load flow analysis, we have the following power equations in polar form:

(a) For a load bus (l)

$$V_l \sum_{j=1}^N [V_j Y_{lj} \cos (\gamma_{lj} - \phi_l + \phi_j)] = P_l \quad (\text{B.1})$$

for all l

$$-V_l \sum_{j=1}^N [V_j Y_{lj} \sin (\gamma_{lj} - \phi_l + \phi_j)] = Q_l \quad (\text{B.2})$$

(b) For a generator bus (g)

$$V_g \sum_{j=1}^N [V_j Y_{gj} \cos (\gamma_{gj} - \phi_g + \phi_j)] - PG_g = P_g \quad (\text{B.3})$$

for all g

$$-V_g \sum_{j=1}^N [V_j Y_{gj} \sin (\gamma_{gj} - \phi_g + \phi_j)] - QG_g = Q_g \quad (\text{B.4})$$

where QG_g , similar to PG_g (as described in Chapter 3), is the imaginary output power generated at bus g. In the transient analysis, the classical model for the generator is used (constant e.m.f. behind the direct axis transient reactance) as shown in figure B.1.

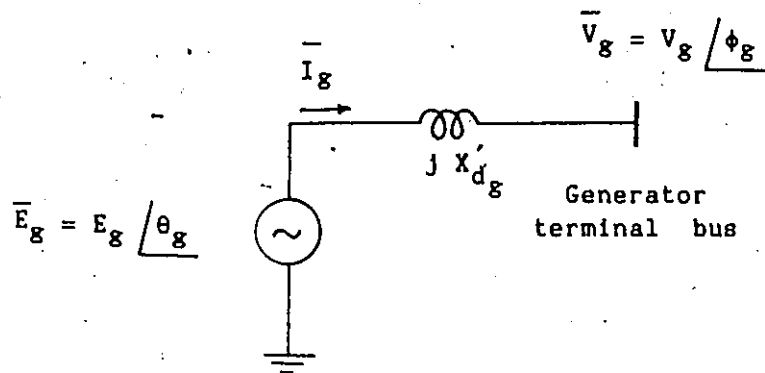


Fig. B.1 Generator classical model.

According to figure B.1, the generator output current is given by:

$$\bar{I}_g = [\bar{E}_g - \bar{V}_g] / jX'_{dg} \quad (\text{B.5})$$

then

$$\bar{I}_g = \frac{-j}{X'_{dg}} [(E_g \cos \theta_g - V_g \cos \phi_g) + j (E_g \sin \theta_g - V_g \sin \phi_g)] \quad (\text{B.6})$$

or

$$\bar{I}_g = B_g [(E_g \sin \theta_g - V_g \sin \phi_g) - j (E_g \cos \theta_g - V_g \cos \phi_g)] \quad \text{for all } g \quad (\text{B.7})$$

where

$$B_g = 1 / X'_{dg} \quad \text{for all } g \quad (\text{B.8})$$

Then, the generator real power output is given by:

$$P_{G_g} = \text{Re} \{ \bar{S}_g \} \quad (\text{B.9})$$

$$P_{G_g} = \text{Re} \{ \bar{E}_g \cdot \bar{I}_g^* \} \quad (\text{B.10})$$

$$P_{G_g} = \operatorname{Re} \left\{ [E_g \cos \theta_g + j E_g \sin \theta_g] \cdot B_g \cdot [(E_g \sin \theta_g - V_g \sin \phi_g) + j (E_g \cos \theta_g - V_g \cos \phi_g)] \right\} \quad (\text{B.11})$$

$$P_{G_g} = B_g [E_g \cos \theta_g (E_g \sin \theta_g - V_g \sin \phi_g) - E_g \sin \theta_g (E_g \cos \theta_g - V_g \cos \phi_g)] \quad (\text{B.12})$$

$$P_{G_g} = B_g E_g V_g (\sin \theta_g \cos \phi_g - \cos \theta_g \sin \phi_g) \quad (\text{B.13})$$

or $B_g E_g V_g \sin (\theta_g - \phi_g) - P_{G_g} = 0 \quad \text{for all } g \quad (\text{B.14})$

Since the armature resistance is neglected, then the generator real power is the same as the real power delivered to the generator terminal bus. This is not the case with the imaginary power; therefore the imaginary power delivered to the generator terminal bus is given by:

$$Q_{G_g} = \operatorname{Im} \left\{ \bar{V}_g \cdot \bar{I}_g^* \right\} \quad (\text{B.15})$$

$$Q_{G_g} = \operatorname{Im} \left\{ [V_g \cos \phi_g + j V_g \sin \phi_g] \cdot B_g \cdot [(E_g \sin \theta_g - V_g \sin \phi_g) + j (E_g \cos \theta_g - V_g \cos \phi_g)] \right\} \quad (\text{B.16})$$

$$Q_{G_g} = B_g [V_g \sin \phi_g (E_g \sin \theta_g - V_g \sin \phi_g) + V_g \cos \phi_g (E_g \cos \theta_g - V_g \cos \phi_g)] \quad (\text{B.17})$$

$$Q_{G_g} = B_g [-V_g^2 + E_g V_g (\sin \theta_g \sin \phi_g + \cos \theta_g \cos \phi_g)] \quad (\text{B.18})$$

$$\text{or } QG_g = B_g [E_g V_g \cos (\theta_g - \phi_g) - V_g^2] \quad \text{for all } g \quad (\text{B.19})$$

Since we are not interested in QG_g , then QG_g can be eliminated using equation (B.4) and we get the following equation:

$$-V_g \sum_{j=1}^N [V_j Y_{gj} \sin (\gamma_{gj} - \phi_g + \phi_j)] - B_g [E_g V_g \cos (\theta_g - \phi_g) - V_g^2] = Q_g \quad \text{for all } g \quad (\text{B.20})$$

(c) Swing equation

The swing equation of an N_g generator system can be written in a synchronous frame of reference as:

$$M_g \dot{\omega}_g = P_m - PG_g \quad \text{for all } g \quad (\text{B.21})$$

The previous equation can be expressed in the COA frame of reference as discussed in chapter 2:

$$M_g \dot{\omega}_g = P_{m_g} - PG_g - \frac{M_g}{M_o} P_{COA} \quad \text{for all } g \quad (\text{B.22})$$

$$\text{where } P_{COA} = \sum_{g=1}^{N_g} [P_{m_g} - PG_g] \quad (\text{B.23})$$

Since our task is to calculate the SEP and UEP as steps to calculate the energy margin, and since the speeds are zero at SEP and UEP, then (by subtracting equation (B.22) of $g=2$ from that of $g=1$, . . . , and the equation of $g=N_g$ from that of $g=N_g-1$)

equation (B.22) can be rewritten in the form:

$$PG_g - \frac{M_g}{M_0} \sum_{i=1}^{N_g} P_i = P_{n_g} - \frac{M_g}{M_0} \sum_{i=1}^{N_g} P_{n_i} \quad \text{for all } g \neq N_g \quad (\text{B.24})$$

Dividing the g^{th} equation of (B.24) by M_g and then subtracting the 2nd equation from the 1st equation, the 3rd equation from the 2nd equation,, the N_g^{th} equation from the $(N_g-1)^{\text{th}}$ equation, we get the following new set of equations:

$$\frac{PG_g}{M_g} - \frac{PG_{g+1}}{M_{g+1}} = \frac{P_{n_g}}{M_g} - \frac{P_{n_{g+1}}}{M_{g+1}} \quad \text{for all } g \neq N_g \quad (\text{B.25})$$

Equations (B.1), (B.2), (B.3), (B.20), (B.14), (B.25)

and (3.1) are the system equations.

APPENDIX C
DERIVATION OF JACOBIAN ELEMENTS

According to figure 3.1, the jacobian elements of each block are formulated as follows (the symbol f_i will denote the L.H.S. of a given equation):

Elements of J_{11}

Taking the partial derivative of the L.H.S. of equation (3.3) or (3.4) w.r.t. ϕ , we get

$$\frac{\partial f_i}{\partial \phi_j} = - V_i V_j Y_{ij} \sin (\gamma_{ij} - \phi_i + \phi_j) \quad , i \neq j \quad (C.1)$$

$$\frac{\partial f_i}{\partial \phi_i} = V_i \sum_{\substack{k=1 \\ k \neq i}}^N [V_k Y_{ik} \sin (\gamma_{ik} - \phi_i + \phi_k)] \quad (C.2)$$

where $i = 1, \dots, N$ and $j = 1, \dots, N$

Elements of J_{12}

Taking the partial derivative of the L.H.S. of equation (3.3) or (3.4) w.r.t. V , we get

$$\frac{\partial f_i}{\partial V_j} = V_i Y_{ij} \cos (\gamma_{ij} - \phi_i + \phi_j) \quad , i \neq j \quad (C.3)$$

$$\frac{\partial f_i}{\partial V_i} = \sum_{\substack{k=1 \\ k \neq i}}^N [V_k Y_{ik} \cos (Y_{ik} - \phi_i + \phi_k)] + 2 V_i Y_{ii} \cos Y_{ii} \quad (C.4)$$

where $i = 1, \dots, N$ and $j = 1, \dots, N$

Elements of J_{21}

Taking the partial derivative of the L.H.S. of equation (3.5) w.r.t. ϕ , we get

$$\frac{\partial f_i}{\partial \phi_j} = - V_i V_j Y_{ij} \cos (Y_{ij} - \phi_i + \phi_j) \quad , i \neq j \quad (C.5)$$

$$\frac{\partial f_i}{\partial \phi_j} = V_i \sum_{\substack{k=1 \\ k \neq i}}^N [V_k Y_{ik} \cos (Y_{ik} - \phi_i + \phi_k)] \quad (C.6)$$

where $i = 1, \dots, N$ and $j = 1, \dots, N$

Elements of J_{22}

Taking the partial derivative of the L.H.S. of equation (3.5) w.r.t. V , we get

$$\frac{\partial f_i}{\partial V_j} = - V_i Y_{ij} \sin (Y_{ij} - \phi_i + \phi_j) \quad , i \neq j \quad (C.7)$$

$$\frac{\partial f_i}{\partial V_i} = - \sum_{\substack{k=1 \\ k \neq i}}^N [V_k Y_{ik} \sin (Y_{ik} - \phi_i + \phi_k)] - 2 V_i Y_{ii} \cos Y_{ii} \quad (C.8)$$

where $i = 1, \dots, N_g$ and $j = 1, \dots, N$

Elements of J_{31}

Taking the partial derivative of the L.H.S. of equation (3.6) w.r.t. ϕ , we get

$$\frac{\partial f_i}{\partial \phi_i} = - V_i V_j Y_{ij} \cos (Y_{ij} - \phi_i + \phi_j) \quad i \neq j \quad (C.9)$$

$$\frac{\partial f_i}{\partial \phi_j} = V_i \sum_{\substack{k=1 \\ k \neq i}}^N [V_k Y_{ik} \cos (Y_{ik} - \phi_i + \phi_k)] - B_i E_i V_i \sin (\theta_i - \phi_i) \quad (C.10)$$

where $i = 1, \dots, N_g$ and $j = 1, \dots, N$

Elements of J_{32}

Taking the partial derivative of the L.H.S. of equation (3.6) w.r.t. V , we get

$$\frac{\partial f_i}{\partial V_j} = - V_i Y_{ij} \sin (Y_{ij} - \phi_i + \phi_j) \quad i \neq j \quad (C.11)$$

$$\frac{\partial f_i}{\partial V_i} = - \sum_{\substack{k=1 \\ k \neq i}}^N [V_k Y_{ik} \sin (Y_{ik} - \phi_i + \phi_k)] \\ - 2 V_i Y_{ii} \sin Y_{ii} - B_i E_i \cos (\theta_i - \phi_i) \\ + 2 B_i V_i \quad (C.12)$$

where $i = 1, \dots, N_g$ and $j = 1, \dots, N$

Elements of D_1

This block is a diagonal matrix for which the elements can be obtained by taking the partial derivative of the L.H.S. of equation (3.6) w.r.t. θ as follows:

$$\frac{\partial f_i}{\partial \theta_i} = B_i E_i V_i \sin (\theta_i - \phi_i) \quad (C.13)$$

where $i = 1, \dots, N_g$

Elements of D_2

This block is a diagonal matrix whose elements can be obtained by taking the partial derivative of the L.H.S. of equation (3.7) w.r.t. ϕ as follows:

$$\frac{\partial f_i}{\partial \phi_i} = - B_i E_i V_i \cos (\theta_i - \phi_i) \quad (C.14)$$

where $i = 1, \dots, N_g$

Elements of D_3

This block is a diagonal matrix whose elements can be obtained by taking the partial derivative of the L.H.S. of equation (3.7) w.r.t. V as follows:

$$\frac{\partial f_1}{\partial V_i} = B_1 E_1 \sin(\theta_i - \phi_i) \quad (C.15)$$

where $i = 1, \dots, N_g$

Elements of D_4

This block is a diagonal matrix whose elements can be obtained by taking the partial derivative of the L.H.S. of equation (3.7) w.r.t. θ as follows:

$$\frac{\partial f_1}{\partial \theta_i} = B_1 E_1 V_i \cos(\theta_i - \phi_i) \quad (C.16)$$

where $i = 1, \dots, N_g$

Elements of B

This block is a bidiagonal matrix whose elements can be obtained by taking the partial derivative of the L.H.S. of equation (3.8) w.r.t. PG . The diagonal elements are

$$\frac{\partial f_1}{\partial PG_i} = 1 / M_i \quad (C.17)$$

The upper-diagonal elements are

$$\frac{\partial f_i}{\partial PG_{i+1}} = -1 / M_{i+1} \quad (C.18)$$

where $i = 1, \dots, N_g - 1$

Elements of \tilde{m}

This block is a vector whose elements can be obtained by taking the partial derivative of the L.H.S. of equation (3.9) w.r.t. θ as follows:

$$\frac{\partial f_{N_g}}{\partial \theta_i} = M_i \quad (C.19)$$

where $i = 1, \dots, N_g$

As shown in figure 3.1, we have two blocks, each is a negative unity matrix. The first one (the upper one) results from taking the partial derivative of equation (3.4) w.r.t. PG, and the second one results from taking the partial derivative of equation (3.7) w.r.t. PG.

It is clear that the Jacobian is very sparse, and most of its elements (J_{11}, \dots, J_{32}) have already been formulated as a part of the load flow solution.

APPENDIX D

A MULTI-STAGE ALGORITHM (STAFP-1)

The algorithm STEFP-1 consists of five stages. In each stage an output screen is displayed which presents the results of that stage. The sample results shown in this appendix are for the 50-Generator, 145-bus system described in section 4.2 with the same fault and clearing conditions.

First Screen

This is an interactive dialogue in which the user inputs the names of load flow and dynamic data files and the name of the output file which contains the results (SEP, UEP and energy margin). Figure D.1 shows the first screen.

Stage 1

This is mainly to read the data, to calculate the generator internal emf in COA frame of reference, and to calculate the clearing angles and speeds. Figure D.2 shows the output screen of stage 1. This screen shows the summary of input data (similar to those in table 4.1), the CPU times consumed in each step as well as the total CPU in this stage.

STEFP-1

Sparse Transient Energy Function Program

micro computer version

Department of Electrical and Computer Engineering
McMaster University

Load flow data file name ? LFD.DAT

Dynamic data file name ? DYN.DAT

Output results file name ? OUT.DAT

To start a session press RETURN

Fig. D.1 The first screen of STEFP-1.

STAGE 1

To read load flow and dynamic data, to calculate internal EMF's, and to calculate clearing angles and speeds.

Input Data :

The total no. of generator buses	50
The total no. of load buses	95
The total no. of lines	647
No. of transformers	63
No. of phase shifters	0
The no. of N-Z elements of [Y] matrix	985
The no. of N-Z elements of [J] matrix	4390.

Details of CPU times :

CPU in reading load flow data	= 131.0	sec
CPU in forming pre-fault [Y]	= 8.5	sec
CPU in calculating internal EMFs	= .3	sec
CPU in reading dynamic data	= 4.2	sec
CPU in calculating cl. angles and speeds	= 29.3	sec
CPU in forming post-fault [Y]	= .1	sec
CPU in writing input data for STAGE 2	= 57.1	sec
Total CPU in STAGE 1	= 230.5	sec

To go to STAGE 2 press RETURN

Fig. D.2 The screen of stage 1 of STEFP-1.

Stage 2

This is to calculate the (post-fault) Stable Equilibrium Point (SEP). Figure D.3 shows the output screen of stage 2. This screen shows the number of iterations needed, the total mismatch and the number of rejections (to ensure non-divergence) of each iteration. The CPU times consumed in each step and the total CPU time in this stage are also shown.

Stage 3

Using the procedure described in section 3.4, the initial value \tilde{x}^0 needed to calculate the UEP is evaluated. This stage has an optional output screen and can be displayed at the user's request.

Stage 4

This stage calculates the Unstable Equilibrium Point (UEP) using \tilde{x}^0 as initial value. Figure D.4 shows the output screen of stage 4.

Stage 5

This is to calculate the energy margin using the procedure described in section 3.4. Figure D.5 shows the output screen of this stage.

<u>STAGE 2</u>		
To calculate SEP using Newton-Raphson method in a sparse matrix formulation.		
<u>The calculation of SEP :</u>		
<u>Iteration No.</u>	<u>Mismatch</u>	<u>No. of rejections</u>
0	33.43542000	0
1	.70515520	0
2	.00437499	0
3	.00000389	0
<u>Details of CPU times :</u>		
CPU in reading data from STAGE 1	= 100.4	sec
CPU in calculating SEP	= 167.8	sec
CPU in writing data for STAGE 3	= 7.6	sec
Total CPU in STAGE 2	= 275.8	sec

To go to STAGE 3 press RETURN

Fig. D.3 The screen of stage 2 of STEFP-1.

STAGE 4

To calculate UEP using Newton-Raphson method in a sparse matrix formulation.

The calculation of UEP :

<u>Iteration No.</u>	<u>Mismatch</u>	<u>No. of rejections</u>
0	379.33860000	0
1	32.13735000	0
2	.26112920	0
3	.00018677	0

Details of CPU times :

CPU in reading data from STAGE 3	=	108.8	sec
CPU in calculating UEP	=	167.3	sec
CPU in writing data for STAGE 5	=	4.8	sec
Total CPU in STAGE 4	=	280.9	sec

To go to STAGE 5 press RETURN

Fig. D.4 The screen of stage 4 of STEFP-1.

<u>STAGE 5</u>			
To calculate kinetic energy, potential energy, and energy margin.			
<u>Energy margin calculation :</u>			
The Corrected Kinetic Energy	=	.399362	
The Potential Energy at UEP	=	.895638	
The Energy Margin	=	.496275	
The Normalized Energy Margin	=	1.242669	
<u>Details of CPU times :</u>			
CPU in reading data from STAGE 4	=	93.6	sec
CPU in calculating kinetic energy	=	.1	sec
CPU in calculating energy margin	=	43.2	sec
Total CPU in STAGE 5	=	136.9	sec

To quit press RETURN

Fig. D.5 The screen of stage 5 of STEFP-1.

REFERENCES

- [1] Yu, Y.N., Electric power system dynamic, New York: Academic Press, 1983.
- [2] Pay, M.A., Power system stability, North-Holland Publishing Company, New York, 1981.
- [3] Teichgraeber, R.D., F.W. Harris, and G.L. Johnson, "New stability measure for multimachine power systems", IEEE Trans. PAS, vol. 89, pp 233-239, Feb. 1970.
- [4] Kimbark, E.W., Power system stability, New York: Wiley, vol. 1, 1948.
- [5] Goordich, R.D., Jr., "Accurate computation of 2-machine stability", AIEE Trans. PAS, vol. 71, pp 577-581, August 1952.
- [6] Aylett, P.D., "Energy-integral criterion of transient stability limits of power systems", Proc. IEE, vol. 105, pp 527-536, 1958.
- [7] Dharma Rao, N., "A new approach to the transient stability problem", IEEE Trans. PAS, vol. 81, pp 186-190, July 1962.
- [8] LaSalle, J.P. and S. Lefschetz, Stability by Liapunov's direct method with applications, New York: Academic Press, 1961.
- [9] LaSalle, J.P., "Recent advances in Liapunov stability theory", SIAM Review, vol. 6, pp 1-11, January 1964.
- [10] Ogata, K., Modern control engineering, Englewood Cliffs, N.J., Prentice hall, 1970.
- [11] Fouad, A.A., et al, "Transient stability margin as a tool for dynamic security assessment", EPRI Report EL-1755, Project 1355-3, March 1981.
- [12] Magnusson, P.C., "transient energy method of calculating stability", AIEE Trans., vol. 66, pp 747-755, 1947.
- [13] Steinmetz, C.P., "Power control and stability of electric generating stations", AIEE Trans., vol. XXXIX, Part II, p 1215, July-December 1920.

- [14] Kunder, P., "Evaluation of methods for studying power system stability", Proceedings of the International Symposium on Power System Stability, Ames, Iowa, 1985.
- [15] Peschon, J., "Case study of optimum control of power systems", 1968 Joint Automatic Control Conf., Ann Arbor, Mich.
- [16] Willems, J.L., "Direct methods for transient stability studies in power system analysis", IEEE Trans. Aut. Control, vol. 16, p 332, 1971.
- [17] Ribbens-Pavella, M., "Critical survey of transient stability studies of multimachine power systems by Lyapunov's direct method", Proceedings of the 9th Annual Allerton Conference on Circuits and System Theory, October, pp 751-767, 1971.
- [18] Fouad, A.A., "Stability theory-criteria for transient stability", Proc. Engineering Foundation Conference on Systems Engineering for Power : Status and Prospects, Henniker, New Hampshire, 1975.
- [19] Ribbens-Pavella, M. and F.J. Evans, "Direct methods for studying Dynamics of large-scale electric power systems - a survey", IFAC World Congress on Control Science and Technology for the Progress of Society, 1984.
- [20] Chorlton, A. and G. Shackshaft, "Comparison of accuracy of methods for studying stability. Northfleet exercise.", Electra, vol. 23, p 1, 1972.
- [21] Dandeno, P.L., "Synchronous machine stability constants; requirements and realization", (prepared by IEEE Joint Working Group on this subject), IEEE-PES Winter Meeting, New York, paper No. 177., 1977.
- [22] Willems, J.L. and J.C. Willems, "Application of Lyapunov methods to the computation of transient stability regions of multi-machine power systems", IEEE Trans. PAS, vol. 89, pp 795-801, May/June 1970.
- [23] Pay, M.A., "Power system stability studies" by Lyapunov-Popov approach", Proc. 5th IFAC World Congress, Paris, 1972.
- [24] Sastry, V.R. and P.G. Murthy, "Derivation of completely controllable and completely observable state models of multi-machine power system stability studies", Internation J. of Control, vol. 16, pp 777-788, Oct. 1972.
- [25] Willems, J.L., "A partial stability approach to the problem of the transient power system stability", Internation J. of Control, vol. 19, pp 1-14, 1974.

- [26] Sastry, V.R. and P.G. Murthy, "Discussion of Willems' paper, "Direct methods of transient stability studies power systems analysis", and reply by author", IEEE Trans. AC, vol. 19, pp 480-481, aug. 1972.
- [27] Pay, M.A. and P.G. Murthy, "New Lyapunov functions for power systems based on minimal realizations", Int. J. Control, vol. 19, pp 401, 1974.
- [28] Chetaev, N.G., Stability of motion, Pergamon Press, 1961.
- [29] Krasovskii, N.N., Stability of motion, Stanford University Press, Stanford, California, 1963.
- [30] Schultz, D.G. and J.E. Gibson, "The variable gradient method for generating Lyapunov functions", AIEE Trans. Part. II, Appl. and Industry, vol. 81, pp 203-210, 1962.
- [31] Zobov, V.I., "Methods of Lyapunov and their application", U.S. Atomic Energy Commission, Transaction AEC-tr-4439, p 83, 1961.
- [32] Popov, V.M., "Absolute stability of non-linear control system of automatic control", Automation and Remote Control, vol. 22, pp 857-875, 1962.
- [33] Tavora, C.J. and O.J.M. Smith, "Stability Analysis of power systems", IEEE Trans. PAS, vol. 91, pp 1138-1139, May/June 1971.
- [34] Stanton, K.N., "Dynamic energy balance studies for simulation of power frequency transient", Proc. PICA Conference, Boston, May 1971.
- [35] Fouad, A.A. and R.L. Lugtu, "Transient stability analysis of power of power systems using Lyapunov's second method", IEEE Winter Power Meeting, Paper No. C72, 145-6, New York, Feb. 1973.
- [36] Padiyar, K.R., C.V. Doraswamy, "Analysis of dynamic equilibrium of Power systems", Proc. 7th Annual South Eastern Symposium on System Theory, pp 123-125, March 1975.
- [37] Skilling, H.H. and M.H. Yamakawa, "A graphical solution of transient stability", Elec. Eng., vol. 59, pp 462-465, Nov. 1940.
- [38] Kimbark, E.W., "Improvement of system stability by switched series Capacitors", IEEE Trans. PAS, vol. 85, pp 180-188, Feb. 1966.
- [39] Kimbark, E.W., "Improvement of power system stability by changes in the network", IEEE Trans. PAS, vol. 88, pp 773-781, May 1969.
- [40] Machida, T., "Improving transient stability of AC system by joint usage of DC system", IEEE Trans. PAS, vol. 85, pp 226-232, March 1966.

- [41] Smith, O.J.M., "Power system transient control by capacitor switching", IEEE Trans. PAS, vol. 88, pp 28-35, Jan. 1969.
- [42] El-Kharashi, A.K., "Some transient stability problems connected with displacement governors", IEEE Trans. PAS, vol. 82, pp 166-175, 1963.
- [43] Abu-Elnaga, M.M. and M.A. El-Kady, "Generalized formulation of the equal area criterion and applications to transient stability analysis of power systems", Dépt. Elec. and Computer Eng., McMaster University, Hamilton, Canada, Report SA-85-02-R, Nov. 1985.
- [44] Dharma Rao, N. and H.N. Ramachandra, "Phase-plane techniques for the solution of the transient stability problems", Proc. Inst. Elec. Eng., vol. 110, pp 1451-1461, 1963.
- [45] Dharma Rao, N. and H.N. Ramachandra, "An extension of conventional phase-plane techniques for the solution of multimachine transient stability problem", IEEE Trans. PAS, Suppl., pp 697-711, 1963.
- [46] Kashkari, C.N., "Effect of feed-back signals on transient stability - phase plane approach", IEEE Trans. PAS, vol. 90, pp 2228-2232, 1971.
- [47] Gless, G.E., "Direct method of Lyapunov applied to transient power system stability", IEEE Trans. PAS, vol. 85, pp 159-168, Feb. 1966.
- [48] El-Abiad, A.H. and K. Nagappan, "Transient stability regions of multimachine power systems", IEEE Trans. PAS, vol. 85, pp 169-178, Feb. 1966.
- [49] Gurel, O. and L. Lapidus, "A guide to the generation of Lyapunov functions", Industrial and Engineering Chemistry, pp 30-41, March 1969.
- [50] Margolis, S.G. and W.G. Vogt, "Control engineering applications of V. I. Zobov's construction procedure for Lyapunov functions", IEEE Trans. AC, vol. 8, pp 104-113, April 1963.
- [51] Yu, Y.N. and K. Vongasuriya, "Nonlinear power system stability study by Lyapunov function and Zobove's method", IEEE Trans. PAS, vol. 86, pp 1480, 1967.
- [52] Luré, A.I. and V.N. Postnikov, "On the theory of stability of control systems", Prikl. Mat. 1. Mehk, vol. 8, No. 3, 1944.
- [53] Kalman, R.E., "Lyapunov functions for the problem of Luré in Automatic control", Proc. Nat. Acad. Sci., vol. 49, pp 210-205, Feb. 1963.

- [54] Yakubovitch, V.A., "The solution of certain matrix inequalities in Automatic control", Dokl. akad. Nauk--S.S.S.R., vol. 143, pp 1304-1307, 1962.
- [55] Moore, K.S. and J.H. Anderson, "A generalization of the Popov criterion", Jour. Franklin Institute, vol. 285, pp 488-492, June 1968.
- [56] Willems, J.L., "Optimum Lyapunov functions and stability regions of multimachine power systems", Proc. IEE, vol. 117, pp 573, 1970.
- [57] ~~Willems, J.L.~~ and J.C. Willems, "The application of Lyapunov methods to the compensation of transient stability regions for multimachine power system", IEEE Trans. PAS, vol. 89, pp 795, 1970.
- [58] Willems, J.L., "Direct methods of transient stability studies in power system analysis", IEEE Tans. AC, vol. 16, pp 332, 1971.
- [59] Sastry, V.R. and P.G. Murthy, "Discussion of J.L. Willems "Direct methods of transient stability studies in power system analysis", and reply by author", IEEE Tans. AC, vol. 17, pp 415, 1972.
- [60] Mansour, M., "Stability analysis and control of power systems", in Handschin, E. (Editor), Real time control of electric power systems, Elsevier Publishing Co., Amsterdam, 1972.
- [61] Kakimoto, N., Y. Ohsawa and M. Hayashi, "Transient stability analysis of electric power systems via Lure type Lyapunov function with effect of transfer conductances", Trans. IEE of Japan, vol. 98, pp 63, 1978.
- [62] Kakimoto, N., Y. Ohsawa and M. Hayashi, "Transient stability analysis of multimachine power systems with field flux decay via Lyapunov direct method", IEEE Trans. PAS, vol. 99, pp 1819, 1980.
- [63] Kakimoto, N. and M. Hayashi, "Transient stability analysis of multimachine power system by Lyapunov direct method", Proc. 20th IEEE Conference on Decision and Control, 1981.
- [64] DiCaprio, V. and F. Saccomano, "Nonlinear stability analysis of multimachine electric power systems", Recherche Di Automatica, vol. 1, No. 1, pp 1-29, Sept. 1970.
- [65] Ribbens-Pavella, M., "Transient stability of multimachine power systems by Lyapunov direct method", IEEE Winter Power Meeting, New York, Paper 71CP17-PWR, Jan. 1971.
- [66] Athay, T., R. Podmore and S. Virmani, "A practical method for direct analysis of Transient tenergy stability", IEEE Trans. PAS, vol. 98, pp 573-584, March/April 1979.

- [67] Athay, T. , et al, "Transient energy stability analysis", Final Report submitted to U.S. Department of Energy by SCI, June, 1979.
- [68] Prabhakara, F.S. and A.H. El-Abiad, "A simplified determination of transient stability regions for Lyapunov methods", IEEE Trans. PAS, vol. 94, pp 672-689, Mar. 1975.
- [69] Gupta, C.L. and A.H. El-Abiad, "Determination of the closest unstable equilibrium state for Lyapunov methods in transient stability studies", IEEE Trans. PAS, vol. 95, pp 1699-1712, Sept./Oct. 1976.
- [70] Pai, M.A. and C.L. Narayana, "Finite regions of attraction for multi-nonlinear systems and its application to the power systems stability problem", IEEE Trans. AC, vol. 12, pp 331-336, Oct. 1967.
- [71] Ribbens-Pavella, M. and B. Lemal, "Fast determination of stability regions for on-line power system studies", Proc. IEE, vol. 123, pp 680-696, July 1976.
- [72] Ribbens-Pavella, M., "On-line measurement of transient stability power system index", in Savulescu, S.C. (Editor), Computerized operation of power systems (Book), Elsevier Scientific Publishing Co., New York, 1976.
- [73] Fouad, A.A. and S.E. Stanton, "Transient stability of a multimachine power system. Part I : Investigation of system trajectories. Part, II : Critical transient energy", IEEE Trans. PAS, vol. 100, pp 3408, 1981.
- [74] Fouad, A.A., S.E. Stanton, K.R.C Mamandur and K.C. Krumpel, "Contingency analysis using the transient energy margin technique", IEEE Trans. PAS, vol. 101, pp 757-766, April 1982.
- [75] Fouad, A.A. and V. Vittal, "Power system response to a large disturbance : Energy associated with system separation", IEEE Trans. PAS, vol. 102, pp 3534-3540, Nov. 1983.
- [76] Fouad, A.A., S.E. Stanton and T.K. Gh, "Critical energy for direct transient stability assessment of a multimachine power system", IEEE Trans. PAS, vol. 103, pp 2199-2206, Aug. 1984.
- [77] Fouad, A.A., V. Vittal, S. Rajagopal, V.F. Carvalho, M.A. El-Kady, C.K. Tang, J.V. Mitsche and M.V. Pereira, "Direct transient stability analysis using energy functions application to large power networks", IEEE Trans. in Power System, vol. PWR5-2, No. 1, pp 37-44, 1987.

- [78] EPRI Report No. EL-4980: "Demonstration of large-scale direct analysis of power system transient stability", 1986.
- [79] Hill, D.J. and A.R. Bergen, "Stability Analysis of multimachine power networks with linear frequency dependent loads", IEEE Trans. CAS, vol. 29, pp 840, 1982.
- [80] Hill, D.T. and C.C. Nai, "Energy functions for power systems based structure preserving models", Proceedings of the 25th Conference on Decision and Control, Athens, Greece, Dec. 1986.
- [81] Abu-Elnaga M.M., M.A. El-Kady, and R.D. Findlay, "Sparse formulation of the transient energy function method for applications to large-scale power systems, submitted to IEEE Winter Power Meeting, Feb. 1988.
- [82] El-Kady, M.A., M.M. Abu-Elnaga, R.D. Findlay and C.G. Bailey, "Sparse formulation of the direct method of transient stability for applications on micro computers", Proceedings of the 29th Symposium on Circuits and Systems, Lincoln, Nebraska, 1986.
- [83] Dhar, R.N., Computer aided power system operation and analysis, Tata McGraw-Hill, New Delhi, 1982.
- [84] T. Athay, et al, "Transient energy analysis", System Engineering for Power, Emergency Operating State Control, Section IV, U.S. Dept. of Energy, Publication No. CONF-790904-PI.
- [85] A.M. Saason, C. Travino and F. Aboytes, "Improved Newton's load flow through a minimization technique", IEEE Trans. PAS, Vol 90, No. 5, pp 1974-1981, 1971.
- [86] Abu-Elnaga M.M., M.A. El-Kady, and R.D. Findlay, "Stability assessment of highly stressed power systems using the sparse formulation of the direct method", submitted to IEEE Winter Power Meeting, Feb. 1988.
- [87] Duff, I.S., "MA28 - a set of FORTRAN subroutines for sparse unsymmetric matrices", Report R8730, A.E.R.E., Harwell, England, 1977.
- [88] Paige, C.C. and M.A. Saunders, "LSQR : Sparse linear equations and least squares problems", ACM Trans. Math. Softw., vol. 8, pp 195-209, June 1982.
- [89] Strang, G., Linear algebra and its applications (Second edition), Academic Press, New York, 1980.
- [90] Fletcher, R. and M.J.D. Powell, "A rapidly convergent descent method for minimization", Computer J., vol. 6, pp 163-168, June 1963.

- [91] Davidon, W.C., "Variable metric method for minimization", AEC Research Development Rept. ANL-5990(Rev.), 1956.
- [92] Davidon, W.C., "Variable metric method for minimization", Computer J., vol. 10, pp 406-410, Feb. 1968.
- [93] Gill, P.E. and W. Murray, "Algorithm for the solution of the nonlinear Least squares problem", Am. J. Numer. Anal., vol. 15, pp 977-992, Oct. 1978.
- [94] Stewart, G.W., "ON the implicit deflation of nearly singular systems of linear equations", SIAM J. Sci. Stat. Comp., vol. 2, pp 136-139, June 1981.
- [95] Hestenes, M.R. and R.J. Stiefel, "Methods of conjugate gradients for solving linear systems", J. Res. N.B.S., vol. 49, pp 409-436, 1952.
- [96] Paige, C.C. and M.A. Saunders, "LSQR : An algorithm for sparse linear equations and sparse least squares", ACM Trans. Math. Softw., vol. 8, pp 43-71, March 1982.
- [97] Wilkinson, J.H., The algebraic eigenvalue problem, Oxford University Press (Clarendon), London and New York, 1965.
- [98] Moler, C.B., "Iterative refinement in floating point", J. Assoc. Comput. Mach., vol. 14, pp 316-321, 1967.
- [99] Stewart, G.W., Introduction to matrix computations, Academic Press, New York, 1973.
- [100] Golub, G.H. and W. Kahan, "Calculating the singular values and pseudoinverse of a matrix", SIAM J. Numer. Anal., vol. 2, pp 205-224, 1965.
- [101] Bandler, J.W., "Optimization methods for computer-aided design", IEEE Trans. on Microwave Theory and Techniques, vol. 17, pp 533-551, Aug. 1969.
- [102] Pike, M.C. and I.D. Hill, "Note on algorithm 2: Fibonacci search", Computer J., vol. 9, pp 416-417, Feb. 1967.
- [103] Calahan, D.A., Computer-aided network design, McGraw-Hill, New York, 1968.
- [104] Abu-Elnaga M.M., M.A. El-Kady, and R.D. Findlay, "Incorporation of load models in the direct method of power system transient stability", submitted to IEEE Winter Power Meeting, Feb. 1988.